Micro-scale measurements of marine microbial interactions with global scale consequences

Marco Giardina

February 2019

A thesis submitted in fulfilment of the requirements for the degree of

Doctor of Philosophy in Science

Climate Change Cluster C3, School of Life Science, University of Technology Sydney

Certificate of Original Authorship

I, Marco Giardina, declare that this thesis is submitted in fulfilment of the requirements for the award of Doctor of Philosophy, in the School of Life Sciences at the University of Technology Sydney.

This thesis is wholly my own work unless otherwise reference or acknowledged. In addition, I certify that all information sources and literature used are indicated in the thesis.

This document has not been submitted for qualifications at any other academic institution.

This research was supported by an Australian Government Research Training Program and an Australian Research Council Discovery Grant DP140101045

Production Note:
Signature: Signature removed prior to publication.

Date: 19/02/2019

Acknowledgements

I have changed a lot throughout the course of my PhD, but one aspect of my personality that hasn't changed (and at this point I guess it never will) is that I do not go straight to the point when I speak/write because I like to start from very…VERY FAR.

In fact, I would like to start my acknowledgements thanking **Manuela Coci** and **Gianluca Corno,** my two Master's supervisors, who five years ago introduced me to aquatic microbial ecology and encouraged me, at the end of my Master's degree, to think about doing a PhD. More importantly, they showed me, for the first time, that science does not have frontiers and that mainly young scientist must be involved to the scientific community. In addition, it is thank to their letter of reference that today I am writing these words, close to the submission of my PhD thesis.

Now I go straight to the point, promised.

I am very grateful to my two PhD supervisors, **Justin Seymour** and **Jean-Baptiste Raina,** for having done such a great job with me. They had always time for me despite their very busy schedule. I thank them for having made me feel always comfortable and positive, without never letting me down even when problems rose up. I also thank both of them for always encouraging me to aim high and take all the good opportunities I encountered during my PhD, and I will encounter in my career.

Particularly, I thank **Justin** for taking me on board despite that 250 words "proposal" I presented him when I started the application process for my PhD. Since I joined the Ocean Microbiology Group, he has been a guide for me.

I am also thankful to **JB**, for the huge patience in teaching me all I know about working in the lab and for the late nights spent helping me out with writing, preparing posters and experiments.

Other people have contributed to my PhD thesis.

In particular, I would like to thank greatly **Mathieu Pernice** for his invaluable scientific support and for his positive attitude in approaching science and life that was essential for me in time of troubles.

I am also thankful to **Peta Clode** who made me feel at home every time I was in Perth. In particular, for having facilitated my work while I was there and to provide always new solution when the experiments were not successful. I also thank her for the beers we had after full days of work.

I would like also to thank **Paul Guagliardo** for the great support provided with the NanoSIMS analysis and for gradually teaching me how to do the analysis by myself.

From the Centre of Microscopy, Characterization and Analysis I would also like to thank **Matt Kilburn, Jeremy Shaw, Lyn Kirilak, John Murphy.**

I am also grateful to **Doug Brumley** for his great enthusiasm and effort put in our collaboration.

It was a pleasure to do my PhD at the Climate Change Cluster C3. It was the perfect environment for me to develop as scientist and personally. The team is very strong and I would like to acknowledge in particular the technical staff that made the impossible possible: **Paul Brooks**, **Graeme Polewesky, Gemma Armstrong**, **Lucia Bennar**, **Sue Fennech.** Also thanks to the director of C3, **Peter Ralph**, for having made of C3 a very dynamic and productive work environment.

I also thank **Anita Giraldo, Stefano Aragone, Zouzou** and **Kate Eiloart** for giving me hospitality in Perth and the great time spent together.

A special thanks to all the people that supported me in editing and formatting my thesis: **Caitlin Lawson**, **Sammy Goyen**, **Kirsty Milner**, **Dave Hughes**, **Deepa Varkey, Mahrita Harahap and Steven Woodcock**.

I also want to thank all of my friends in Australia, my old friends in Italy and all those spread around the World for the support and the good times (I would need other 121 pages to acknowledge you all).

Voglio ringraziare mio zio **Fulvio** per avermi consigliato saggiamente quando mi sono trovato di fronte a delle scelte professionali: e' grazie a lui che sono venuto in Australia nel momento giusto. Ringrazio anche mio fratello **Stefano** e mia zia **Gabriella** per essere sempre presenti nei momenti importanti della mia vita.

Ringrazio **Oriana** per avermi sostenuto ed avermi aiutato ad alleviare lo stress in questi ultimi due anni di dottorato.

Infine, il piu' grosso ringraziamento va' ai miei genitori: dedico a loro questa tesi.

Table of Contents

List of Figures

List of Tables

List of Supplementary Figures

List of Supplementary Tables

Declaration of the contribution to each chapter

Chapter 2

MG, JRS, MP and JBR conceived and designed the study; MG, PG and PLC carried out the NanoSIMS data acquisition; SC and MG carried out the ToF-SIMS data acquisition; CM: carried out the peak deconvolution; MG and RP carried out the EA-IRMS data acquisition. MG and JBR drafted the manuscript. All authors read and approved the final manuscript.

Chapter 3

MG, JRS, MP and JBR conceived and designed the study; MG performed the experiments; MG, PG, MK and PLC carried out the NanoSIMS data acquisition; MG analysed the data and did the statistics. MG drafted the manuscript. All authors read and approved the final manuscript.

Chapter 4

MG, JRS, JBR, SS and RS conceived and designed the study; MG performed the laboratory experiments; MP and SS provided support in setting up the experiment; MG, PG and PLC carried out the NanoSIMS data acquisition; ES and MU developed and provided the *M. adhaerens* strains; DRB developed the theoretical model; UK performed the IRMS analysis; MG analysed the data and tested them statistically. MG, JBR, DRB and JRS drafted the manuscript. All authors read and approved the final manuscript.

Summary

Interactions between marine phytoplankton and heterotrophic bacteria are emerging as key ecological processes that control marine biogeochemical cycles and ecosystem productivity. While these interactions have large-scale implications, they are generally played out across very small spatiotemporal scales and often involve intimate ecological relationships involving the exchange of a diverse suite of metabolites and infochemicals. Previous studies have focussed on the ecological relationships between heterotrophic bacteria and large phytoplankton cells, such as diatoms and dinoflagellates, however, the photosynthetic biomass across much of the global ocean is dominated by picocyanobacteria, mainly comprising two genera, *Prochlorococcus* and *Synechococcus*. It has recently been suggested that the nitrogen-rich exudates of *Synechococcus* may be consumed by heterotrophic bacteria, potentially establishing metabolic, and eventually physical interactions. Yet, due to extremely small size of both partners (0.8-2 μm), it is extremely challenging to observe and quantify their metabolic exchanges at the single-cell level using conventional methods. This means that some of the ecological and biogeochemical consequences of these interactions have potentially been overlooked until now. Recently, technological breakthroughs in high-resolution single-cell imaging techniques, such as Secondary Ion Mass Spectrometry (SIMS), have opened the door for studying microbial associations at relevant scales, allowing for more accurate quantification of their impact on nutrient cycling and oceanic productivity.

This thesis focused on the associations between the picocyanobacteria *Synechococcus* and heterotrophic bacteria, I applied a combination of stable isotope labelling approaches and SIMS to study the metabolic exchanges and the behavioural mechanisms underpinning the onset of the interaction between these two partners, at the single-cell level. First, I compared bulk-scale mass spectrometry with two SIMS techniques (NanoSIMS and ToF-SIMS) to define their advantages and limitations in measuring nutrient uptake at both community and single-cell level. After determining that NanoSIMS was the most suitable tool to investigate *Synechococcus*-heterotrophic bacteria interactions, I applied this technique to determine if nutrient exchanges between *Synechococcus* and two of its culture-associated bacterial isolates were reciprocal. Finally, I determined the role that bacterial behaviour may have on the exploitation of *Synechococcus*-derived nutrients.

This thesis demonstrates the single-cell variability and heterogeneity of the nutrient uptake and cycling between these small and ubiquitous marine microbes, this observed heterogeneity would have been completely missed by large-scale approaches. The associations between *Synechococcus* and different bacterial species lead to species-specific differences in nutrient exchanges. Cells can access significantly more *Synechococcus* derived nutrients by means of physical attachment and despite the small size of *Synechococcus* cells, this association is likely mediated by bacterial behaviour such as chemotaxis. The dynamics that determine these single-cell microbial interactions can have vast implications for global-scale processes.

1 Chapter 1 – General Introduction

1.1 A Microbial Ocean

The ocean is a major feature of the biosphere, covering 70 % of the earth's surface, with a total volume of 1.3 billion cubic kilometres and an average depth of 3.6 km (Eakins and Sharman, 2010). Among all of the living biomass inhabiting this vast ecosystem, 90% are microbial. One litre of seawater typically contains 10^{10} viruses, 10^{9} bacteria and 10^{7} phytoplankton cells (Whitman, Coleman and Wiebe, 1998; Suttle, 2005). This huge microbial abundance coupled with their highly diverse metabolic activities, places marine microbes as key drivers of the marine biogeochemical cycles that mediate the nutrient cycles that underpin ocean productivity and control the rates and directions of ocean-atmosphere gas exchange, which strongly influences global climate (Falkowski, Fenchel and Delong, 2008; Strom, 2008).

From a biogeochemical perspective, the two most important groups of marine microorganisms are phytoplankton and heterotrophic bacteria. In fact, phytoplankton, both eukaryotic microalgae (e.g. diatoms and dinoflagellates) and cyanobacteria, govern global carbon and oxygen fluxes, by fixing ~40 Gt C $year^{-1}$, and thereby contributing to approximately 40 % of the global photosynthesis (Falkowski, 1994; Field *et al.*, 1998). In contrast, marine heterotrophic bacteria respire ~37 Gt C $year^{-1}$ (del Giorgio and Duarte, 2002), while contributing to key steps in the carbon, nitrogen, sulphur, oxygen, phosphorus and iron cycles (Falkowski, Fenchel and Delong, 2008). When considered in isolation, phytoplankton and bacteria are alone tremendously important in marine systems, however, the metabolic and ecological interactions between these groups further strongly influence the primary productivity and biogeochemistry of the ocean (Cole, 1982; Azam and Malfatti, 2007).

1.2 Phytoplankton-bacteria interactions

Phytoplankton cells exude up to 50 % of their photosynthetically-fixed carbon into the water surrounding them (Biddanda and Benner, 1997). Marine bacteria can efficiently assimilate many of the highly labile substrates released by phytoplankton and, in turn, supply phytoplankton with micronutrients, such as iron (Amin *et al.*, 2009), regenerated limiting nutrients such as nitrogen and phosphorous (Cole, 1982; Legendre and Rassoulzadegan, 1995), or complex molecules such as vitamins (e.g. vitamin B_{12}) (Croft *et al.*, 2005).

Some bacterial taxa are commonly identified in association with phytoplankton, both *in situ* and *in vitro*, including members of the Flavobacteraceae, Alphaproteobacteria (especially members of the Roseobacter clade), and Gammaproteobacteria (especially members of the family Alteromonadaceae) (Kirchman, 2002; Buchan and Moran, 2005; Amin, Parker and Armbrust, 2012; Teeling *et al.*, 2012; Goecke *et al.*, 2013). The metabolic properties of these bacteria allow them to readily respond to transient nutrient pulses, which are a distinctive feature of phytoplankton blooms, and to positively and negatively influence phytoplankton physiology (Mayali and Azam, 2004; Durham *et al.*, 2014; Amin *et al.*, 2015; van Tol, Amin and Armbrust, 2017). Although, these interactions ultimately influence ocean-scale biogeochemistry and productivity, they occur over extremely small spatial and temporal scales, which can make them challenging to study.

1.2.1 The Phycosphere

Because many marine bacteria exhibit chemotactic attraction to phytoplankton-derived chemicals, Bell and Mitchell (1972) hypothesised that the interactions between phytoplankton and heterotrophic bacteria might occur in the specific microenvironment they termed the 'phycosphere' (Figure 1.1) "the region that extends outward from an algal cell an undefined distance in which bacterial growth is stimulated by extracellular products of the alga" (Bell and Mitchell, 1972). The phycosphere is the aquatic analogue of the terrestrial 'rhizosphere', which is the region surrounding plant roots that is enriched in plant exuded organic substrates, where physiological interactions between the plant and bacteria in the surrounding soil take place (Philippot *et al.*, 2013). The release of photosynthate by healthy phytoplankton cells occurs either as a passive, but constant flow of molecules through the cell membrane, either when photosynthetic rates are faster than incorporation into biomass (Fogg, 1983; Marañón *et al.*, 2004) or as an active physiological response (Smith and Wiebe, 1976; Obernosterer and Herndl, 1995) that may be stimulated by environmental factors such as nutrient availability, light and temperature (Morana *et al.*, 2014; Thornton, 2014). These exuded molecules form concentration gradients of dissolved organic matter that stretch up to several cell diameters from the phytoplankton surface (Stocker, 2012) and influence the chemical composition of seawater in their vicinity (Biddanda and Benner, 1997). Phycosphere sizes are directly correlated to phytoplankton cell diameter however, growth, exudation rates, along with the diffusivity of the exuded compounds, also contributes to the size of the phycosphere (Seymour *et al.*, 2017).

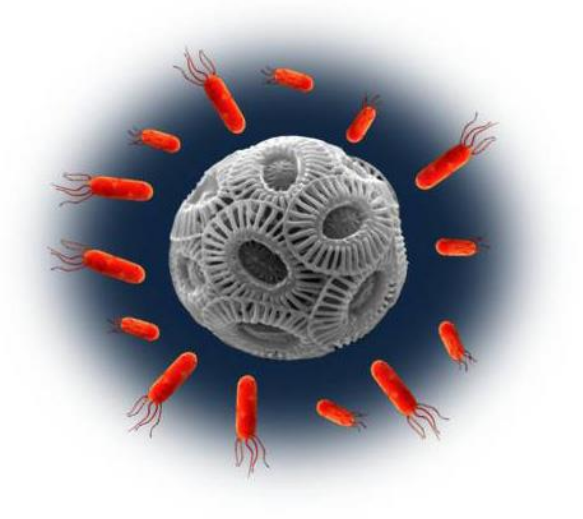

Figure 1.1 A schematic representation of the phycosphere of the coccolithophore *Emiliania huxleyi*

Phytoplankton cells can therefore be considered as localised point sources of dissolved organic matter (DOM) within the water column, whereby they release a myriad of molecules that can be divided in two functional groups: low molecular weight (LMW) and high molecular weight (HMW) compounds (Hellebust, 1965; Buchan *et al.*, 2014). In aquatic environments, phytoplankton-derived LMW molecules, such as amino acids, organic acids, carbohydrates and sugar alcohols, are produced during the early stages of a phytoplankton bloom (Hellebust, 1965; Bjørnsen, 1988; Buchan *et al.*, 2014), conversely, HMW molecules such as complex polysaccharides, and lipids, as well as particulate material, are mostly produced during the declining, stages of the bloom (Buchan *et al.*, 2014). This latter group of molecules are mainly released as result of cell lysis, although several HMW compounds are also released via exudation from viable cells (Biddanda and Benner, 1997; Fukao, Kimoto and Kotani, 2010; Buchan *et al.*, 2014; Iuculano *et al.*, 2017). The production rates of these molecules depend on multiple factors, such as the abundance and types of phytoplankton species (Buchan *et al.*, 2014), the rate of bacterial degradation of particulate organic matter (POM) and DOM (Buchan *et al.*, 2014), the stage of the bloom (e.g. Phytoplankton release of photosynthetic products is higher during the stationary phase) (Obernosterer and Herndl, 1995), and availability of mineral nutrients (Obernosterer and Herndl, 1995).

1.2.2 How bacteria encounter phycospheres

At the scale of marine microbes, the ocean is far from homogenous in its nutrient distribution (Stocker, 2012). Most bacteria are passive drifters, adapted to survive on trace levels of nutrients and are characterised by their streamlined genomes and lower metabolic rates (Morris *et al.*, 2002). However, other copiotrophic bacteria, employ a different strategy, whereby they actively forage within the water column, using motility and chemotaxis – the ability to alter their swimming behaviours in response to a chemical gradient – to search for microscale resource hotspots (Koch, 2001; Lauro *et al.*, 2009; Roman Stocker and Seymour, 2012). Such hotspots can be derived from zooplankton excretions (Turner, 2002), marine snow particles (Azam and Long, 2001), or phycospheres (Bell and Mitchell, 1972; Seymour *et al.*, 2017). These bacterial life-styles strongly determine their probability to encounter phycospheres and, to establish interactions with phytoplankton. For example, it has been predicted that non-motile bacteria only encounter 0.0035 phytoplankton cells day^{-1}, while bacteria that move randomly via motility can encounter up to 9 cells day^{-1} (Seymour *et al.*, 2017). This encounter rate further increases when the cells are motile and chemotactic, enhancing the probability of bacteria to be exposed to the high nutrient concentrations present in the phycosphere, and this behaviour might enhance chemical cycling between phytoplankton and bacteria (Blackburn, Fenchel and Mitchell, 1998). However, the role of chemotaxis in gaining nutrient exposure has been assessed solely by qualitative observations of bacterial accumulation around nutrient hotspots (Blackburn, Fenchel and Mitchell, 1998; Seymour *et al.*, 2008; Smriga *et al.*, 2016) or via theoretical models (Stocker *et al.*, 2008; Smriga *et al.*, 2016) and a direct quantification of the impact of chemotaxis on nutrient uptake derived from the phycosphere is still lacking.

1.2.3 Ups and downs of chemical trading on the phytoplankton-bacteria market

The close spatial interactions between phytoplankton and bacteria occurring in the phycosphere favour the exchange of molecules between these two partners, which can ultimately influence the physiology of both partners. Heterotrophic bacteria may either affect the growth of phytoplankton positively (Amin *et al.*, 2009) or negatively (Mayali and Azam, 2004). Beyond the classic transfer of remineralized nutrients from bacteria in exchange for organic matter from phytoplankton (Legendre and Rassoulzadegan, 1995; Buchan *et al.*, 2014), more complex chemical interactions have recently been identified, such as the provision of B vitamins by bacteria to phytoplankton (Croft *et al.*, 2005; Tang,

Koch and Gobler, 2010; Kazamia *et al.*, 2012; Xie *et al.*, 2013; Grant *et al.*, 2014), or the transfer of specific organosulfur compounds (e.g. 2,3-dihydroxypropane-1-sulfonate) (Durham *et al.*, 2014). For instance, Amin et al. (2015) recently demonstrated that the marine heterotrophic bacteria *Sulfitobacter* takes-up tryptophan produced by the diatom *Pseudo-nitzschia multiseries*, and subsequently converts it into Indole-3-acetate acid before transferring this growth-promoting compound back to the diatom. Furthermore, it has been shown that heterotrophic bacteria can facilitate iron uptake by phytoplankton (Amin *et al.*, 2009) and that they can also promote N_2 fixation in the diazotrophic cyanobacteria *Anabaena* (Paerl, 1977).

Heterotrophic bacteria can also compete for limiting inorganic nutrients with phytoplankton (Bratbak and Thingstad, 1985), display algicidal activities (Mayali and Azam, 2004; Amaro *et al.*, 2005; Su *et al.*, 2007; Wang *et al.*, 2010), or inhibit phytoplankton cell division. For example, *Croceibacter atlanticus* attaches to the surface of the diatom *Thalassiosira pseudonana* and ultimately enhances plastid accumulation (van Tol, Amin and Armbrust, 2017). Interestingly, there are cases where bacteria can establish dynamic interactions according to the growth phase of the phytoplankton. For example, the Roseobacter *Phaeobacter gallaeciensis* promotes the growth of healthy *Emiliania huxleyi* by producing the growth-promoting hormone phenylacetic acid and the broad spectrum antibiotic tropodithietic acid (Seyedsayamdost *et al.*, 2011). As *E. huxleyi* cells senesce, they release the breakdown product p-coumaric acid that signals *P. gallaeciensis* to operate a switch from mutualistic to pathogenic. *P. gallaeciensis* releases algicidal molecules (roseobacticides A and B) to kill the microalga and gain access to more carbon. These dynamic interactions seem to be widespread in nature: in fact it has also been recently observed in another association between the Rhodobacteriaceae, *Dinoroseobacter shibae*, and the dinoflagellate *Prorocentrum minimum* (Wang *et al.*, 2015). However, most of our knowledge on phytoplankton-bacteria interactions derives from studies on eukaryotic photoautotrophs, while small prokaryotic photosynthesizers have been mostly overlooked.

1.3 Picocyanobacteria: the dominant photosynthetic organisms in the ocean

The marine picocyanobacteria are largely comprised by two globally important genera, *Prochlorococcus* and *Synechococcus*, which are characterized by their small size (~0.8 - 2 μm) (Morel *et al.*, 1993) and their high abundance, accounting respectively for 10^{27} and 10^{26} cells in the global ocean (Flombaum *et al.*, 2013). In fact, they dominate the photosynthetic biomass across much of the ocean. *Prochlorococcus* is the most abundant phototrophic microorganism on the planet and dominates the tropical oligotrophic ocean (Partensky, Blanchot, et al. 1999; Partensky, Hess, et al. 1999). On the other hand, *Synechococcus* is relatively ubiquitous, and generally present in high abundance in both coastal waters and the open ocean (Partensky, Blanchot, et al. 1999).

One of the most important phytoplankton-bacteria interaction might occur between marine heterotrophic bacteria and picocyanobacteria (Partensky, Hess and Vaulot, 1999). Recent studies have started to delineate the dynamics of the interactions of picocyanobacteria-heterotrophic bacteria. We now know that the presence of heterotrophic bacteria can have both positive and negative effects on the growth of picocyanobacteria in co-culture (Sher *et al.*, 2011; Christie-Oleza *et al.*, 2017). In fact, it has been observed that, when in co-culture with heterotrophic microbes, both *Prochlorococcus* and *Synechococcus* upregulate their photosynthetic machinery (Tai *et al.*, 2009; Aharonovich and Sher, 2016; Biller, Coe and Chisholm, 2016), while heterotrophic bacteria such as *Vibrio parahaemoliticus*, *Shewanella* W3-18-1 and *Alteromonas macleodii* MIT1002 and HOT1A3, seem to upregulate pathways that diminish stress condition induced by oxygen radicals and facilitate iron uptake in these cyanobacteria (Tai *et al.*, 2009; Beliaev *et al.*, 2014; Aharonovich and Sher, 2016; Biller, Coe and Chisholm, 2016). These interactions may involve reciprocal chemical exchanges. For instance, *Synechococcus* cells exude nitrogen-rich photosynthates, such as simple amino acids or polypeptides that may be utilised by heterotrophic bacteria, while *Ruegeria pomeroyi* uses exoenzymes (Christie-Oleza, Scanlan and Armengaud, 2015) to return re-mineralized nitrogen to *Synechococcus* (Christie-Oleza *et al.*, 2017).

Nutrient exchanges between small cells such as *Synechococcus* and heterotrophic bacteria would require particularly close spatial proximity. However, it has been theorised that the *Synechococcus* phycosphere will be too small to be detected by chemotactic bacteria (Jackson, 1987). However, evidence of the physical attachment of

Synechococcus and heterotrophic bacteria suggests that microscale associations might exist (Malfatti and Azam, 2009), but visualizing and quantifying nutrient exchange between these two small microorganisms at the sub-cellular scale still remains a challenge.

1.4 Tools to examine microscale chemical exchanges between marine microbes

Omics approaches such as metagenomics, transcriptomics and proteomics have allowed for enhanced understanding of metabolic interactions between phytoplankton and bacteria at the community level. However, they do not allow quantification of nutrient fluxes between microbes at the single-cell level.

1.4.1 Secondary Ion Mass Spectrometry (SIMS)

The advent of Secondary Ion-Mass Spectrometry (SIMS), such as nano-scale SIMS (NanoSIMS) and Time of Flight-SIMS (ToF-SIMS) has enabled single-cell scale investigations into the metabolic activities and functions of specific micro-organisms within complex microbial communities at the single-cell level (Wagner, 2009; Watrous and Dorrestein, 2011; Gao, Huang and Tao, 2015). The power of these instruments relies on their capacity to visualize and quantify ions at micro-scale resolution. Both NanoSIMS and ToF-SIMS use a high energy primary ion beam to blast the sample surface (Wagner, 2009; Gao, Huang and Tao, 2015), ejecting secondary ions derived from the sample in a process called sputtering (Watrous and Dorrestein, 2011). The secondary ions produced are subsequently directed into a mass spectrometer then separated by different mass-to-charge ratios using an electrostatic field (NanoSIMS) or time-of-flight tube (ToF-SIMS) (Kilburn and Clode, 2014). While both ToF-SIMS and NanoSIMS employ a high energy primary ion beam (Passarelli and Winograd, 2011; Kilburn and Clode, 2014), they differ in their currents and beam diameters, which has significance for determining the spatial resolution of the instruments - the smaller the beam the higher the resolution. The primary ion beam in ToF-SIMS can be narrowed down to the sub-micron scale providing a spatial resolution between 1-5 μm. The comparatively gentler sputtering of this instrument, relative to NanoSIMS, leads to the production of fewer secondary ions, impacting the accuracy of quantitative analyses, but generating intact molecular ions and allowing their identification (Watrous and Dorrestein, 2011; Hoefler and Straight, 2014; Kilburn and Clode, 2014). In contrast, the smaller primary ion beam of the NanoSIMS enables a spatial resolution of analysis close to 50 nm, while the more intense sputtering of this

instrument generates higher secondary ion flux allowing for very accurate elemental quantification but destroying the chemical structure of the molecules (Watrous and Dorrestein, 2011; Kilburn and Clode, 2014).

ToF-SIMS has been used to characterize the spatial distribution of microbial biomarkers (Thiel et al., 2007) and detect the distribution of intact molecules in cells (Vaidyanathan *et al.*, 2008). NanoSIMS has been used extensively in microbial ecology since the early 2000s to quantify nutrient uptake rates by individual cells (Alonso *et al.*, 2012; Foster, Sztejrenszus and Kuypers, 2013; Krupke *et al.*, 2013), characterise bacterial metabolisms (Finzi-Hart *et al.*, 2009; Musat *et al.*, 2012; Terrado *et al.*, 2017) and to study microbe-microbe (Foster *et al.*, 2011; Thompson *et al.*, 2012; Bonnet *et al.*, 2016; Arandia-Gorostidi *et al.*, 2017; Raina *et al.*, 2017; Carpenter *et al.*, 2018; Samo *et al.*, 2018), animal-microbe (Lechene *et al.*, 2006, 2007; Pernice *et al.*, 2012; Rädecker *et al.*, 2018) and plant-microbe (Tarquinio *et al.*, 2018) interactions at the single-cell level (Musat *et al.*, 2016). Recently, ToF-SIMS and NanoSIMS were also coupled to quantify the transfer of organosulfur molecules between microalgae and bacteria (Raina *et al.*, 2017) and nutrient transfer between fungi and bacteria (Worrich *et al.*, 2017).

1.5 Study aims and objectives

Picocyanobacteria and heterotrophic bacteria are the most abundant microbes in the ocean and play an integral role in driving biogeochemical processes and sustaining the marine food-web. Important questions remain unanswered regarding how the metabolism and the behaviour of these two partners affect their interactions at the single-cell level. Quantifying the nutrient exchange between picocyanobacteria and heterotrophic bacteria at their relevant scale will allow to assess more accurately their impact on nutrient cycling in the ocean.

The over-arching goal of this thesis is to provide a comprehensive characterization of the microscale interactions between the small, but ubiquitous and ecologically significant marine microbes, *Synechococcus* and heterotrophic bacteria. Principally, I focused on visualizing and quantifying how single-cell metabolic exchanges and microbial behaviours influence chemical exchanges between these two groups. To accomplish this goal, my specific aims are:

1. **To compare and validate single-cell approaches for measuring nutrient uptake in the marine model microbe *Synechococcus*.** Here I aim to compare three different mass-spectrometry techniques to measure the enrichment of *Synechococcus*. I compare Elemental analysis isotope ratio mass spectrometry (EA-IRMS), with ToF-SIMS and NanoSIMS to determine the most suitable technique to explore *Synechococcus*-bacteria interactions at ecologically relevant scales and resolution.
2. **To quantify nutrient exchange between *Synechococcus* and heterotrophic bacteria at sub-cellular scale.** Here I aim to determine if reciprocal chemical exchanges between *Synechococcus* and bacteria can be quantified at the single cell level and assess the level of species-specificity involved in these interactions.
3. **To characterize the role of bacterial chemotaxis in the consumption of *Synechococcus*-derived organic matter.** Here I aimed to explore if bacterial behaviour could play a role in the exploitation of the small phycospheres surrounding *Synechococcus* through experimental and theoretical approaches

2 Chapter 2

Quantifying inorganic nitrogen assimilation by *Synechococcus* using bulk and single-cell mass spectrometry: a comparative study

Published in *Frontiers in Microbiology* on November 2018

Marco Giardina[1], Soshan Cheong[2], Christopher E. Marjo[2], Peta L. Clode[3,4], Paul Guagliardo[3], Russell Pickford[5], Mathieu Pernice[1*], Justin R. Seymour[1], Jean-Baptiste Raina[1]

[1]Climate Change Cluster, University of Technology Sydney, Sydney, Broadway NSW 2007, Australia

[2]Mark Wainwright Analytical Centre, University of New South Wales, Kensington, Australia

[3]Centre for Microscopy Characterisation and Analysis, The University of Western Australia, Perth, Australia

[4]UWA School of Biological Sciences and UWA Oceans Institute, The University of Western Australia, Perth, Australia

[5]Bioanalytical Mass Spectrometry Facility, University of New South Wales, Sydney, NSW, Australia

2.1 Abstract

Microorganisms drive most of the major biogeochemical cycles in the ocean, but the rates at which individual species assimilate and transform key elements is generally poorly quantified. One of these important elements is nitrogen, with its availability limiting primary production across a large proportion of the ocean. Nitrogen uptake by marine microbes is typically quantified using bulk-scale approaches, such as Elemental Analyser-Isotope Ratio Mass Spectrometry (EA-IRMS), which averages uptake over entire communities, masking microbial heterogeneity. However, more recent techniques, such as secondary ion mass spectrometry (SIMS), allow for elucidation of assimilation rates at the scale at which they occur: the single cell level. Here, we combine and compare the application of bulk (EA-IRMS) and single-cell approaches (NanoSIMS and Time-of-Flight-SIMS) for quantifying the assimilation of inorganic nitrogen by the ubiquitous marine primary producer *Synechococcus*. We aimed to contrast the advantages and disadvantages of these techniques and showcase their complementarity. Our results show that the average assimilation of ^{15}N by *Synechococcus* differed based on the technique used: values derived from EA-IRMS were consistently higher than those derived from SIMS, likely due to a combination of previously reported systematic depletion as well as differences in sample preparation. However, single-cell approaches offered additional layers of information, whereby NanoSIMS allowed for the quantification of the metabolic heterogeneity among individual cells and ToF-SIMS enabled identification of nitrogen assimilation into peptides. We suggest that this coupling of stable isotope-based approaches has great potential to elucidate the metabolic capacity and heterogeneity of microbial cells in natural environments.

2.2 Introduction

Stable isotopes have been used extensively in microbial ecology (Boschker and Middelburg, 2002) to quantify microbial metabolic activities (Dumont and Murrell, 2005), determine the uptake rate of specific molecules (Pelz *et al.*, 1998; Bronk, 1999), track nutrient transfer between different organisms (Van Den Meersche *et al.*, 2004; Van Den Meersche, Soetaert and Middelburg, 2011; Raina *et al.*, 2017), and monitor chemical transformations through a range of biotic or abiotic processes (Matwiyoff and Ott, 1973; Post, 2002). In microbial oceanography, the assimilation rate of inorganic nitrogen by marine micro-organisms is traditionally quantified using large sample volumes (Garside, 1981; Mccarthy, Garside and Nevins, 1992), whereby molecules labelled with the rare stable isotope ^{15}N are often employed as a tracer used to enrich litres of seawater, during incubation periods ranging from hours to days (Evrard *et al.*, 2010; Van Den Meersche, Soetaert and Middelburg, 2011). The microbial biomass is then concentrated (by filtration or centrifugation) before measuring the $^{15}N/^{14}N$ ratio of the entire community with mass spectrometry.

One of the most widely used techniques to measure stable isotope ratios is elemental analyser – isotope ratio mass spectrometry (EA-IRMS) (Boschker and Middelburg, 2002; Muccio and Jackson, 2009). EA-IRMS has been widely applied for studying microbially-mediated biogeochemical cycles (Montoya *et al.*, 1996; Boschker *et al.*, 1998; Hinrichs *et al.*, 1999) and has become an important tool for tracking nutrient transfer among microbes (Pel, Hoogveld and Floris, 2003). However, bulk-scale approaches such as EA-IRMS are, by definition, disconnected from the metabolic activities of the individual microscopic organisms targeted, averaging out their metabolic activities. Single-cell approaches, on the other hand, offer the potential to unveil the metabolic and phenotypic diversity present in microbial communities and to more accurately quantify how their activities might scale-up to affect oceanic processes.

The application of imaging mass spectrometry, such as nano-scale secondary ion mass spectrometry (NanoSIMS) and Time of Flight-SIMS (ToF-SIMS), enables direct investigation of the metabolic activities and functions of specific micro-organisms within complex microbial communities at the single-cell level (Wagner, 2009; Watrous and Dorrestein, 2011; Gao, Huang and Tao, 2015). The power of these instruments relies on their capacity to visualise and quantify ions at micro-scale resolution. Both NanoSIMS

and ToF-SIMS use a high energy primary ion beam to blast the sample surface (Wagner, 2009; Gao, Huang and Tao, 2015), ejecting secondary ions derived from the sample in a process called sputtering (Watrous and Dorrestein, 2011). The secondary ions produced are subsequently directed into a mass spectrometer then separated by different mass-to-charge ratios using an electrostatic field (NanoSIMS) or time-of-flight tube (ToF-SIMS) (Kilburn and Clode, 2014). While both ToF-SIMS and NanoSIMS employ a high energy primary ion beam (Passarelli and Winograd, 2011; Kilburn and Clode, 2014), they differ in their currents and beam diameters, which has significance for determining the spatial resolution of the instruments - the smaller the beam the higher the resolution. The primary ion beam in ToF-SIMS can be narrowed down to the sub-micron scale providing a spatial resolution between 1-5 μm. The comparatively gentler sputtering of this instrument, relative to NanoSIMS, leads to the production of fewer secondary ions, impacting the accuracy of quantitative analyses, but generating intact molecular ions and allowing their identification (Watrous and Dorrestein, 2011; Hoefler and Straight, 2014; Kilburn and Clode, 2014). In contrast, the smaller primary ion beam of the NanoSIMS enables a spatial resolution of analysis close to 50 nm, while the more intense sputtering of this instrument generates higher secondary ion flux allowing for very accurate elemental quantification but destroying the chemical structure of the molecules (Watrous and Dorrestein, 2011; Kilburn and Clode, 2014).

NanoSIMS has been used extensively in microbial ecology since the early 2000s to quantify nutrient uptake rates by individual cells (Alonso *et al.*, 2012; Foster, Sztejrenszus and Kuypers, 2013; Krupke *et al.*, 2013), characterise bacterial metabolisms (Finzi-Hart *et al.*, 2009; Musat *et al.*, 2012; Terrado *et al.*, 2017) and study microbe-microbe (Foster *et al.*, 2011; Thompson *et al.*, 2012; Bonnet *et al.*, 2016; Arandia-Gorostidi *et al.*, 2017; Raina *et al.*, 2017; Carpenter *et al.*, 2018; Samo *et al.*, 2018) and animal-microbe (Lechene *et al.*, 2006, 2007; Pernice *et al.*, 2012; Rädecker *et al.*, 2018) interactions at the single-cell level (Musat *et al.*, 2016). ToF-SIMS has been used to characterise the spatial distribution of microbial biomarkers (Thiel et al., 2007) and detect the distribution of intact molecules in cells (Vaidyanathan *et al.*, 2008). Recently, ToF-SIMS and NanoSIMS were coupled to quantify the transfer of organosulfur molecules between microalgae and bacteria (Raina *et al.*, 2017) and nutrient transfer between fungi and bacteria (Worrich *et al.*, 2017).

Here we combine EA-IRMS, NanoSIMS and ToF-SIMS to quantify nitrogen uptake and metabolism by the ubiquitous marine cyanobacteria *Synechococcus* from the bulk-scale down to the scale of individual cells. While there is extensive literature on nitrogen requirements of this important microorganism at the bulk scale (Glibert and Ray, 1990; Bronk, 1999; Moore *et al.*, 2002), little is known about these dynamics at the scale of individual cells. By using three different stable isotope analytical techniques, we aim to contrast their specific advantages and disadvantages and highlight their complementarity when studying small bacterial cells.

2.3 Materials and Methods

2.3.1 Synechococcus culture maintenance

Synechococcus sp. CS-94 RRIMP N1 (S1) was cultured for seven days in a modified form of f/2 (-Si) medium that combines the nutrients of f/2 medium (Guillard, 1975) and the artificial salt solutions of the Enriched Seawater Artificial Water (ESAW) (Berges *et al.*, 2001), with the latter used instead of natural filtered seawater, which can contain biologically available nitrogen. The culture was maintained under conditions mirroring the natural environmental preferences of this organism: e.g. temperature of 23 °C and illumination with an incident photon irradiance of ~ 180 µmol photons m^{-2} s^{-1} (12 h: 12 h light: dark cycle).

2.3.2 Experimental design and samples collection

On the day of the experiment, 50 ml of *Synechococcus* culture was centrifuged at 1,500 g for 15 minutes. To quantify the assimilation of nitrogen by the *Synechococcus* cells, the supernatant was removed and replaced with fresh growth media containing ^{15}N-labelled Sodium Nitrate ($NaNO_3$; final concentration 8.82×10^{-4}M; ^{15}N, 98%+, Cambridge Isotopes Laboratories, Inc., Cambridge, MA), as the sole source of biologically available nitrogen. A *Synechococcus* culture subsample was centrifuged, as described above, but resuspended in fresh growth medium containing natural abundance of ^{15}N and acted as an unlabelled control. A six-hour incubation was performed with 1.5 ml samples collected sequentially through time at the following time-points: 0 minutes (T_0; sample not exposed to ^{15}N enrichment, see above), 15 minutes (T_1), 30 minutes (T_2), 1 hour (T_3), 2 hours (T_4), 4 hours (T_5), 6 hours (T_6). Samples were collected in triplicate for IRMS analysis and in duplicate for ToF-SIMS and NanoSIMS. All samples were centrifuged for 15 min at 1,500g, the supernatant was removed and replaced with 500 µl of paraformaldehyde (1% final concentration) diluted in buffer (0.1 M Sucrose, 1× PBS). Samples were fixed for 24 hours at 4°C, washed three times with buffer (0.1 M Sucrose in 1×PBS) in order to eliminate any residual paraformaldehyde before being prepared for specific instruments.

2.3.3 EA-IRMS: sample preparation and analysis

Cells were collected by centrifuging the samples at 1,500 g for 15 minutes, the buffer was removed and the pellet dried in the oven at 60°C for 48 hours. Glutamic acid was used as a standard, whereby different ratios of ^{15}N-labelled glutamic acid (^{15}N-Glu) (L-Glutamic acid, 98 atom% ^{15}N , Sigma-Aldrich) and non-labelled glutamic acid (^{nat}N-Glu)

(L-Glutamic acid, ≥99% HPLC-grade, Sigma-Aldrich) were prepared at a final concentration 1 mg ml^{-1}: 100% ^{nat}N-Glu, 1:50,000 (^{15}N-Glu:^{nat}N-Glu), 1:10,000, 1:5,000, 1:1,000, 1:500, 1:100, 1:50, 1:10. The different standard solutions were reduced to dryness in an oven at 60°C for 48 hours. Approximately 0.250 mg of either samples or standards were weighed into tin capsules and loaded into the autosampler of the EA-IRMS. Samples were analysed on a ThermoFisher Scientific EA-IRMS system featuring Flash 2000 organic elemental analyser and Delta Plus IRMS coupled via an EA-Isolink. The carbon and nitrogen in the sample was converted to CO_2 and N_2 within the elemental analyser before transfer to the mass spectrometer for isotope ratio analysis. Values obtained were corrected using the Vienna Pee Dee Belemnite (VPDB) standard. Instrument operation was performed using IsoDat software (ThermoFisher Scientific, Waltham, MA). To ensure the accuracy of the EA-IRMS, we measured the dilution series of glutamic acid standards (i.e. increasing ratios of ^{15}N/^{14}N). These standards were used as the reference to quantify the assimilation of ^{15}N by the *Synechococcus* culture (Supplementary Figure 1). The measured ^{15}N atom fraction in the ^{nat}N-Glu standard was 0.36%, and the value measured in the highest dilution, 1:10 (^{15}N:^{14}N), was 9.21% (Supplementary Figure 1).

2.3.4 Sample preparation for SIMS

In order to remove the sucrose buffer and obtain a monolayer of cells, the samples were diluted ten times in sterile, filtered MilliQ water (0.22 µm pore size, Minisart syringe filters, Sartorius, Göttingen, Germany) and 50 µl were immediately placed onto silicon wafers (7.07 mm × 7.07 mm, Type P, diameter: 4 inches, orientation: <111>, ProSciTech, Townsville, Australia), dried at 45°C and stored inside a desiccator, protected from light until SIMS analysis.

2.3.5 NanoSIMS analysis

We used the NanoSIMS 50 (Cameca, Gennevilliers, France) at the Centre for Microscopy, Characterisation and Analysis (CMCA) at The University of Western Australia. This instrument allows for simultaneous collection of up to five isotopic species (here: $^{12}C_2^-$, $^{12}C^{13}C^-$, $^{12}C^{14}N^-$, $^{12}C^{15}N^-$, and ^{32}S). Enrichment of the rare isotope ^{15}N was confirmed by an increase in the ^{15}N/^{14}N ratio above the natural abundance value recorded in controls (equal to 0.374% ± 0.001 for nitrogen). Different pre-sputtering lengths and current intensities were tested. The analysis was performed as followed:

samples were pre-sputtered for 3.5 minutes at 500 pA Cs^+beam (D1=1) on 30 µm² areas (256 × 256 pixel), followed by automatic horizontal and vertical secondary ion beam centering. We selected the above conditions because counts did not increase with longer sputtering, we therefore assumed that the beam reached the inner part of the cells. The analysis was then performed by rastering a 2 pA beam (D1=2) over 25 µm² areas (256 × 256 pixels); three planes were recorded per area with a dwell time of 3 ms per pixel. The instrument was operated with a high mass resolving power (in the range of 9,000), allowing the separation of isobaric interferences. Images were analysed using the Fiji software package (http://fiji.sc/Fiji) (Schindelin *et al.*, 2012) combined with the Open-MIMS plug-in (http://nrims.harvard.edu/software). All images were dead-time corrected (Hillion *et al.*, 2008); the individual planes were then summed prior to extracting counts from the images. Isotopic quantification data were extracted from the mass images by manually drawing regions of interest around each single bacterial cell using the $^{12}C^{14}N^-$ image as mask.

2.3.6 ToF-SIMS analysis

ToF-SIMS is a surface analysis technique where only the uppermost molecular layers are analysed. The data collected by ToF-SIMS can be visualised as both (i) an accumulated mass spectrum from the bulk surface, and (ii) a two-dimensional image showing the intensity distribution of the specific secondary ions in the area analysed (Fearn, 2015). In order to probe the ^{14}N and ^{15}N species within the cells, and not only on the cell surfaces, depth profiling analysis was performed, where the cells were sputtered through in a dual beam configuration with alternating analysis and sputtering cycles. Using this approach, the resultant spectrum in images is a composite of all spectra collected throughout the depth profile and is more comparable to data obtained using NanoSIMS that also sputters through the sample. ToF-SIMS analysis was conducted using the TOF.SIMS 5 instrument (ION-TOF GmbH, Münster, Germany) at the Mark Wainwright Analytical Centre (MWAC), University of New South Wales. This instrument is equipped with a bismuth liquid metal cluster ion gun for analysis, an argon gas cluster ion gun for depth profile sputtering, and an electron flood gun for charge compensation. The 'non-interlaced' mode was employed, with each cycle consisting of 1 scan of sputtering (~1.5 s), followed by 2 scans of data acquisition, and a 0.5 s pause in between the analyses. Sputtering was performed using a 10 keV Ar_{2000}^+ cluster ion beam rastering over a 340 × 340 μm^2 area. Mass spectral data for the images was acquired using

a 30 keV Bi_3^+ ion beam, analysing a 100 × 100 μm^2 square in the central region. The analysis beam was operated in the 'spectrometry' mode that compromises the lateral spatial resolution of the image but maximises the mass resolution (m/Δm >5000). All analyses were conducted in the negative polarity. Spectra were mass calibrated using the masses of C^-, C_2^-, C_3^-, C_4^- and C_5^- molecules. Prior to each depth profiling analysis, the analysis area was first identified by surveying the $^{12}C^{14}N^-$ (m/z 26) maps acquired in the 'fast-imaging' mode for high-lateral-resolution (~195 nm) images. During this initial imaging analysis, no more than two scans were acquired for each area of analysis to ensure the ion dose density was kept below the static SIMS limit that ensures minimal damage to the sample surface. Data processing and evaluation was conducted using the SurfaceLab six software package (ION-TOF GmbH, Munster, Germany).

2.3.7 Peak deconvolution following ToF-SIMS analysis

Incorporation of ^{15}N into a biological system using imaging ToF-SIMS is best studied using the $^{12}C^{15}N$ (m/z 27.000109) and $^{12}C^{14}N$ (m/z 26.0003074) anions that can be subsequently used to calculate the $^{12}C^{15}N/^{12}C^{14}N$ ratio. However, $^{12}C^{15}N$ has a significant overlap with $^{13}C^{14}N$ (m/z 27.006429) and a nearby peak at $^{12}C_2{}^1H_3$ (m/z 27.023475). The mass spectral resolution of ToF-SIMS is less than NanoSIMS, so a deconvolution of the data is required to extract the true peak intensities around m/z 27. In addition to the peak overlap, the peaks in ToF-SIMS mass spectra are asymmetric, exhibiting a tail toward higher mass, so a Gaussian-Lorenzian function incorporating a tailing term was used to fit the data correctly (Beamson and Briggs, 1992). For multi-peak fitting, the tailing term and peak width were fixed for each peak, with only position and height varying for individual peaks. Fitting was achieved by minimizing Chi^2 against the experimental data. The $^{12}C^{14}N$ peak at m/z 26 is substantially more intense than the $^{12}C^{15}N$ peak at m/z 27, leading to poor fits in the latter region unless each region is fitted separately. The m/z 26 region was fitted using a single peak for $^{12}C^{14}N$, while the region at m/z 27 was fitted with two peaks representing $^{12}C^{15}N$, $^{13}C^{14}N$ (the peak at $^{12}C_2{}^1H_3$ was sufficiently well resolved and did not require fitting; Supplementary Figure 2.2). A batch fitting process was performed on the average spectrum within each ROI and implemented by the authors in Python 3.1 using the curve_fit function found in the Scipy Optimize module. Peak fitting of the $^{12}C^{14}N$ peak was readily performed in a single step using this code. In the case of the 3-peak fitting of the m/z 27 region, each fit was evaluated graphically by eye, and poor fits were reprocessed individually using different start values for position and

height to ensure all peaks appeared in the expected positions based on their theoretical m/z values. An equivalent process was adopted for calculation of the higher mass molecular ion ratios of $^{12}C_3{}^{15}N$ / $^{12}C_3{}^{14}N$ and $^{12}C^{15}N^{16}O$ / $^{12}C^{14}N^{16}O$. However, the mass resolution of the ToF-SIMS was not sufficient to enable deconvolution of the ^{13}C-containing interferences ($^{13}C_3{}^{14}N$ and $^{13}C^{14}N^{16}O$), resulting in anomalously high peak fitting ratios (approximately 4 atom percent higher than natural abundance in T_0-T_3). Nevertheless, the full time-series data clearly showed a positive trend confirming the increasing incorporation of ^{15}N in these molecular ions.

2.3.8 ^{15}N atom fraction

The measured isotope ratios were converted to Atomic Percentage (Atom %), which gives the percentage of a specific atom within the total number of atoms. In this case, we calculated the percentage of ^{15}N within the total number of nitrogen atoms (^{15}N + ^{14}N) following the formula:

$$Atom\% = \frac{^{15}\mathrm{N}}{(^{15}\mathrm{N} + {}^{14}\mathrm{N})} \times 100$$

2.3.9 Statistical Analysis

All statistical analyses were carried out using SPSS (version 23; IBM Corporation, Armonk, USA). Data were first tested for normality and homogeneity of variance using Shapiro-Wilk and Levene's tests, respectively. When the data was not normally distributed and/or the variances were not homogeneous, comparisons of ^{15}N enrichment between T_0 and measurements of each respective instrument were carried out using the Mann-Whitney U-test. Pairwise comparisons between each method, at each time point, were conducted using Kruskal-Wallis H-test with Dunn's post hoc tests and Bonferroni adjustment. A summary of the statistical results is reported in Supplementary Table 2.1 and 2.2.

2.4 Results and discussions

EA-IRMS, NanoSIMS, and ToF-SIMS were used to quantify $^{15}NO_3^-$ assimilation by *Synechococcus* at both the bulk and single-cell level. Correlations between EA-IRMS and NanoSIMS approaches have previously been reported, whereby these two techniques have been combined to measure the metabolic activities of multiple marine microorganisms, including the mixotrophic alga *Ochromonas* spp. BG-1 (Terrado *et al.*, 2017), a subseafloor chemoautotrophic member of the *Campylobacteria* (Mcnichol *et al.*, 2018) and several nitrogen-fixing cyanobacteria (Popa *et al.*, 2007; Ploug *et al.*, 2010; Foster, Sztejrenszus and Kuypers, 2013; Krupke *et al.*, 2013). However, this study is the first to additionally compare the use of EA-IRMS and NanoSIMS with ToF-SIMS, which can provide further insight on the fate of nitrogen within *Synechococcus* cells.

All three techniques revealed that the *Synechococcus* cells became significantly enriched in ^{15}N after only 15 minutes of incubation (T_0 vs. T_1: EA-IRMS t-test p=0.000; ToF-SIMS p=0.002; NanoSIMS p=0.000; Supplementary Table 2). The ^{15}N atom fraction increased over the six hours incubation period, from 0.371% ± 0.003 (T_0) to 12.89% ± 0.06 (T_6) for EA-IRMS; 0.374% ± 0.007 to 9.2% ± 3.2 for NanoSIMS; and 0.46% ± 0.08 to 11.6% ± 4.2 for ToF-SIMS (Figure 2.1A). However, the three instruments exhibited substantial discrepancies (Figure 2.1A, Supplementary Table 2.1): after six hours of incubation, the enrichment values quantified by EA-IRMS were on average 10% higher than those recorded by ToF-SIMS, and 28% higher than those from NanoSIMS (Supplementary Table 2.1). Previous studies have also reported imperfect matches between EA-IRMS and NanoSIMS (Kopf *et al.*, 2015; Terrado *et al.*, 2017), which have been ascribed to a combination of differences in sample preparations together with known systematic depletion (by 1-10% of the heaviest isotope) due to systematic fractionation during SIMS analysis (Fitzsimons, Harte and Clark, 2000). In addition to fractionation effect, the differences between instruments observed here are most likely due to two factors: (i) although all samples were prepared using the same protocol, SIMS samples had to be subsequently diluted ten-fold directly prior to drying in order to obtain an even layer of cells and avoid their superimposition. Because this dilution was the only difference between EA-IRMS and the two SIMS techniques, it is likely that this step triggered a loss of water-soluble nitrogen compounds from the cells. In addition, (ii) the mass resolving power of the two SIMS instrument is not equal. This point is best exemplified by the artefactual enrichment of the ToF-SIMS samples at T_0 and is due to a

combination of peak overlap (differences between isobaric peaks such as $^{11}B^{16}O^-$ and $^{12}C^{15}N^-$ cannot be resolved) and peak asymmetry (exhibiting a tail toward higher mass). This latter point likely explains why the ToF-SIMS-derived enrichments are higher on average than the NanoSIMS ones (Supplementary Table 2.1). Despite variations between techniques, linear regression analyses showed a strong positive relationship between measurements from the three instruments (Figure 1B-D). This indicates that the measured increase in ^{15}N enrichment through time was consistent across all three techniques.

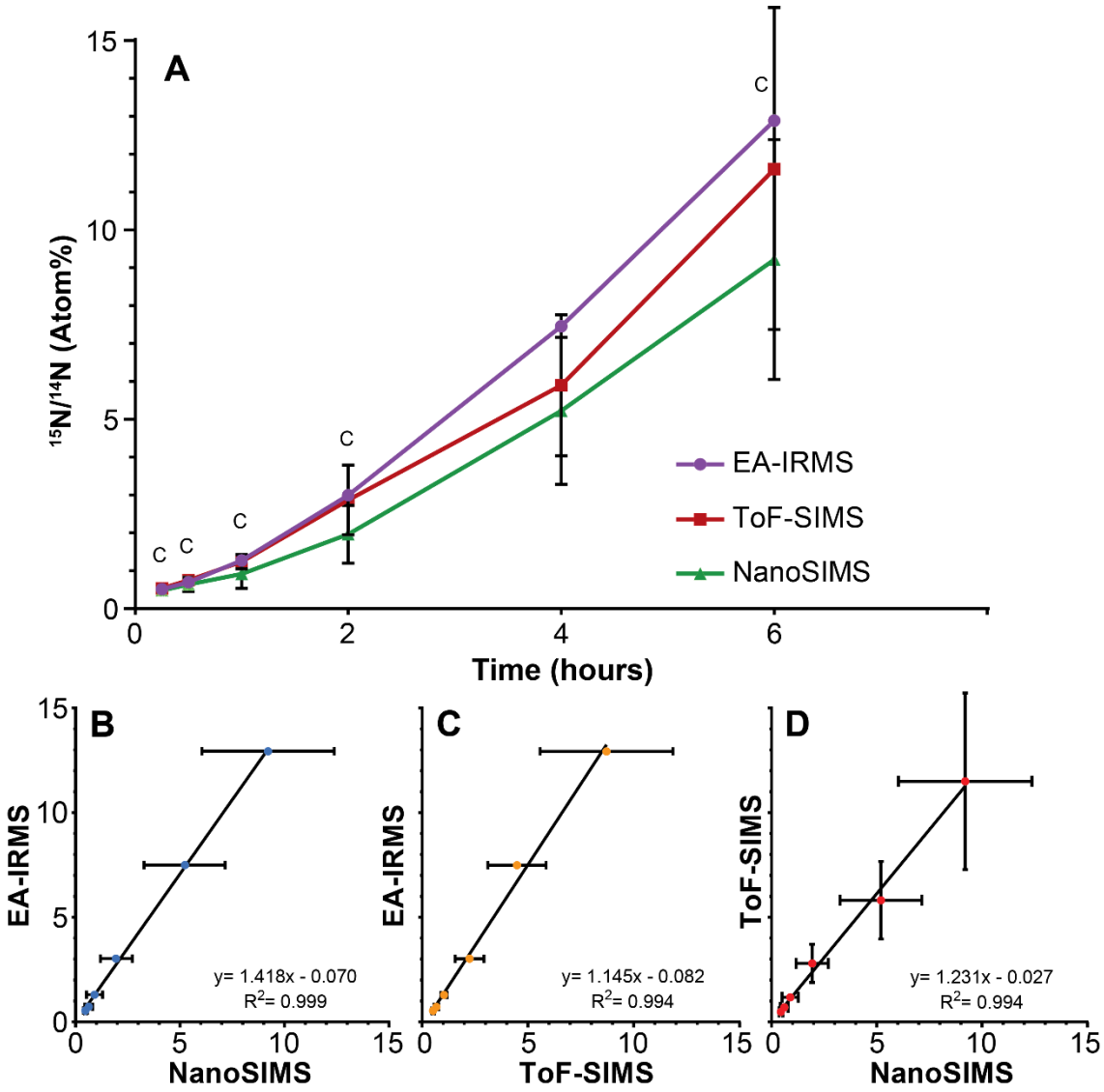

Figure 2.1 ^{15}N assimilation by *Synechococcus* sp. between (**A**) EA-IRMS (purple), ToF-SIMS (red) and NanoSIMS (green). Asterisk denote significant differences between ToF-SIMS and NanoSIMS (see Supplementary Table 1). Relationship between different ^{15}N measurement (in Atom %) performed with (**B**) EA-IRMS and NanoSIMS, (**C**) EA-IRMS and ToF-SIMS and (**D**) NanoSIMS and ToF-SIMS. All slopes differed significantly from 0 (ANOVA, $p<0.05$). All measurements were carried out on different samples collected from the same culture flask (n=1 biological replicate). Error bars: standard deviation of 3 technical replicates measured with EA-IRMS (technical replicates) and single cells measured with NanoSIMS and ToF-SIMS. For number of replicates refer to Supplementary Table 2.2.

^{15}N enrichments recorded using SIMS were considerably more variable than the values reported with EA-IRMS. Although bulk measurements with EA-IRMS provided an accurate quantification of the metabolic activities in the whole *Synechococcus* culture, it inherently masked the disparities in nitrogen enrichment at the single cell level. The averaged nitrogen ratio recorded through NanoSIMS indicated significant ^{15}N uptake after 15 minutes of incubation (0.48% ± 0.09), but this technique also allowed us to identify a high variability in ^{15}N enrichment between single cells (Figure 2.2A). Up to an hour after the start of the ^{15}N exposure, approximately 7% of the cells were not enriched, while up to 5% of the cells were more than twice as enriched as the population average. In comparison, after 4 hours, even the cells that were the least enriched exhibited ^{15}N levels that were twice as high as the natural abundance. The heterogeneity in ^{15}N content between cells, in the 50 ml culture flask we investigated, became more pronounced in the later time points, which was quantified using two different measures of the dispersion of observations: the interquartile range (IQR) and the Fano factor (Figure 2.2). The IQR increased from 0.9 after 2 hours to 3.3 after 6 hours of incubation, similarly the Fano factor increased from 0.01 after 15 min to 1.08 after 6 hours. This variability in enrichment among cells exposed to the same conditions is time-dependent but its underlying causes can result from several biological and methodological factors which have previously been identified (Musat *et al.*, 2008; Finzi-Hart *et al.*, 2009; Ploug *et al.*, 2010; Woebken *et al.*, 2012).

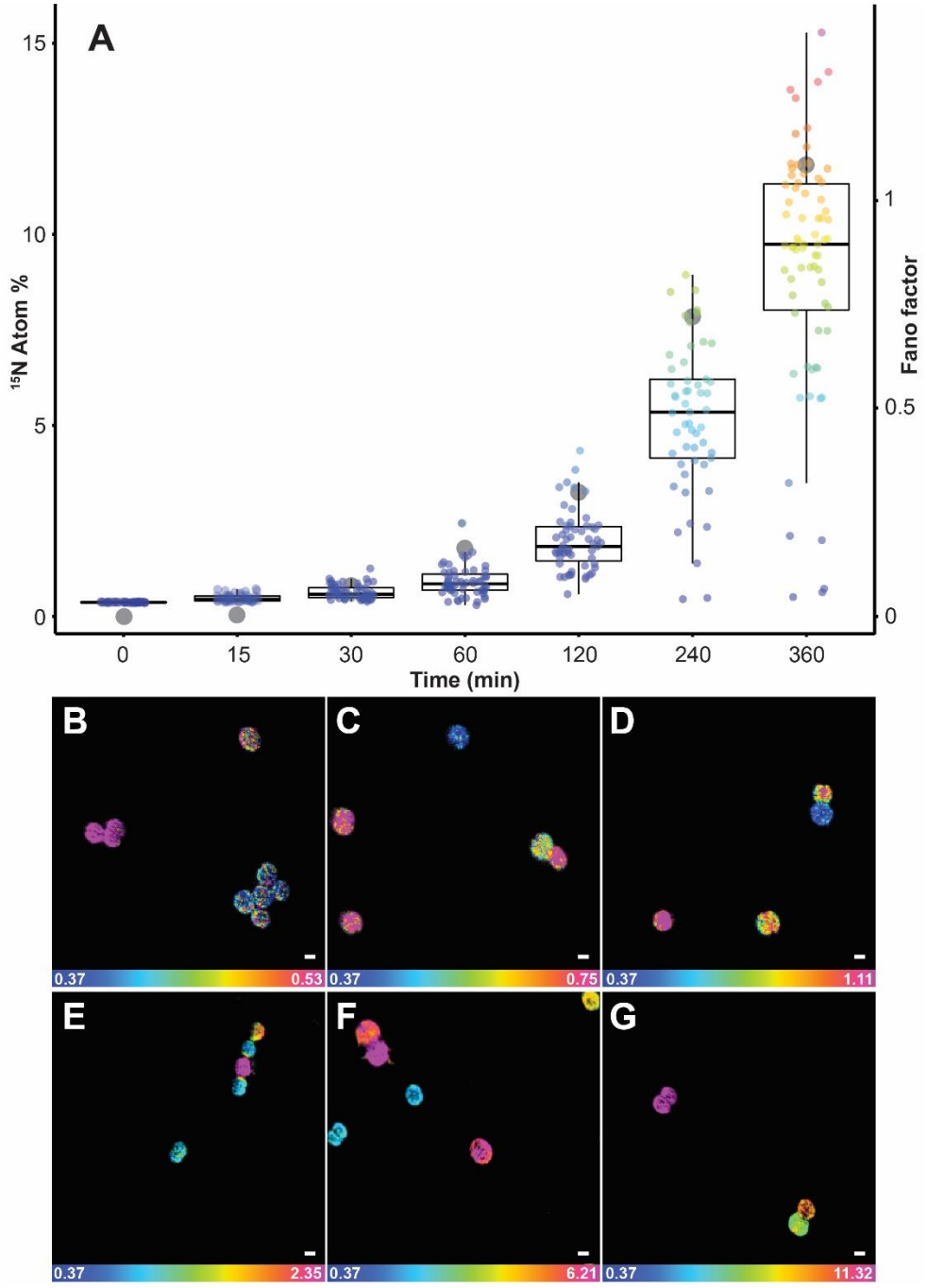

Figure 2.2 Quantification of ^{15}N uptake by *Synechococcus* cells through time at single-cell level using NanoSIMS. (**A**) Box plot showing an increase in single-cell heterogeneity (lower and upper hinges correspond to the 25th and 75th percentiles) as well as the Fano factor (ratio of sample variance to sample mean; indicated in the figure by grey dots) which measures the heterogeneity of the ^{15}N assimilation. Representative NanoSIMS images showing the distribution of ^{15}N/^{14}N ratio after (**B**) 15 minutes, (**C**) 30 minutes, (**D**) 1 hour, (**E**) 2 hours, (**F**) 4 hours and (**G**) 6 hours. Scale bar: 1µm. Note: the scale of the images increase from **B-G** to highlight the cellular heterogeneity: blue represent natural ^{15}N atom fraction and magenta represent the third quartile of each respective data point. For number of analysed cells refer to Supplementary Table 2. All measurements were carried out on a sample taken from the same culture flask (n=1 biological replicate).

Among the biological factors impacting cell-to-cell variation in NanoSIMS-derived ^{15}N enrichment, heterogeneity in the assimilation rate is likely to play an important role. Indeed, microbial populations are composed of a collective of individual cells, each potentially displaying different metabolic activity (Adams, 2000; Johnson *et al.*, 2012) and behavioural traits (Crespi, 2001). In some cases, the differences between cells are not due to genetic diversity, but are the result of phenotypic heterogeneity, which is based on the stochasticity of several molecular mechanisms that induce differences between single cells, even in the absence of genetic and environmental variation (Ackermann, 2015). For example, unequal cell division may lead to a different distribution of key components, such as enzymes, ribosomes, or pigments, inducing significant physiological differences in the daughter cells (Huh and Paulsson, 2011). Heterogeneity in ^{15}N-enrichment observed in NanoSIMS can also be due to differences in cells life cycle, in cell sizes (Lidstrom and Konopka, 2010) or in metabolic rates, which is consistent with observations among other unicellular cyanobacteria (Foster et al. 2013). This heterogeneity within a cell population might deliver ecological benefits, including the division of labour between individuals and the survival of specific phenotypes in fluctuating environments (Lidstrom and Konopka, 2010; Ackermann, 2015; Schreiber *et al.*, 2016). Within natural marine ecosystems, where the distribution of nutrients is highly patchy at the microscale (Stocker, 2012), such inter-cellular variability in metabolism is highly likely to be widespread. In addition, a range of methodological factors can also affect cell-to-cell heterogeneity in enrichment measured by NanoSIMS including the orientation of the cells, their biovolume and elemental density (Musat *et al.*, 2014, 2016; Pernice *et al.*, 2015; Achlatis *et al.*, 2018).

An increase in the variability of ^{15}N enrichment among single cells/aggregates was also recorded over time using ToF-SIMS (Figure 2.1), and became more pronounced in the later time-points (IQR: 2 hours = 1.3; 4 hours = 1.7; 6 hours = 4.7). We subsequently investigated the ^{15}N incorporation into organic molecules, targeting specifically amino acids and peptides. We followed the CNO^- (m/z 42) and C_3N^- (m/z 50) peaks which, along with CN^-, were the three most intense peaks in the samples and are characteristic of protein fragmentation (L. J. Chen *et al.*, 2011), commonly used in negative ToF-SIMS analyses (Sanni *et al.*, 2002; Wagner *et al.*, 2002; Sjövall, Johansson and Lausmaa, 2006). However, deconvolution interferences, caused by neighbouring hydrocarbon peaks, induced an overestimation of ^{15}N enrichment into peptides by approximately 4 Atom% (Figure 2.3). This issue was specific to the CNO^- and C_3N^- peaks and did not impact previous quantification of $^{12}C^{15}N$ and $^{12}C^{14}N$ peaks (Figure 2.1). Although the signals exhibited an overall increase through time, these deconvolution artefacts prevented an accurate quantification of the proportion of ^{15}N channelled by *Synechococcus* towards amino-acid synthesis. Besides CNO^- and C_3N^-, we were not able to detect or reliably quantify other ^{15}N-labelled organic nitrogen compounds in *Synechococcus* cells. Prior studies of biological material using ToF-SIMS used positive polarity, which enables a degree of separation for specific amino acids in the mass spectrum. Since we were focusing on comparing the two SIMS techniques, we used the negative polarity mass spectra to image and quantify CN^- ions. However, our data clearly show that using negative polarity provides insufficient information to identify specific amino acids.

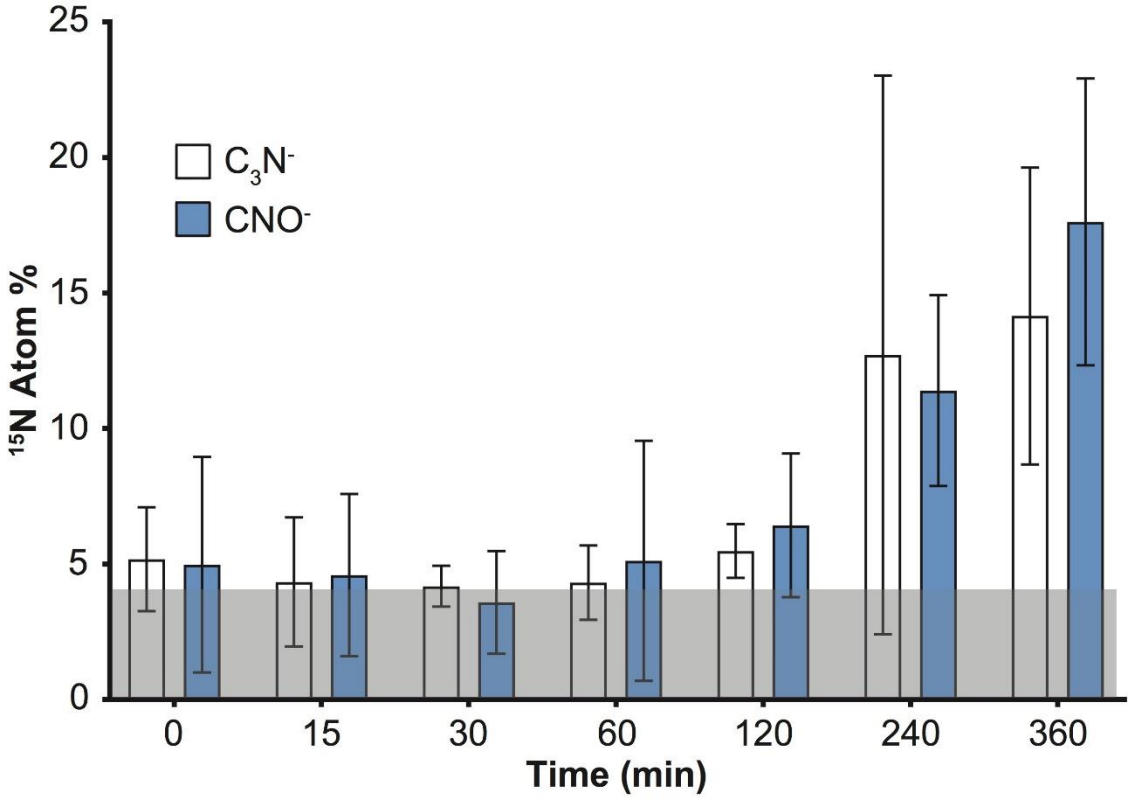

Figure 2.3 Detection of ^{15}N incorporation into peptides by quantifying C_3N^- and CNO^- in *Synechococcus* cells with ToF-SIMS. Note: deconvolution of neighbouring peaks ($^{13}C^{12}C_2{}^{14}N$ and $^{13}C^{14}N^{16}O$), resulted in erroneously offset values (by approximately 4 Atom% throughout the time series; shaded grey area). Error bars: standard deviation of single cell measurements. For number of replicates refer to Supplementary Table 2. All measurements were carried out on a sample taken from the same culture flask (n=1 biological replicate).

In conclusion, the three instruments do not require extensive sample preparation to analyse stable isotope incorporation in microbial populations. EA-IRMS provides quick, accurate and relatively inexpensive quantification but is restricted to large sample amounts: the dried biomass needed for analysis should be higher than 0.15 mg per sample, which is equivalent to the microbial biomass present in hundreds of millilitres of oceanic water. Conversely, SIMS methods require longer analysis, but can push measurements beyond the population average, unravelling cellular heterogeneity and enabling access to complex biological processes, or rare microorganisms (Musat *et al.*, 2008; Zimmermann *et al.*, 2015). Currently, NanoSIMS is the only instrument that allows the visualization and quantification of stable isotope tracers within any cell type (from multicellular organisms to virus particles). In comparison, the use of ToF-SIMS has been limited in microbiology, mainly because of its lower spatial resolution, however our data clearly show that this instrument enables the detection of isotopic enrichment in cells as small as 2 µm. Although peak overlap and asymmetry can prevent accurate isotopic quantification when enrichment levels are very low, this instrument can reliably detect microscale enrichments of $^{12}C^{15}N$ as soon as they exceed 0.2 Atom% (Figure 2.1; Supplementary Table 2.2). Therefore, ToF-SIMS is a useful technique for detecting enrichment in biological samples, especially if researchers do not have access to a NanoSIMS. Recent technological developments - increasing ToF-SIMS resolution to less than 200 nm for inorganic molecules and less than 2 µm for organic compounds (Passarelli *et al.*, 2017) - will undoubtedly increase the relevance of this instrument to study microbial interactions. SIMS approaches hold great potential to unravel some more intricate aspects of *Synechococcus* ecology by quantifying more accurately fluxes of the major elements, localizing where these elements are stored intracellularly and in which form, and visualizing how these cells interact with other microbes such as heterotrophic bacteria or zooplankton. Future research coupling the approaches used here to examine the dynamics of single cell ecophysiology will deliver more precise insights into the metabolic interactions of microbes at the micro-scale, which in-turn promises to contribute to a clearer understanding of the importance of microbial processes in ocean-scale chemical fluxes.

3 Chapter 3

Reciprocal nutrient exchanges between a ubiquitous marine cyanobacterium and heterotrophic bacteria

Marco Giardina[1], Mathieu Pernice[1], Peta L. Clode[2,3], Matthew R. Kilburn[2], Paul Guagliardo[2], Jean-Baptiste Raina[1*], Justin R. Seymour[1]

[1] Climate Change Cluster (C3), University of Technology Sydney, Broadway NSW 2007, Australia

[2] Centre for Microscopy, Characterisation and Analysis, University of Western Australia, 35 Stirling Highway, Perth 6009, Australia

[3] UWA School of Biological Sciences and UWA Oceans Institute, The University of Western Australia, Perth, Australia

3.1 Abstract

Interactions between marine phytoplankton and bacteria play critical roles in oceanic biogeochemical cycles and stimulate biomass production at the base of the marine food web. Although picocyanobacteria dominate the photosynthetic biomass of the world ocean, their interactions with heterotrophic bacteria have been mostly studied at the bulk-scale. However, technological advances enable us to zoom in on these microscale interactions in order to quantify nutrient exchange at the single-cell level and investigate potential reciprocal transfers. Here we used nano-scale Secondary Ion Mass Spectrometry (NanoSIMS) to visualize and quantify the exchange of nitrogen and carbon between the ubiquitous picocyanobacterium *Synechococcus* and two of its Alphaproteobacteria associates (*Erythrobacter* sp. MG_01 and *Shimia* sp. MG_02). *Synechococcus* cells were pre-enriched in ^{15}N, which was increasingly taken up by the two heterotrophs over time although *Erythrobacter* sp. consumed approximately 3 times more nitrogen than *Shimia* sp. Both strains of heterotrophic bacteria regularly attached to the *Synechococcus* cells, which increased their uptake of *Synechococcus*-derived nitrogen by one order of magnitude relative to non-attached cells. Additionally, we also quantified translocation of ^{13}C from the two labelled Alphaproteobacteria to *Synechococcus* cells, revealing that these picocyanobacteria can actively assimilate carbon compounds produced by heterotrophic bacteria, but exhibited a preference for *Shimia* sp. exudates. The observations provide single-cell evidence for complex reciprocal nutrient exchanges between ecologically important picocyanobacteria and their associated heterotrophic partners. Furthermore, the ability of heterotrophic bacteria to physically attach and engage in previously unsuspected chemical cycling with one of the most abundant photosynthetic organisms on the planet may have profound ecological and biogeochemical implications.

3.2 Introduction

Interactions between phytoplankton and heterotrophic bacteria shape the base of the marine food-web, regulating nutrient cycling and primary productivity globally (Cole, 1982). These interactions can span the continuum of symbiotic interactions from mutualistic (Aota and Nakajima, 2001; Amin *et al.*, 2015) to antagonistic (Mayali and Azam, 2004; van Tol, Amin and Armbrust, 2017), involving reciprocal nutrients exchanges or exploitation.

Most studies which investigate phytoplankton-bacteria interactions have focused on large phytoplankton cells, such as diatoms and dinoflagellates (Mayali, Franks and Burton, 2011; Amin *et al.*, 2015; Smriga *et al.*, 2016; Raina *et al.*, 2017). However, much of the phototrophic biomass of the ocean is dominated by small organisms, including the picocyanobacteria *Synechococcus* and *Prochlorococcus* (Partensky, Blanchot and Vaulot, 1999; Flombaum *et al.*, 2013). With an estimated 10^{26} cells present in the world's oceans (Flombaum *et al.*, 2013), *Synechococcus* is the second most abundant photosynthetic organism on this planet. Emerging evidence indicates that *Synechococcus* may establish metabolic interactions with a wide diversity of heterotrophic bacteria, with direct impacts on the physiology of both partners (Tai *et al.*, 2009; Beliaev *et al.*, 2014; Christie-Oleza *et al.*, 2015, 2017; Christie-Oleza, Scanlan and Armengaud, 2015; Arandia-Gorostidi *et al.*, 2017; Kaur *et al.*, 2018; Zheng *et al.*, 2018). For example, recent proteomic studies have revealed mutual nutrient exchanges between *Synechococcus* and the Roseobacter *Ruegeria pomeroyi* (Christie-Oleza *et al.*, 2017). *Synechococcus* exudes nitrogen-rich dissolved organic matter that is assimilated by the Roseobacter and transformed into ammonia that, in turn, is consumed by the *Cyanobacteria* (Christie-Oleza *et al.*, 2017).

While previous studies have revealed important metabolic interactions between *Synechococcus* and heterotrophic bacteria, they have generally been carried out in bulk-scale scenarios, prohibiting the examination of these processes at the scale at which these interaction occur, the microscale. Single-cell approaches, such as NanoSIMS, thanks to their sub-micron resolution, hold the great potential of directly visualizing and quantifying these interactions

Our goal was to quantify the potential for reciprocal chemical exchanges between these groups by zooming in on single-cell chemical interactions, allowing us to consider how the ecological interactions between these important functional groups will influence chemical cycling in the upper ocean. Here we used nano-scale Secondary Ion Mass Spectrometry (NanoSIMS) in combination with stable isotope labelling to measure the microscale dynamics of Nitrogen and Carbon transfer between *Synechococcus* and two of its culture-associated bacteria, *Erythrobacter* sp. MG_01 and *Shimia* sp. MG_02, both members of the Alphaproteobacteria commonly reported in association with phytoplankton (Schäfer and Abbas, 2002; Jasti *et al.*, 2005; Goecke *et al.*, 2013; Behringer *et al.*, 2018).

3.3 Materials and methods

3.2.1 Synechococcus culture maintenance

Synechococcus sp. CS-94 RRIMP N1 (S1) was purchased form the Australian National Algae Culture Collection (ANACC, CSIRO, https://anacc-db-cdc.it.csiro.au/fmi/webd/CMARC%20Database) and maintained in culture in the Phytoplankton Culture Collection of the Climate Change Cluster C3 at UTS. The strain, was cultured in f/2 (-Si) medium (Guillard, 1975). Instead of using natural filtered sea water which can contain biologically available nitrogen, the nutrients of f/2 medium were added to an artificial salts solution (Enriched Seawater Artificial Water (ESAW)) (Berges *et al.*, 2001). The culture was maintained at 23 °C on a 12:12 h dark:light cycle at ~ 180 µmol photons m^{-2} s^{-1}.

3.2.2 Bacterial isolation and identification

Heterotrophic bacteria were isolated from *Synechococcus* culture by serially diluting aliquots into sterile Artificial Sea Water (ASW) (Seymour, Marcos, and Stocker, 2009) reaching 1:100 dilutions. Ten microliters of each dilution was spread onto separate 2216 Marine Agar plates (Difco Laboratories, Detroit, Michigan) which were incubated at room temperature. After 4-6 days, six single colonies from each plate (6 isolates in total) were grown overnight in 2216 Marine Broth (Difco Laboratories, Detroit, Michigan) in a shaking incubator (180 rpm). Each isolate was cryopreserved in triplicate in 20% glycerol, snap frozen in liquid nitrogen and stored at -80°C until required. In addition, 1.8 ml of each isolate grown in marine broth was extracted using UltraClean® Microbial DNA Isolation Kit (MO BIO Laboratories, Inc.), according to the manufacturer's

instructions. The 16S rRNA gene was amplified by polymerase chain reaction (PCR) and the universal primers 27F 5'-GAGTTTGATC(AC)TGGCTCAG-3'; and 1492R 5'-GGTTACCTTGTTACGACTT-3' (Weisburg *et al.*, 1991) to determine the taxonomy of the isolated strains. PCR reactions were performed in 25 µl reaction volumes containing: 12.5 µl of GoTAQ Mix, 1µl of forward primer 27F, 1µl of reverse primer 1492R, 9.5 µl of DNA free H_2O, DNA sample 1 µl. PCR conditions consisted of an initial denaturing step at 94°C for 5 minutes, followed by 30 cycles of 94°C for 1 minute, 55°C for 1 minute and 72°C for 3 minutes and a final extension of 72°C for 10 minutes. PCR products were purified using UltraClean® PCR Clean-up Kit (MO BIO Laboratories, Inc.) according to the manufacturer's protocol. The PCR products were then sequenced by the Australian Genome Research Facility (AGRF Ltd) using Sanger sequencing. The resulting sequences were trimmed using Bio Edit Sequence Alignment Editor version 7.2.5 (Hall, 1999) to obtain amplicons of 600-700 bp. Finally, the amplicons were aligned using Basic Local Alignment Search Tool (BLAST; http://blast.ncbi.nlm.nih.gov/Blast.cgi). Among the six isolates two strains, belonging to the Alphaproteobacteria class, were chosen for the experiment because of their swimming capabilities (assessed through phase-contrast at 20X) with light microscopy. Their 16S rRNA genes were respectively 99% similar to *Erythrobacter citreus* strain RE35F/1 (Denner *et al.*, 2002) and *Erythrobacter pelagi* UST081027-248 (Wu *et al.*, 2012), and 99% similar to *Shimia marina* strain CL-TA03 (Choi and Cho, 2006) and *Shimia isoporae* strain SW-6 (M.-H. Chen *et al.*, 2011).

3.2.3 Isotopic labelling

To trace the transfer of nitrogen from *Synechococcus* to bacteria, the stable isotope ^{15}N was used. *Synechococcus sp.* was inoculated into f/2 medium with the ^{15}N-labelled Sodium Nitrate ($NaNO_3$, ^{15}N, 98%+, Cambridge Isotopes Laboratories, Inc.) as sole source of nitrogen. The culture was grown in batch for four months until the day of the experiment, at its optimal light and temperature conditions, to ensure the total replacement of ^{14}N with ^{15}N in the cells. The day before the experiment, the two bacterial strains were grown overnight at room temperature in ESAW medium enriched with ^{13}C (in amino-acids form; Celtone Base Powder; Cambridge Isotope Laboratories, Tewksburry, MA; final concentration 10%). The stable isotope labelling of the bacteria was carried out to: (*i*) facilitate their localisation with NanoSIMS (Raina *et al.*, 2017); (*ii*) investigate potential reciprocity in the nutrient they exchanges.

3.2.4 Experimental design

On the day of the experiment, 120 ml of ^{15}N-labelled *Synechococcus* culture were aliquoted into three 50 ml tubes (final volume 40 ml per tube) and then rinsed three times, by centrifuging at 1,500 g for 15 minutes, with fresh f/2 medium containing natural abundances of ^{15}N in order to remove all residual of ^{15}N–labelled compounds from the medium. The cells were finally re-suspended in 40 ml of f/2 (with natural abundance of ^{15}N). This medium exchange (from ^{15}N enriched f/2 to natural abundance) was carried out in order to ensure that the ^{15}N measured in the bacterial cells was not derived from the growth medium, but instead was only a consequence of uptake of ^{15}N molecules exuded from phytoplankton cells. The overnight bacterial cultures were washed three times in ESAW before inoculation. After washing, the heterotrophs were inoculated in each respective tube in a ratio 1:10 *Synechococcus*:heterotrophs. The concentrations of both *Synechococcus* and the two heterotrophic bacteria were determined by flow cytometry (Accuri C6; BD Scientific). A 100 µl aliquot was taken from each 50 ml tube of *Synechococcus* and the bacteria cultures before washing. The cultures were diluted respectively 1,000 and 10,000 times in artificial seawater and fixed with glutaraldehyde (final conc. 2%). Prior to analysis, heterotrophic bacteria samples were stained with SYBRGreen-I (final conc. 1:10,000) for 15 minutes in the dark (Marie *et al.*, 1997). *Synechococcus* population was discriminated according to cell side scatter (SSC) and red fluorescence (650 nm). On the other hand, bacterial population were discriminated according to SSC and green fluorescence (488 nm) (Seymour, Seuront and Mitchell, 2007). The inoculums were performed according to the following scheme: (1) *Synechococcus* + *Erythrobacter* (S+MG_01); (2) *Synechococcus* + *Shimia* (S+MG_02). We performed a six-hour incubation (based on results from a pilot study; Supplementary Figure 1) under illumination at the same light and temperature conditions at which the *Synechococcus* culture was maintained. Samples were collected as a time series following the addition of bacteria. 1.5 ml of samples were collected in triplicate after 30 minutes (T_1), 2 hours (T_2) and 6 hours (T_3). The samples were centrifuged at 1,500 g for 15 minutes, the surnatant was removed and replaced with 500 µl of 1% paraformaldehyde (PFA) in 0.1 M Sucrose and 1× phosphate buffer saline (PBS), and then were fixed for 24h at 4 °C. The next day, samples were washed three times with sucrose-PBS buffer by centrifuging the samples at 1,500 g for 15 minutes (in order to remove any residual PFA) before being filtered onto gold-palladium pre-coated polycarbonate filters (GTTP type;

pore size 0.22 µm; diameter 25 mm; Millipore) (Musat *et al.*, 2008) using a 12 position vacuum filtrating manifold (Millipore). In order to avoid superimposition of cells, before filtration the samples were diluted 100 times in 2 ml volume of Sucrose-PBS buffer. A *Synechococcus* culture maintained in the presence of natural abundance of ^{15}N (0.37%), was used as a control, and treated identically to all experimental cultures. The filters were stored at -20 °C until NanoSIMS analysis. For loading the samples in the NanoSIMS, the filters were taken out of the freezer and let air-dry overnight inside a desiccator. A 5×5 mm piece was cut from each filter and mounted on different stubs. Finally, the filters were coated with 5 nm of gold before being loaded in the NanoSIMS.

3.2.5 Scanning Electron Microscope (SEM)

Samples that had been prepared on filters and mounted on Si wafers were sputter coated with 3 nm Pt and imaged with the in lens secondary electron detector at 3 kV in a field emission SEM (Zeiss 55 SUPRA).

3.2.6 NanoSIMS analysis

We used the NanoSIMS 50 (Cameca, Gennevilliers, France) at the Centre for Microscopy, Characterisation and Analysis (CMCA) at The University of Western Australia. This model allows simultaneous collection and counting of up to five isotopic species (in this case; $^{12}C_2^-$, $^{12}C^{13}C^-$,$^{12}C^{14}N^-$, $^{12}C^{15}N^-$, ^{32}S) enabling the determination of the $^{15}N/^{14}N$ and $^{13}C/^{12}C$ ratios. Enrichment of the rare isotopes ^{15}N and ^{13}C was confirmed by an increase in their ratio above the natural abundance value recorded in controls (0.00367 for nitrogen and 0.022 for carbon). The NanoSIMS was performed as chain analysis: samples were pre-sputtered for 3.50 minutes at 500 pA Cs^+ beam (D1=1) on 30 µm² areas (256 x 256 pixel), followed by automatic horizontal and vertical secondary ion beam centring and finally the analysis was performed by rastering a 2 pA beam (D1=2) over 25 µm² areas (256 x256 pixels). We used Fiji software (http://fiji.sc/Fiji) (Schindelin *et al.*, 2012) with the Open-MIMS plug-in (http://nrims.harvard.edu/software) to process the NanoSIMS data. All images were dead-time corrected (Hillion *et al.*, 2008). Isotopic quantification data of the heterotrophic bacteria were extracted from the mass images by manually drawing regions of interest around each single bacterial cell using the $^{12}C^{13}C^-$ image as mask (Supplementary Figure 3.2).

3.2.7 Normalisation of ^{13}C levels

The two bacterial species used here exhibited vastly different ^{13}C atomic fraction at the beginning of the experiment (13.293 % ± 0.344 for *Erythrobacter* sp. MG_01 and 22.365 % ± 0.4242 for *Shimia* sp. MG_02). To account for these initial differences in enrichment, all measured $^{13}C/^{12}C$ ratio from *Synechococcus* cells were normalised to the respective initial $^{13}C/^{12}C$ ratio of the bacterial cells. The normalised values were calculated as follow: for both bacterial species, the means of ^{13}C enrichment was calculated at 30 minutes (as it was the highest level of enrichment), obtaining values that here we name as A for simplicity

A = means of ^{13}C enrichment of both bacterial species at 30 minutes

As no difference in ^{13}C enrichment was found between attached and not-attached bacteria both groups were included in the calculation of the mean. Then, the ^{13}C values of each *Synechococcus* cell were subtracted by the ^{13}C value measured in the control, obtaining values here named as B for simplicity

B = ^{13}C value of single *Synechococcus* cell – mean value of ^{13}C in the control

Finally, each values B (^{13}C *Synechococcus* minus ^{13}C control) were then divided by the values A (mean values of ^{13}C enrichment of the bacteria at 30 minutes) of the respective bacterial specie which the Synechococcus cells were co-incubated with during the experiment obtaining the normalized ^{13}C values showed in Figure 3.3

Normalized ^{13}C values = B/A

3.2.8 Atom fraction

The measured isotope ratios were converted to Atomic Percentage (Atom %), which gives the percentage of a specific atom within the total number of atoms. In this case, we calculated the percentage of ^{13}C and ^{15}N within the total number of nitrogen and carbon atoms following the formula:

$$Atom\% = \frac{^{15}\mathrm{N}}{(^{15}\mathrm{N} + {}^{14}\mathrm{N})} \times 100$$

Or

$$Atom\% = \frac{^{13}\mathrm{C}}{(^{13}\mathrm{C} + {}^{12}\mathrm{C})} \times 100$$

3.2.9 Statistics

The data were first tested for normality and homogeneity of variance using respectively Shapiro-Wilk and Levene's test. Since the data were not normally distributed and/or not homogeneous, nitrogen and carbon incorporation within same microbial groups for all incubation times were tested using Kruskal-Wallis H-test with multiple comparisons. Instead Mann-Whitney U-test instead (paired two-tailed *t*-test) was applied for pairwise comparisons between groups at each time point. All statistics were carried out through SPSS (version 23; IBM Corporation, Armonk, USA). The outcomes of the tests are reported in Supplementary Table 3.1, 3.2 and 3.3.

3.4 Results and Discussion

To track potential reciprocal nutrient exchanges, *Synechococcus* cells were enriched with the stable isotope ^{15}N, while the two heterotrophic bacteria, *Shimia* sp. and *Erythrobacter* sp., were enriched with ^{13}C. Both strains are commonly found in the ocean (Denner *et al.*, 2002; Wu *et al.*, 2012; Buchan *et al.*, 2014)) and have also been found to develop intimate associations with several phytoplankton taxa in culture (Schäfer and Abbas, 2002; Jasti *et al.*, 2005; Goecke *et al.*, 2013; Behringer *et al.*, 2018). However, in the literature there is no direct evidence of association between *Synechococcus* and these two bacterial species. After enriching cells from each group separately, we co-incubated *Synechococcus* with each of the two heterotrophs and measured ^{15}N and ^{13}C transfer throughout a six-hour period using NanoSIMS.

3.4.1 Synechococcus-derived nitrogen uptake by free-living bacteria

Following co-incubation with *Synechococcus*, both bacteria strains exhibited significant increases in intracellular ^{15}N through time (Kruskal-Wallis (KW), $p<0.001$) (Figure. 3.1). After thirty minutes of co-incubation with enriched *Synechococcus* cells, *Erythrobacter* MG_01 and *Shimia* MG_02 cells became respectively 8.6- and 3.5-times more enriched in ^{15}N than cells the control. After six hours, these levels of enrichment were respectively 14.7- and 6-times higher than control. Single-cell mass spectrometry analysis allowed to probe for differences in the metabolic capacity of the heterotrophic bacteria examined here. When compared directly, the *Erythrobacter* MG_01 assimilated approximately 3 times significantly more *Synechococcus*-derived ^{15}N than the *Shimia* MG_02 (Mann-Whitney (MW), $p<0.001$) at each time point. This is notable given that *Shimia* MG_02 belongs to the Roseobacter clade, which are well known for close metabolic associations with phytoplankton (Sarmento and Gasol, 2012; Buchan *et al.*, 2014; Behringer *et al.*, 2018), including *Synechococcus* (Christie-Oleza et al. 2017).

The significant levels of enrichment in ^{15}N observed in the two heterotrophic associates of *Synechococcus* confirm previously observations from Christie-Oleza et al. (2017): *Synechococcus* cells release high amounts of nitrogen-containing organic matter into the surrounding media, which can be rapidly assimilated by heterotrophic bacteria. Heterotrophic bacteria from the Roseobacter clade utilize nitrogen-rich *Synechococcus* exudates, mainly composed of amino acids, which serves two important functions: *i*) the assimilation of organic nitrogen by Roseobacter leads to detoxification of the environment has and prevent a negative effect on the growth of *Synechococcus*; and *ii*) the re-mineralization of these nutrients further sustain *Synechococcus* growth. Our work clearly shows that the amount of organic nitrogen assimilated by heterotrophic bacteria is species-specific and reveals that, contrary to previous assumptions, certain members of the Roseobacter clade are not the main consumers of available nitrogen.

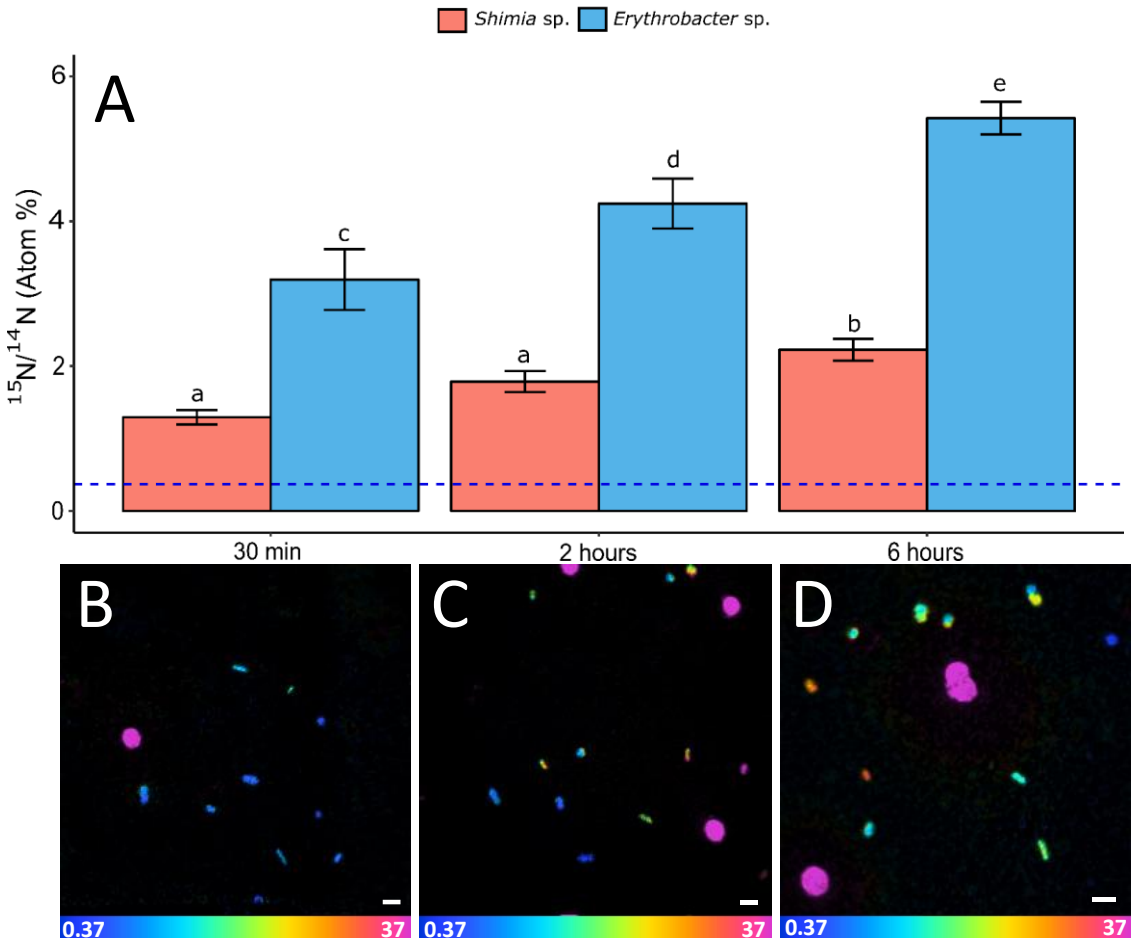

Figure 3.1 (A) Increasing ^{15}N enrichment of *Shimia* sp. (pink) and *Erythrobacter* sp. (blue) ; Error bars: standard errors; dashed line: $^{15}N/^{14}N$ ratio in natural abundance calculated from the control (0.367 % ± 0.002 mean ± SEM, n = 154); *Erythrobacter* MG_01: 30 minutes (3.194 % ± 0.419 mean ± SEM, n = 71), 2 hours (4.243 % ± 0.343 mean ± SEM, n = 132), 6 hours (5.422 % ± 0.224 mean ± SEM, n = 283); *Shimia* MG_02: 30 minutes (1.294 % ± 0.101 mean ± SEM, n = 150), 2 hours (1.786 % ± 0.145 mean ± SEM, n = 270), 6 hours (2.225 % ± 0.151 mean ± SEM, n = 237). Representative NanoSIMS images showing $^{15}N/^{14}N$ ratio distribution in the samples: (**B**) 30 minutes, (**C**) 2 hours and (**D**) 6 hours; Blue = $^{15}N/^{14}N$ ratio in natural abundance, calculated from the control; Magenta = arbitrary value selected to highlight increase in colour intensity over time. Scale bars: 2 µm.

3.4.2 Synechococcus-derived nitrogen uptake by attached bacteria

Scanning electron microscope (SEM) measurements revealed that both heterotrophic bacteria regularly became directly attached to *Synechococcus* cells during the co-incubation period (Figure 3.2). The common occurrence of this process, along with its consistency with previous observations (Malfatti and Azam, 2009; Beliaev *et al.*, 2014), strongly suggests that these attachments are not an artefact derived from the sample preparation.

Heterotrophic bacteria attached to *Synechococcus* cells exhibited differential uptake dynamics than unattached cells. Thirty minutes after the start of the co-incubation, attachment was prevalent for both *Erythrobacter* MG_01 and *Shimia* MG_02, and these cells were respectively 75-times and 56-times significantly more enriched in ^{15}N than the control cells (KW, $p<0.001$) and one order of magnitude significantly more enriched than the non-attached cells (MW, $p<0.001$) (Fig. 3.2E). However, contrary to the increasing enrichment shown by the free-living bacteria, the attached cells maintained a steady level of ^{15}N enrichment over time and no significant difference was recorded between them. These patterns indicate that attachment of heterotrophic bacteria to *Synechococcus* cells leads to a higher rate of nitrogen cycling and in the environment will influence the biogeochemistry of the ocean.

While the capacity of heterotrophic bacteria to attach to phytoplankton cells or particles is a well-recognised ecological strategy for enhancing exposure to growth substrates (Grossart *et al.*, 2007; Mayali, Franks and Burton, 2011), the mode of attachment in the case of *Synechococcus* is potentially paradoxical: typical mode of particle or phytoplankton attachment in the ocean involve motility and chemotaxis (Kiørboe and Jackson, 2001; Sonnenschein *et al.*, 2012) – the ability of bacteria to direct their movement based on concentration gradients – however, with its 2 µm diameter, *Synechococcus* cells are considered to be too small to be detected by chemotactic bacteria (Seymour *et al.*, 2017). However, physical attachment of heterotrophic bacterial cells to *Synechococcus* cells has previously been reported under culture conditions as well as in environmental samples (Malfatti and Azam, 2009; Beliaev *et al.*, 2014; Arandia-Gorostidi *et al.*, 2017). Our results extend upon these observations to show that associations between these small marine microbes can enhance rates of nutrient exchange,

pointing to a potentially important, but overlooked role of microscale associations between picocyanobacteria and heterotrophic bacteria in marine nutrient cycling.

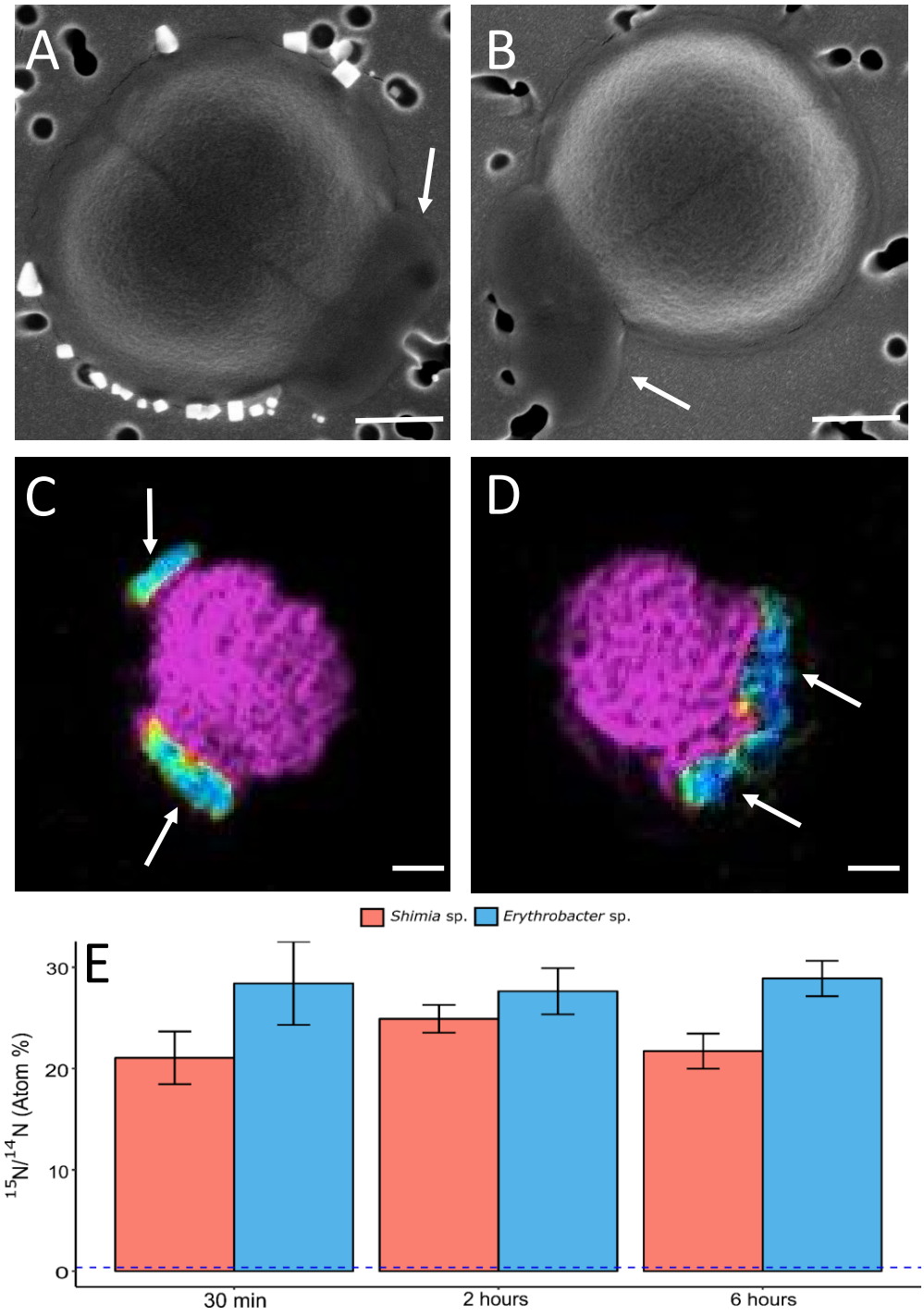

Figure 3.2 Attached bacteria. (**A, B**) SEM image of a bacterial cell attached at a *Synechococcus* cell. (**C, D**) NanoSIMS image showing the distribution of $^{15}N/^{14}N$ ratio in two bacterial cells attached to a *Synechococcus* cell. Arrows indicate attached bacteria.^{15}N enrichment of attached bacteria. (**E**) Steady ^{15}N enrichment of attached *Shimia* sp. (pink) and *Erythrobacter* sp. (blue). Error bars: Standard error. Dashed line: $^{15}N/^{14}N$ ratio in natural abundance calculated from the control (0.367 % ± 0.002 mean ± SEM, n = 154). *Erythrobacter* MG_01: 30 minutes (28.401 % ± 4.094 mean ± SEM, n = 8), 2 hours (27.625 % ± 2.278 mean ± SEM, n = 13), 6 hours (28.887 % ± 1.744 mean ± SEM, n = 20); *Shimia* MG_02: 30 minutes (21.048 % ± 2.602 mean ± SEM, n = 19), 2 hours (24.907 % ± 1.375 mean ± SEM, n = 38), 6 hours (21.717 % ± 1.729 mean ± SEM, n = 21). Scale bar: 0.5 µm

3.4.3 Bacterial-derived Carbon uptake by Synechococcus.

While the provision of remineralised nutrients has traditionally been considered the most important contribution of marine heterotrophic bacteria to phototrophic associates (Azam, Fenchel and Field, 1983; Azam, 1998; Buchan *et al.*, 2014), it is increasingly clear that bacteria can also provide important vitamins and other organic molecules to promote the growth of phytoplankton cells (Croft *et al.*, 2005; Durham *et al.*, 2014; Amin *et al.*, 2015). Both heterotrophic bacterial strains were pre-enriched with ^{13}C, as a means to localize these cells using NanoSIMS, but also to track eventual transfer of carbon to *Synechococcus* cells. *Erythrobacter* MG-01 and *Shimia* MG_02 were respectively approximately 6-times and 10-times significantly more enriched in ^{13}C than the control cells (Mann-Whitney, p <0.001) (Supplementary Figure 3.3 and Supplementary Table 3.3). Although they were grown in the presence of ^{13}C for the same amount of time, the level of ^{13}C enrichment of the two heterotrophs differed, with *Shimia* MG_02 cells being twice as enriched as *Erythrobacter* MG_01 (Supplementary Figure. 3.3). After normalising our results to take into account the initial differences in ^{13}C enrichments between the two heterotrophic bacteria (see methods), we determined that *Synechococcus* assimilated bacterial-derived ^{13}C-labelled compounds during the experimental period, and the enrichment level was strongly influenced by the identity of the heterotrophic partner (Figure. 3.3). Specifically, the *Synechococcus* cells in co-culture with *Shimia* MG_02 were 6-times more enriched in ^{13}C after 30 minutes of co-incubation compared to those with *Erythrobacter* MG_01 (MW, p<0.001). *Synechococcus* cells in co-culture with *Erythrobacter* MG_01 only became significantly enriched (relatively to control) after six hours of co-incubation (MW, p<0.001). These patterns indicate that the Roseobacter *Shimia* MG_2, although not taking up as much nitrogen from *Synechococcus* as *Erythrobacter* MG_01, was clearly involved in active transfer of carbon compounds with the cyanobacteria, in line with its mutualist interactions with other larger phytoplankton. These reciprocal exchanges support: *i*) the photoheterotrophic metabolism of *Synechococcus* cells (Cottrell and Kirchman, 2009) and, *ii*) the first evidence of carbon exchanges with heterotrophic bacteria, which might support this type of metabolism.

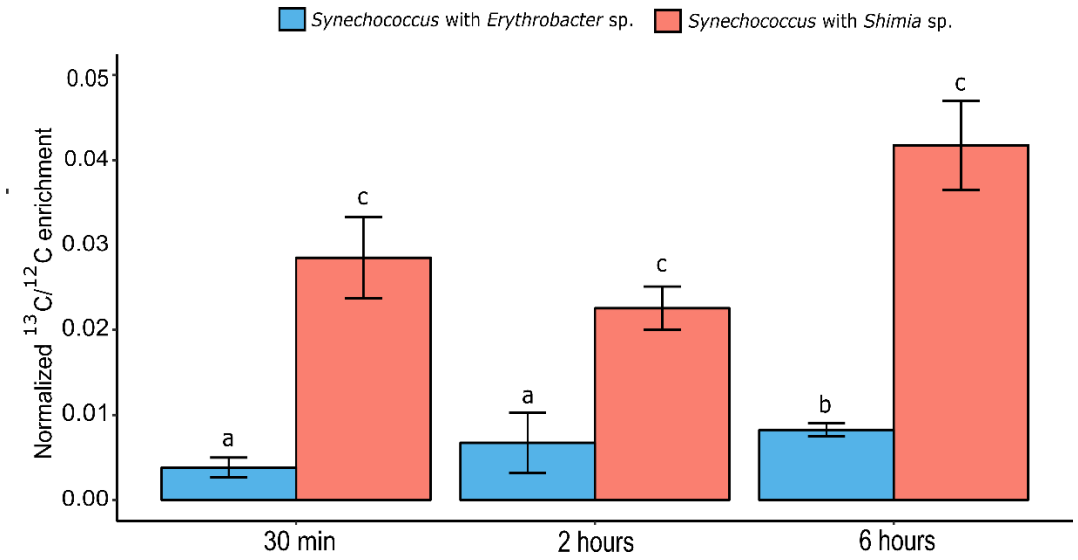

Figure 3.3 Normalized ^{13}C enrichment of *Synechococcus* cells in incubation with *Erythrobacter* (blue) and *Shimia* (pink); Error bars: standard error; *Synechococcus* with *Erythrobacter* MG_01: 30 minutes (0.004 % ± 0.001 mean ± SEM, n = 48), 2 hours (0.007 % ± 0.003 mean ± SEM, n = 54), 6 hours (0.008 % ± 0.001 mean ± SEM, n = 147); *Synechococcus* with *Shimia* MG_02: 30 minutes (0.028 % ± 0.005 mean ± SEM, n = 26), 2 hours (0.023 % ± 0.003 mean ± SEM, n = 49), 6 hours (0.042 % ± 0.005 mean ± SEM, n = 24). Note: all the values displayed are above natural abundance.

3.4.4 Conclusions

We quantified the microscale spatiotemporal dynamics of carbon and nitrogen transfer between one of the most abundant and ecologically important photoautotrophic microorganisms, *Synechococcus*, and two of its associated heterotrophic bacteria, providing the first quantitative evidence for mutual exchange of nutrients between these groups of microorganisms at the single cell-level. Both free-living *Erythrobacter* and *Shimia* cells, as well as those physically attached to *Synechococcus* cells assimilated *Synechococcus* derived organic nitrogen. Attached cells acquired significantly higher levels of *Synechococcus* exudates, indicating that the physical attachments observed here and elsewhere (Arandia-Gorostidi *et al.*, 2017), have the potential to profoundly influence the rate of nutrient cycling and the productivity of microbial populations in the upper ocean. Our NanoSIMS analysis also provided the first direct evidence for *Synechococcus* usage of carbon produced by heterotrophic associates, suggesting that the phototrophic metabolism of *Synechococcus* may in some instances be supported by associated heterotrophic bacteria. Together, these findings are indicative of a mutualistic interaction between *Synechococcus* and specific heterotrophic bacterial associates, with the relationship based on the reciprocal exchange of nitrogen and carbon compounds, which might in part help to explain the ecological success of *Synechococcus* across the global ocean.

4 Chapter 4

Chemotaxis enhances bacterial uptake of chemicals exuded by abundant marine picocyanobacteria

Marco Giardina[1], Douglas R. Brumley[2,3], Peta Clode[4,5], Mathieu Pernice[1], Steven Smriga[3], Eva Sonnenschein[5], Matthias Ullrich[5], Paul Guagliardo[4], Unnikrishnan Kuzhiumparambil[1], Roman Stocker[3], Jean-Baptiste Raina[1], Justin R. Seymour[1]

[1] Climate Change Cluster (C3), University of Technology Sydney, Broadway NSW 2007, Australia;

[2] School of Mathematics and Statistics, The University of Melbourne, Parkville, Victoria 3010, Australia;

[3] Institute of Environmental Engineering, Department of Civil, Environmental, and Geomatic Engineering, ETH Zürich, 8093 Zürich, Switzerland

[4] Centre for Microscopy, Characterisation and Analysis, University of Western Australia, 35 Stirling Highway, Perth 6009, Australia;

[5] UWA School of Biological Sciences and UWA Oceans Institute, The University of Western Australia, Perth, Australia

[6] Molecular Life Science Research Centre, Jacobs University Bremen, Bremen, Germany

4.1 Abstract

While intimate reciprocal chemical exchanges under-pin important phytoplankton-bacteria interactions in the ocean, these cells are often separated by hundreds to thousands of body-lengths, limiting the capacity for localised chemical exchanges. Motile heterotrophic bacteria can enhance their chances of encountering and maintaining close proximity with phytoplankton cells using chemotaxis – the ability of modulating their movement in response to chemical gradients. While the importance of chemotaxis for allowing marine bacteria to colonise the phycosphere surrounding larger phytoplankton cells (e.g. dinoflagellates and diatoms) has been established, much of the photosynthetic biomass in the ocean is comprised of small picophytoplankton (e.g. *Prochlorococcus* and *Synechococcus*), which have been considered too small to be detected by chemotactic bacteria. Here we used NanoSIMS to empirically demonstrate that chemotactic bacteria can exploit the phycosphere surrounding *Synechococcus* cells, and therefore gain access to more *Synechococcus*-derived nutrients. Using the chemotactic phytoplankton-associate *Marinobacter adhaerens*, as well as two mutants unable to swim or unable to chemotax, we showed that chemotaxis enabled the wild type bacteria to take up more than twice the amount of *Synechococcus*-produced photosynthates relative to non-chemotactic and non-motile mutants. The advantage of chemotaxis was more pronounced when *Synechococcus* density was low (10^3 and 10^4 cells ml^{-1}), relative to a *Synechococcus* bloom scenario (10^5 cells ml^{-1}) where there was no measurable difference in nutrient uptake between the three phenotypes. These patterns were corroborated by a mathematical model that predicted similar dynamics, which could be explained by the overall increase in background nutrient concentration for higher *Synechococcus* cell densities. These results highlight the, previously overlooked, importance of swimming behaviour in ecological and metabolic interactions between heterotrophic bacteria and small cyanobacteria that dominate photosynthetic biomass across vast regions of the ocean.

4.2 Introduction

Phytoplankton-bacteria interactions drive global biogeochemical cycles and mediate oceanic productivity (Cole, 1982; Azam and Malfatti, 2007). These interactions are thought to take place within the phycosphere - the microenvironment directly surrounding individual phytoplankton cells, which is enriched in organic compounds derived from photosynthetic activity (Bell and Mitchell, 1972; Mitchell, Okubo and Fuhrman, 1985; Seymour *et al.*, 2017). Bacteria exposed to the high nutrient concentrations present in the phycosphere are predicted to play a disproportionally higher role in chemical cycling than those in the adjacent nutrient-limited seawater (Blackburn, Fenchel and Mitchell, 1998). Motile heterotrophic bacteria typically establish and maintain contact with phycospheres through chemotaxis - the ability to direct their movements in response to chemical gradients (Stocker & Seymour 2012). This behaviour is key to the microscale associations between phytoplankton and bacteria (Blackburn, Fenchel and Mitchell, 1998; Stocker *et al.*, 2008). For instance, chemotaxis by the marine bacterium *Marinobacter adhaerens* towards the diatom *Thalassiosira weissflogii* is essential for cellular aggregation between the bacterium and the alga (Sonnenschein *et al.*, 2012). Chemotaxis has mostly been studied between heterotrophic bacteria and large phytoplankton (Smriga *et al.*, 2016; Seymour *et al.*, 2017). However, most of the phytoplanktonic biomass of the oceans is comprised of small picoplankton – including *Prochlorococcus* and *Synechococcus* (Flombaum *et al.*, 2013), which according to prevailing theory may not develop microscale associations with heterotrophic bacteria.

The ability of heterotrophic bacteria to chemotactically detect and exploit a phycosphere is strictly governed by the size of the phytoplankton cell, with larger cells producing larger phycospheres (Seymour *et al.*, 2017). According to modelling approaches, which have largely used chemotactic parameters derived from enteric bacteria (Mitchell, Okubo and Fuhrman, 1985; Jackson, 1987; Bowen *et al.*, 1993), there is a theoretical size threshold below which a phycosphere should no longer be detected by chemotactic marine bacteria (Jackson, 1987; Seymour *et al.*, 2017). This threshold corresponds to a phytoplankton cell smaller than 4 μm (Jackson, 1987), which would rule out the detection and exploitation of the phycosphere surrounding *Synechococcus* (2 μm on average) and *Prochlorococcus* (0.8 μm on average) (Waterbury *et al.*, 1979; Morel *et al.*, 1993). This would imply that the photosynthates exuded by these small cyanobacteria will ultimately diffuse into the surrounding seawater, rather than being consumed by

phycosphere-dwelling heterotrophic bacteria. However, marine bacteria exhibit swimming speeds and chemotactic sensitivities that substantially exceed those of the enteric species typically used as models for bacterial chemotaxis (Mitchell et al. 1995, 1996; Stocker et al. 2008; Son et al. 2016), and may in fact have the capacity to home in on much smaller phycospheres than theoretical models have suggested (Seymour et al. 2017).

With approximately 10^{27} *Prochlorococcus* and 10^{26} *Synechococcus* cells in the ocean (Flombaum *et al.*, 2013), elucidating the ecological links between these numerically dominant picocyanobacteria and heterotrophic bacteria is critical to determine the fate of the abundant pool of organic compounds they release. Indirect evidence for a potential role for bacterial behaviours in these interactions comes from observations of chemotaxis by marine bacterial isolates towards the molecules exuded by *Synechococcus* and *Prochlorococcus* cells (Seymour *et al.*, 2010), along with evidence for physical associations between *Synechococcus* cells and heterotrophic bacteria using atomic force microscopy (Malfatti and Azam, 2009) and NanoSIMS (Chapter 3). However, while there are emerging evidence for tight metabolic coupling between *Synechococcus* and heterotrophic bacteria (Arandia-Gorostidi *et al.*, 2017), an understanding of the role of bacterial behaviours, such as chemotaxis, in these profoundly important interactions is lacking.

4.3 Materials and methods

4.1.1 Synechococcus culture maintenance

Synechococcus sp. CS-94 RRIMP N1 (S1) was cultured in a modified form of f/2 (-Si) medium that combines the nutrients of f/2 medium (Guillard, 1975) and the artificial salts solutions of the Enriched Seawater Artificial Water (ESAW) (Berges *et al.*, 2001) instead of using natural filtered sea water which can contain biologically available nitrogen. The culture was maintained at 23 °C on a 12:12 h dark:light cycle at ~ 180 µmol photons m^{-2} s^{-1}.

4.1.2 Marinobacter adhaerens HP15

The wild type (WT) of the marine bacterium *Marinobacter adhaerens* HP15 and two mutant strains (Δ*che*A and Δ*fli*C) were used as model organisms for this experiment. *Marinobacter adhaerens* HP15 (WT) is a heterotrophic, motile and chemotactic bacteria that was isolated from marine particulate samples collected from surface waters of the German Bight (Grossart *et al.*, 2004). Mutant strains were generated by homologous recombination to delete the genes *che*A, which encode for one of the first enzymes of the chemotaxis signalling cascade (Sonnenschein *et al.*, 2012), and the gene *fliC* encoding for flagellin, the protein responsible of the production of the flagella (Sonnenschein *et al.*, 2011).

4.1.3 Isotopic labelling

To trace the transfer of nitrogen from *Synechococcus* to bacteria the stable isotope ^{15}N was used. *Synechococcus sp.* was inoculated into the modified f/2 medium with the ^{15}N-labelled sodium nitrate ($NaNO_3$, ^{15}N, 98 %+, Cambridge Isotopes Laboratories, Inc.) as sole source of nitrogen. The culture was grown in a 50 ml batch for one week until the day of the experiment, under the same conditions as above, to ensure high level of the ^{15}N enrichment in the cells. Two days before the experiment, glycerol stocks of the three strains were streaked onto respective Difco 2216 Marine Broth agar plates (Difco Laboratories, Detroit, Michigan) and incubated at 30 °C. On the day of the experiment, single colonies of each of the bacterial strains were suspended into ESAW medium enriched with ten times diluted ^{13}C-labelled nutrients (in amino-acids form; Celtone Base Powder; Cambridge Isotope Laboratories, Tewksburry, MA) and grown overnight at 30°C and 180 r.p.m.. The stable isotope labelling of the bacteria was carried out to facilitate their localisation with NanoSIMS as presented in Raina et al. (2017).

4.1.4 Experimental design

On the day of the experiment, the concentrations of both *Synechococcus* and the three bacterial strains were determined by flow cytometry (Accuri C6; BD Scientific). A 100 µl aliquot was taken from the *Synechococcus* and the bacteria cultures before washing them. The cultures were diluted respectively 1,000 and 10,000 times in artificial seawater and fixed with glutaraldehyde (final conc. 2%) for 20 minutes. Prior to analysis, the bacteria samples were stained with SYBRGreen-I (final conc. 1:10,000) for 15 minutes in the dark (Marie *et al.*, 1997). The *Synechococcus* population was discriminated according to cell side scatter (SSC) and red fluorescence (650 nm). On the other hand, bacterial populations were discriminated according to SSC and green fluorescence (488 nm) (Seymour et al.2007). Then, to remove all residual ^{15}N–labelled compounds from the medium, the ^{15}N-labelled *Synechococcus* culture was rinsed three times, by centrifuging at 1,500 g for 15 minutes, with fresh f/2 medium containing natural abundances of ^{15}N. The cells were finally re-suspended in 50 ml of f/2 (with natural abundance of ^{15}N). This medium exchange (from ^{15}N enriched f/2 to natural abundance) was carried out in order to ensure that the ^{15}N measured in the bacterial cells was not derived from the growth medium, but instead was only a consequence of uptake of ^{15}N molecules exuded from phytoplankton cells. On the other hand, to remove any residual of ^{13}C-compounds, the overnight bacterial cultures were washed three times in ESAW before inoculation. Three sets of three different dilutions were made with the washed *Synechococcus* culture inside separate 50 ml centrifuge tubes containing 40 ml of the modified version of f/2 media. The dilutions were the following: 1,000 cells ml^{-1}, 10,000 cells ml^{-1} and 100,000 cells ml^{-1}. The three strains of *M. adhaerens* were inoculated singularly in each respective treatment at a final concentration of 10^6 cells ml^{-1} and the tubes were gently mixed by flipping them three times. Aliquots of 1.5 ml were collected from each treatment and transferred into a 1.5 ml centrifuge tube. We performed a three-hour incubation (based on the results from chapter 2) under illumination at the at the same light and temperature conditions used for maintaining *Synechococcus* and, at the end of the experiment, samples were fixed with glutaraldehyde 2.5% for 30 minutes. A *Synechococcus* culture maintained in the presence of natural abundance of ^{15}N (0.37%), was used as the control, which was treated identically to all experimental cultures. To remove any residual glutaraldehyde, the samples were washed three times by centrifugation. The first two centrifugation steps were carried out at 1,500 g for 15 minutes. After the first step, the

supernatant was removed and replaced with 500 µl of ESAW and after the second step the supernatant was replaced with sterile filtered MilliQ water (0.22 µm pore size, Minisart syringe filters, Sartorious Stedim Biotech, Göttingen, Germany) to remove the salts of the ESAW. To avoid prolonged contact of the cells with MilliQ and eventual osmotic effect that may damage the cells, the third centrifugation step was carried out at 2,500 g for 5 minutes and the supernatant was removed and replaced with 50 µl of sterile filtered MilliQ water. The samples were re-suspended by pipetting and finally placed onto silicon wafers (7.07 mm x 7.07 mm, Type P / <111>, ProSciTech), dried at 45 °C and stored inside a desiccator, protected from light until NanoSIMS analysis. Finally, the samples were coated with 5 nm of gold before being loaded in the NanoSIMS.

4.1.5 Measurements of Synechococcus exudation rates

Highly enriched ^{15}N-labelled *Synechococcus* cells were washed 3 times in f/2 medium (as described above) before being re-suspended in 30 ml of f/2 medium (with natural abundance of ^{15}N). A culture aliquot was then inoculated into two litres of f/2 to reach a concentration of 100,000 cells/ml. We performed a three hour incubation collecting samples at three time points: T1) 1 hour, T2) 2 hours, T3) 3 hours. After collection, the cell suspensions were centrifuged at 1,500 g for 15 minutes and filtered through a 0.2 µm syringe filter. The filtrate was acidified to pH = 2 using 10 % HCl (made with HPLC-water from HCl puriss. 32 %, Fluka, Sigma). HLB cartridges (6 cc, 200 mg sorbent, Oasis) were first mounted onto a vacuum manifold, then conditioned using 6 ml of methanol and finally equilibrated with 6 ml of milliQ. The filtrate was loaded inside its respective cartridge and run at 3 ml per minute. The cartridges were washed twice with 6 ml of 0.01 N HCl to remove residual salts and dried for 20 minutes under vacuum. Finally, the metabolites were eluted with 4 ml methanol into glass vials and stored at -20 ºC until needed for Isotope Ratio Mass Spectrometry (IRMS) analyses.

4.1.6 NanoSIMS analysis

We used the NanoSIMS 50 (Cameca, Gennevilliers, France) at the Centre for Microscopy, Characterisation and Analysis (CMCA) at The University of Western Australia. This instrument allows for simultaneous collection of up to five isotopic species (in this case; $^{12}C_2^-$, $^{12}C^{13}C^-$, $^{12}C^{14}N^-$, $^{12}C^{15}N^-$, ^{32}S). Enrichment of the rare isotope ^{15}N was confirmed by an increase in the $^{15}N/^{14}N$ ratio above the natural abundance value recorded in the control (equal to 0.374 % ± 0.001 for nitrogen). The NanoSIMS was

performed using a chain analysis: samples were pre-sputtered for 3.5 minutes at 500 pA Cs^+ beam (D1=1) on 30 µm² areas (256 × 256 pixel), followed by automatic horizontal and vertical secondary ion beam centring. The analysis was then performed by rastering a 2 pA beam (D1=2) over 25 µm² areas (256 × 256 pixels); three planes were recorded per area with a dwell time of 3 ms per pixel. The instrument was operated with a high mass resolving power (in the range of 9,000), allowing the separation of isobaric interferences. Images were analysed using the Fiji software package (http://fiji.sc/Fiji) (Schindelin *et al.*, 2012) combined with the Open-MIMS plug-in (http://nrims.harvard.edu/software). All images were dead-time corrected (Hillion *et al.*, 2008); the individual planes were then summed prior to extracting counts from the images. Isotopic quantification data were extracted from the mass images by manually drawing regions of interest around each single bacterial cell using the $^{12}C^{14}N^-$ image as mask. In contrast to the sample preparation used in Chapter 3 where samples had to be diluted 100 times prior filtration in order to avoid superimposition of cells, the opposite problem occurred in Chapter 4: samples had to be concentrated because of the relatively low densities of *Synechococcus* (10^3, 10^4, 10^5 cells ml^{-1}) and bacterial cells (10^6 cells ml^{-1}) used in the experiment. This concentration sometimes led to unwanted superimposition of cells. Particularly, we noticed that in the ^{15}N raw images generated by NanoSIMS, large areas of ^{15}N enrichment (here named 'halo') could be visualized around single *Synechococcus* cells. The $^{15}N/^{14}N$ ratio of regions of interests (ROIs) drawn within and outside these ^{15}N enriched halos showed that they were abnormally enriched. These halos artificially altered the $^{15}N/^{14}N$ ratio measured in the bacteria occurring within these areas relatively to those outside. We therefore used the raw ^{15}N images to draw ROIs (ROI-halo) that clearly defined the boundaries of each halo around single *Synechococcus* cells, we then excluded from our dataset all the bacterial cells that fell within the ROI-halo, considering only bacteria outside the ROI-halo for our data analysis.

4.1.7 Atom fraction

The measured isotope ratios were converted to Atomic Percentage (Atom %), which gives the percentage of a specific atom within the total number of atoms. In this case, we calculated the percentage of ^{13}C and ^{15}N within the total number of carbon and nitrogen atoms following the formula:

$$Atom\% = \frac{^{15}\mathrm{N}}{(^{15}\mathrm{N} + {}^{14}\mathrm{N})} \times 100$$

Or

$$Atom\% = \frac{^{13}\mathrm{C}}{(^{13}\mathrm{C} + {}^{12}\mathrm{C})} \times 100$$

4.1.8 Statistical analysis

Shapiro-Wilk and Levene's test were respectively used to test the data for normality and homogeneity of variance. Since the data were not normally distributed and/or not homogeneous, Kruskal-Wallis H-test with multiple comparisons was used to test the ^{15}N enrichment of the three mutants at the same *Synechococcus* concentration and across different *Synechococcus* concentrations. The statistical software SPSS (version 23; IBM Corporation, Armonk, USA) was used to carry out all statistical tests. The outcomes of the tests are reported in Supplementary Table 4.3.

4.1.9 Normalisation of ^{13}C levels

The three bacterial phenotypes used here exhibited slightly different ^{13}C Atomic fractions (Supplementary Figure 4.2). To account for these initial differences in enrichment, all measured ^{13}C Atom% from *Synechococcus* cells were normalised to the respective initial ^{13}C Atom% of the bacterial cells. The normalised values were calculated as follow: firstly, the ^{13}C values of each *Synechococcus* cell were subtracted by the ^{13}C mean value measured in the control, obtaining values that can be named as A for simplicity.

A = ^{13}C value of *Synechococcus* cell – ^{13}C mean value of control

Secondly, each values A were then divided by the mean values of ^{13}C enrichment of the respective bacterial type which the *Synechococcus* cells were co-incubated with during the experiment. For example, the value A calculated from a *Synechococcus* cell

that was incubated with the WT bacteria at 1,000 *Synechococcus* cell ml^{-1} was divided by the mean of ^{13}C enrichment calculated for that bacterial group at that concentration, obtaining values B.

B = value A of *Synechococcus* incubated with WT bacteria / ^{13}C mean value of WT bacteria

Finally, the means of all the values B were calculated and used to generate Figure 4.2.

4.1.10 Model for single Synechococcus phycosphere landscape

In order to model the dissolved organic matter (DOM) landscape, individual *Synechococcus* cells were considered as point-wise particles, exuding DOM at a rate of *L* molecules/second. We began by considering the DOM concentration around a single *Synechococcus* cell in an unbounded, quiescent fluid. The molecules released diffused radially and were consumed by bacteria distributed throughout the domain. Owing to the spherical symmetry of the problem, both the DOM concentration, $C(r, t)$, and the bacterial concentration, $B(r, t)$, may be written as functions of radius *r* and time *t* only. The nutrient profile varied in space and time according to the diffusion equation (1) (Smriga *et al.*, 2016):

$$\frac{\partial C}{\partial t} = D\nabla^2 C - [4\pi a D B(r,t)]C$$

The molecular diffusion of DOM is captured by the first term on the right hand side of Eq. (1). We assumed a single molecular species, with diffusivity *D* ($\mu m^2/s$). The second term represents diffusion-limited consumption of the DOM source by bacteria. The parameter *a* is the bacterial cell radius of *Marinobacter adhaerens*. The distribution of bacteria, $B(r, t)$, will in general not be uniform, and will depend on $C(r, t)$. However, if we assume that bacteria are approximately uniformly distributed with concentration $B0$, Eq. (1) may be rewritten as (2):

$$\frac{\partial C}{\partial t} = D\nabla^2 C - kC$$

where the consumption rate is given by $k = 4\pi D B_0$. The steady state solution to Eq. (2) in spherical coordinates, which is finite at $r \to \infty$, is given by (3)

$$C(r) = \frac{A}{r}\exp\left(-\sqrt{\frac{k}{D}}r\right) = \frac{A}{r}\exp(-\sqrt{4\pi a B_0}\, r)$$

where $A > 0$ is an arbitrary constant. The radial flux of DOM through a spherical surface at $r = \epsilon \ll 1$ must match the leakage rate from the *Synechococcus* cell. That is, (4)

$$J = \lim_{r\to 0}\left(-D\,\frac{dC}{dr}\Big| \times 4\pi r^2\right) = 4\pi AD = L$$

It follows that (5)

$$C(r) = \frac{L}{4\pi Dr}\exp\left(-\sqrt{4\pi B_0}\, r\right)$$

Note that the above expression diverges at $r \to 0$. However, for any bacterium in the vicinity of the nutrient source, the maximum concentration of DOM occurs at the surface of *Synechococcus* (with radius $r_0 = 2\ \mu m$). The DOMD profile is therefore capped by this value, so that (6)

$$C(r) = \begin{cases} \dfrac{L}{4\pi D r_0}\exp\left(-\sqrt{4\pi a B_0}\, r_0\right), & \mathrm{r} \le r_0 \\ \dfrac{L}{4\pi Dr}\exp\left(-\sqrt{4\pi a B_0}\, r\right), & r > r_0 \end{cases}$$

We note that the total amount of DOM present in the domain, $\int C(r)dV$, is finite, as the phytoplankton leakage is balanced by bacterial consumption. It is possible to recover the nutrient profile in the absence of bacterial consumption by setting $B_0 = 0$. This functional form $C(r) = L/4\pi Dr$ is used elsewhere (Seymour *et al.*, 2017) in the case of single nutrient sources. However, for a suspension of *Synechococcus* cells, the long range nature of this function results in a divergent nutrient concentration. It is therefore necessary to utilise the profile shown in Eq. (6).

4.1.11 Model for multiple resources

To mimic the experimental system, we considered a rectangular ox with dimension l_x, l_y, l_z in the x, y, z directions respectively. This box is randomly seeded with N identical DOM sources at positions $\{x_i = (x_i, y_i, z_i)|i = 1,2, \dots, N\}$, so that the total density of *Synechococcus* cells is $\rho = N/(l_x l_y l_z)$. Linearity of the diffusion equation enables the

superposition of multiple solutions from Eq. (6). It follows that the total DOM concentration at position **x** is given by (7)

$$c(x) = \sum_{i=1}^{N} C_i(d_i)$$

where C_i is the expression in Eq. (6) and d_i is the distance between points **x** and $\mathbf{x}_i$. We utilized periodic boundary conditions to evaluate d_i, so that $d_i = |v_i|$ where $v_i = (x - x_i, y - y_i, z - z_i)\ mod(l_x, l_y, l_z)$. That is, the concentration from each pulse is evaluated by taking the shortest distance to it within the periodic domain. From Eqs. (6) and (7), it is also possible to directly evaluate the spatial gradient of the DOM field, given by $\nabla c(x)$. Note, however that there is no time-dependence in the field. A single 2D slice of the nutrient profile through the box domain with *Synechococcus* density $\rho = 10^3$ cells ml^{-1} is shown in Supplementary Figure 4.1.

4.1.12 Model for bacterial chemotaxis

We introduced bacteria to the three-dimensional DOM field defined by Eq. (7), and investigated their collective dynamics. The relative performance (nutrient exposure) of wild type bacteria compared to their non-chemotactic or non-motile counterparts was examined. To begin with, we outlined the agent-based model for bacterial chemotaxis. In the laboratory frame, the nutrient concentration was given by the smooth function c(x). In each simulation time-step Δt = 0.05 s, a bacterium with velocity **v** and position **X** performs a (noisy) measurement of the concentration change in its reference frame $\frac{\partial c_N}{\partial t} = N(\mu, \sigma^2)$. This stochastic measurement is normally distributed with mean $\mu = v \cdot \nabla c$ and standard deviation $\sigma = \prod[3c(\boldsymbol{X}, t)/\pi aDT^3]^{1/2}$, and therefore directly incorporates the fundamental precision with which a cell can measure the gradient. This measurement modifies the cell's mean run time according to the following equation (8):

$$\tau = \tau_0 \exp[\Gamma \times N(\mu, \sigma^2)]$$

A value of τ_0 = 0.25 s was chosen to ensure the unbiased bacterial diffusivity matched the observed experimental value. During each time-step, the probability of reorientation was given by $\Delta t/\tau$. Run-reverse-flick reorientation dynamics were included explicitly using known parameters derived for *Vibrio alginolyticus* (Son, Guasto and Stocker, 2013), and rotational diffusion with D_r = 0.0349 rad^2 s^{-1} perturbed the swimming direction at each time-step. Cell motility occurs in three dimensions, as in experiments, with swimming

bacteria subject to periodic boundary conditions. The sensory integration timescale is given as $T = 0.1$ s, the cell radius is taken to be $a = 0.5$ μm, the swimming speed $v = |\mathbf{v}| = 45$ μms^{-1}, and we use the diffusivity for glutamate, $D = 608$ μm^{2}s^{-1}. For the WT cells, we utilise recently measured parameters for *Vibrio ordalii*, $\prod_{sim} = 6.16$ and $\Gamma_{sim} = 0.0223$ s/μM. Initially seeded randomly within the domain, we simulated the 3D motion of 10^3 bacteria as they respond to the DOM landscape. Within the context of this model, it is straightforward to simulate non-chemotactic (Δ*che*A) or non-motile (Δ*fliC*) mutants by setting $\Gamma = 0$ or $v = 0$ respectively. We assessed the dynamics of wild type and non-chemotactic strains across a range of different DOM landscapes. Specifically, we considered the same concentrations of phytoplankton cells (10^3, 10^4 and 10^5 cells ml^{-1}) as used in the experiment. Results for non-motile mutants are not shown, as they are equal to the non-chemotactic case.

4.4 Results and discussion

Here we aimed to quantify the role of motility and chemotaxis on the exploitation of the *Synechococcus* phycosphere, by combining stable isotope labelling and NanoSIMS to compare the uptake of *Synechococcus*-derived ^{15}N molecules by three phenotypes of the same bacterial strain (*Marinobacter adhaerens* HP15): *i*) a chemotactic and motile bacteria (wild type, WT); *ii*) a non-chemotactic but motile mutant (Δ*che*A) (Sonnenschein *et al.*, 2012); and *iii*) a non-motile mutant (Δ*fli*C) (Sonnenschein *et al.*, 2011). We exposed each of these phenotypes to different ^{15}N-labelled-*Synechococcus* densities (10^3, 10^4 and 10^5 cells ml^{-1}), mimicking different natural scenarios (oligotrophic water, coastal water and bloom, respectively), and measured the bacterial incorporation of *Synechococcus*-derived ^{15}N at the single-cell level, over a three-hour incubation time. We employed ^{15}N as the principal chemical tracer in these experiments, because *Synechococcus* exudates are particularly rich in organic nitrogen and these compounds may be fundamental for the establishment of mutualistic interactions with heterotrophic bacteria (Chapter 3, (Christie-Oleza *et al.*, 2017)). Furthermore, the *M. adhaerens* were labelled with ^{13}C, in order to facilitate the localization of the bacteria with NanoSIMS and investigate potential reciprocal nutrient transfers.

All three bacterial phenotypes were significantly enriched in ^{15}N after three hours of co-incubation with *Synechococcus* (Kruskal Wallis Test (KW), $p<0.001$; Figure 4.1). However, their respective enrichments were strongly influenced by *i*) their behaviour (i.e. capacity for motility and chemotaxis) and *ii*) the background density of *Synechococcus* cells. For all *Synechococcus* densities, the average ^{15}N enrichment of the wild-type strain of *M. adhaerens* was always higher than the non-chemotactic and non-motile mutants (Figure. 4.1). These differences were most pronounced in the treatment with the lowest *Synechococcus* concentration (10^3 cells ml^{-1}) (Figure. 4.1 A), where the wild type strain was 2.4-fold more enriched than the non-motile mutants and 1.8-fold more than the non-chemotactic mutants (KW, $p<0.001$). At intermediate *Synechococcus* density (10^4 cells ml^{-1}) (Figure. 4.1 B), the wild type bacteria were 1.8-fold more enriched than non-chemotactic bacteria (KW, $p<0.001$) and 2.1-fold more enriched than non-motile bacteria, although this comparison was not statistically different. At both low and intermediate *Synechococcus* densities (10^3 and 10^4 cells ml^{-1}), the ^{15}N enrichment of non-chemotactic and non-motile mutants were not statistically different. The higher levels of enrichment of the wild type strain is manly determined by between 26 % and 22 % of cells that were

more enriched than the respective mean values measured in these two scenarios (Supplementary Figure 4.3 A and B). On the other hand, only between 10 % and 18 % of single cells of the non-chemotactic and non-motile bacteria had levels of enrichment higher than the mean values of the wild type strain.

These results not only provide the first experimental evidence that chemotaxis enhances the consumption of photosynthates by motile bacteria in heterogeneous resource landscapes, but demonstrate that even the phycosphere associated with small picocyanobacteria can be exploited. This latter point implies that previous theoretical approaches have underestimated the sensitivity and precision of chemotactic bacteria in the pelagic ocean, and have overlooked the importance of chemotaxis in the establishment of interactions between *Synechococcus* and heterotrophic bacteria. Given the high abundance of these key microbes, chemotaxis may have a large impact on the rate of biogeochemical transformations in the ocean.

At the highest *Synechococcus* density (10^5 cell ml^{-1}), differences in ^{15}N enrichment between the three phenotypes were not statistically different (Figure. 4.1C), but *M. adhaerens* cells were between 2.3 and 6.3-folds more enriched than they were in lower *Synechococcus* densities (Kruskal-Wallis $p<0.001$). In fact, all three bacterial strains showed that between 27 % and 30 % had higher levels of enrichment than the highest mean value (wild type) at high concentration of *Synechococcus* cells (Supplementary figure 4.3 C). This means that beyond a specific phytoplankton cell density, during bloom conditions for example, chemotaxis becomes less important to get access to photosynthates. This can be ascribed to higher concentrations of organic matter in the bulk seawater caused by the diffusion of photosynthates from *Synechococcus* phycospheres, together with the closed nature of our experimental system.

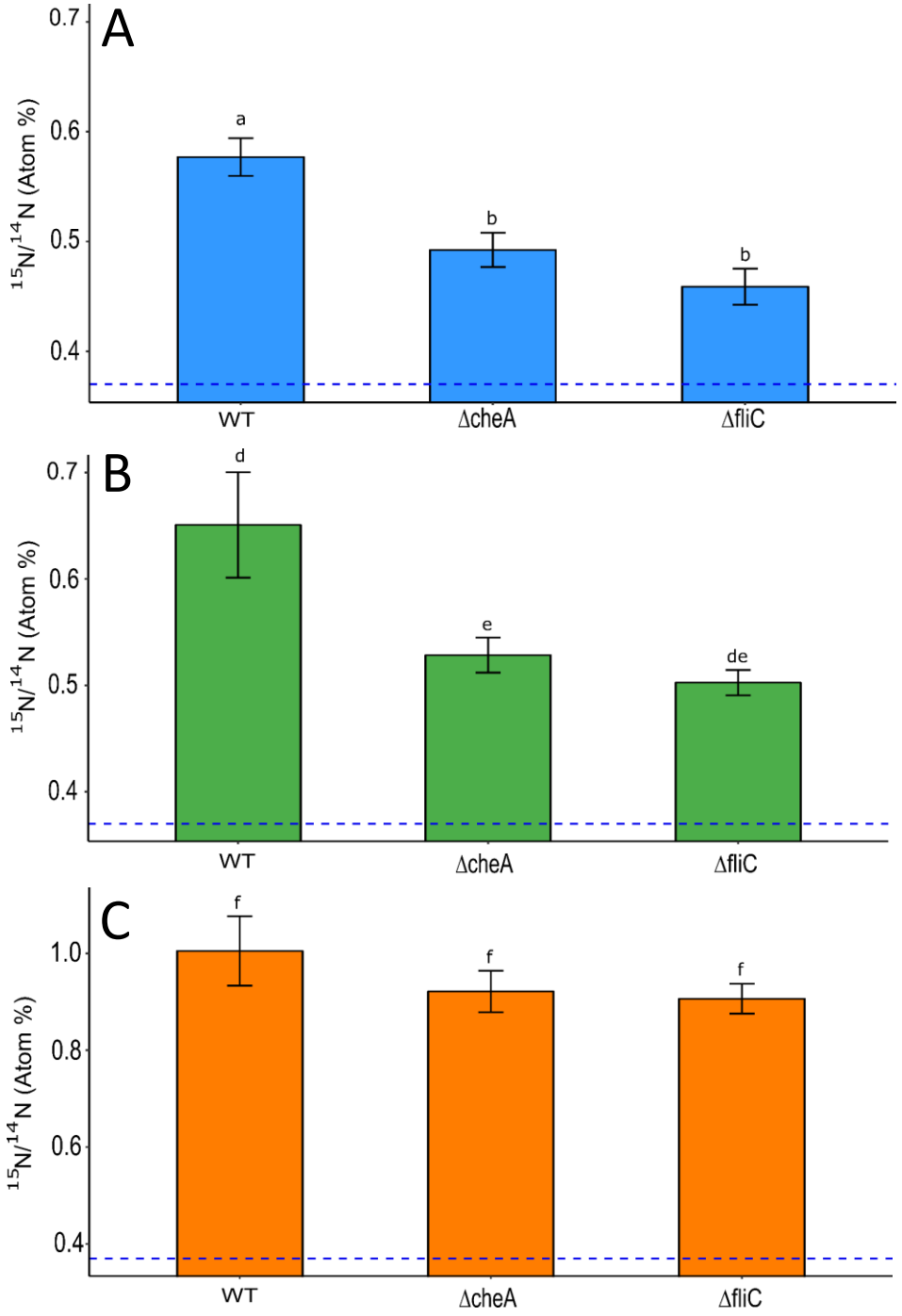

Figure 4.1 ^{15}N enrichment of *Marinobacter adhaerens* HP15 wild type (WT), motile and non-chemotactic (Δ*che*A), and non-motile (Δ*fli*C) at different *Synechococcus* concentrations: (**A**) 1,000 cells ml^{-1} (WT: 0.577 % ± 0.171, n = 376; Δ*che*A: 0.492 % ± 0.015, n = 262; Δ*fli*C: 0.458 % ± 0.016, n = 166; mean ± SEM); (**B**) 10,000 cells ml^{-1} (WT: 0.651 % ± 0.049, n = 470; Δ*che*A: 0.528 % ± 0.016, n = 419; Δ*fli*C: 0.502 % ± 0.012, n = 286; mean ± SEM); (**C**) 100,000 cells ml^{-1} (WT: 1.005 % ± 0.071, n = 181; Δ*che*A: 0.921 % ± 0.043, n = 172; Δ*fli*C: 0.907 % ± 0.031, n = 195; mean ± SEM). Dashed line: $^{15}N/^{14}N$ ratio in natural abundance calculated from the control (0.374 % ± 0.001 mean ± SEM, n = 120). Letters indicate statistics: significant differences are indicate by using different letters.

The exudates of *Synechococcus* are mainly constituted of low molecular weight compounds (Fiore *et al.*, 2015) and previous work has shown that they can attract chemotactic bacteria (Seymour *et al.*, 2010). These exuded compounds are enriched in amino acids and peptides (Fiore *et al.*, 2015; Christie-Oleza *et al.*, 2017; Ma, Coleman and Waldbauer, 2018) and bacteria, such as *Ruegeria pomeroyi*, when co-incubated with *Synechococcus*, increase the production of membrane transport proteins that allow their uptake (Christie-Oleza *et al.*, 2017). Given that amino acids are well known chemotactic cues (Bell and Mitchell, 1972; Mesibov and Adler, 1972; Gaworzewska and Carlile, 1982; Malmcrona-Friberg, Goodman and Kjelleberg, 1990), this class of molecules may play a role in the establishment of *Synechococcus*-heterotrophic bacteria interactions in the phycosphere. Further investigations should aim to assess the relative contribution of specific compounds exuded by *Synechococcus* to the chemotaxis response observed here.

Similarly to Chapter 3, all three bacterial phenotypes were pre-labelled with ^{13}C, as a means to identify these cells using NanoSIMS, but also to track eventual transfer of carbon to the cyanobacteria. *Synechococcus* assimilated bacterial-derived ^{13}C-labelled compounds during the co-incubation and after normalising our results to take into account the initial differences in ^{13}C enrichments between the three bacterial phenotypes (see methods), we determined that the ^{13}C enrichment in *Synechococcus* was influenced by the phenotype of the bacterial partners. Irrespectively of the *Synechococcus* density, the cyanobacterial cells co-incubated with the wild type *M. adhaerens*, exhibited consistently higher ^{13}C enrichment than the cells co-incubated with non-motile and non-chemotactic mutants (Figure. 4.2). However, *Synechococcus* uptake of bacterial-derived ^{13}C was only significantly different between wild type and non-chemotactic cells at the highest *Synechococcus* densities (10^5 cells ml^{-1}; Kruskal-Wallis $p<0.001$). This result suggest that prolonged close spatial interaction is required for *Synechococcus* to take up ^{13}C originating from the heterotrophic bacteria. These prolonged interactions are more likely to occur with chemotactic or non-motile cells, some of which will maintain their position in the phycosphere (either through active behaviour (wild type) or serendipity (non-motile)), than with the ever-moving non-chemotactic cells.

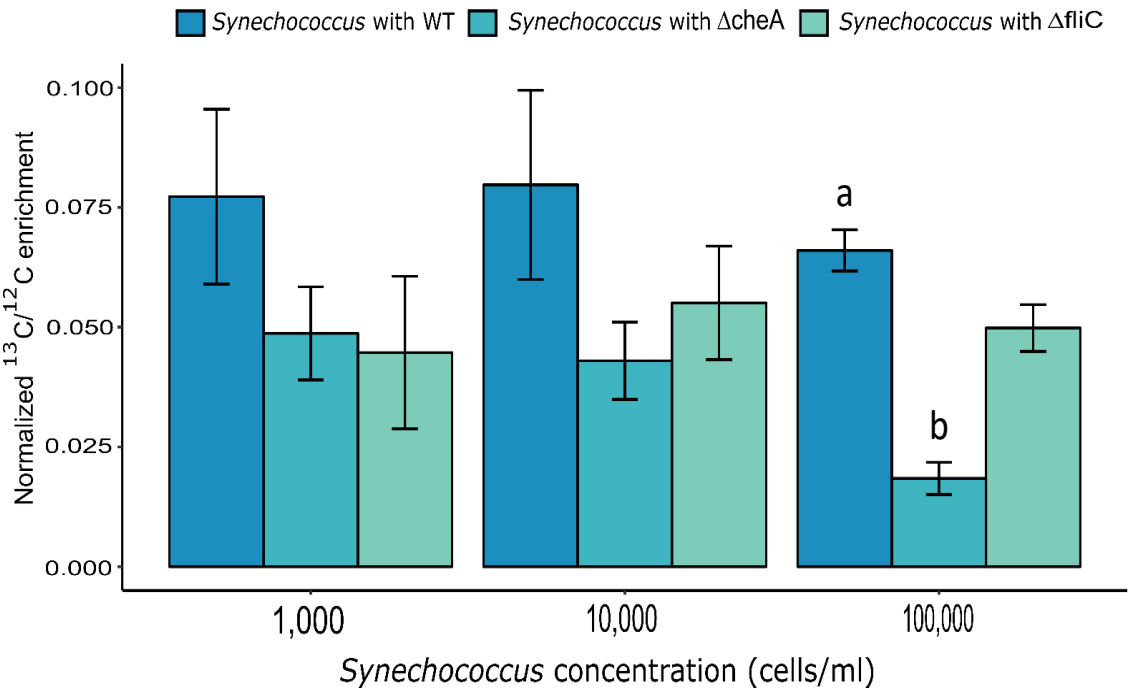

Figure 4.2 Normalized ^{13}C enrichment of *Synechococcus* cells in incubation with *Marinobacter adhaerens* wild type (WT), non-chemotactic (Δ*che*A) and non-motile (Δ*fli*C) in the three *Synechococcus* concentrations; Error bars: standard error; density 1,000 cells ml^{-1}: *Synechococcus* with WT (0.077 % ± 0.018 mean ± SEM, n = 10), *Synechococcus* with Δ*che*A (0.048 % ± 0.009 mean ± SEM, n = 11), *Synechococcus* with Δ*fli*C (0.045 % ± 0.016 mean ± SEM, n = 10); density 10,00 cells ml^{-1}: *Synechococcus* with WT (0.079 % ± 0.019 mean ± SEM, n = 23), *Synechococcus* with Δ*che*A (0.043 % ± 0.003 mean ± SEM, n = 17), *Synechococcus* with Δ*fli*C (0.055 % ± 0.012 mean ± SEM, n = 16); density 100,000 cells ml^{-1}: *Synechococcus* with WT (0.066 % ± 0.004 mean ± SEM), *Synechococcus* with Δ*che*A (0.018 % ± 0.003 mean ± SEM), *Synechococcus* with Δ*fli*C (0.049 % ± 0.005 mean ± SEM). Note: all the values displayed are above natural abundance.

To further explore the effect of behaviour on nutrient uptake, we developed a theoretical model that predicted the relative performance (nutrient exposure and uptake) of chemotactic bacteria to non-chemotactic or non-motile bacteria across a range of different dissolved organic matter (DOM) landscapes generated by *Synechococcus* cells, with conditions mimicking the experimental system. Specifically, we considered three different concentrations of 2 µm radius phytoplankton cells: 10^3, 10^4 and 10^5 cells ml^{-1}. Regarding the chemotactic cells, we considered a standard concentration of 10^3, 0.5 µm cell radius and 45 µm s^{-1} swimming speed calculated experimentally. The parameters used in the model are summarized in Table 4.1.

Table 4.1 Minimal model parameters used throughout, unless stated otherwise.

Variable	*Symbol*	*Value*
Nutrient diffusivity	D	608 $\mu m^2/s$
Nutrient leakage rate	L	2.04×10^{-17} mol/s
Phytoplankton radius	r_0	2 μm
Bacterial radius	a	0.5 μm
Swimming speed	v	45 $\mu m/s$
Mean run time	τ_0	0.25 s
Rotational diffusivity	D_r	$0.0349\,rad^2 s^{-1}$
Domain width	l_x	1100 - 5000 μm

Within the model, the positions of 10^3 bacteria, initially seeded randomly in a three dimensional realm (width 5,000 µm), were measured relative to modelled phycospheres, over the course of three hours, thereby matching the time in the experiments. The spatial distribution of chemotactic and non-chemotactic bacteria at the conclusion of the simulation were compared (Figure. 4.3). After the three hour period, 33 % of chemotactic bacteria were situated within the higher nutrient concentrations present in the *Synechococcus* phycosphere (Figure. 4.3A). Conversely, only 14 % of the non-chemotactic cells encountered the *Synechococcus* phycosphere by chance alone (Figure 4.3B). However, while the chemotactic bacteria aggregated within individual phycospheres, we emphasise that the trapping effect – the capacity of bacteria to satellite within the same phycosphere for extended periods – was not extremely strong, relatively to what was observed for larger phytoplankton (Smriga *et al.*, 2016), due to the small size of *Synechococcus* phycospheres and chemotactic cells did stochastically swim between different phycospheres.

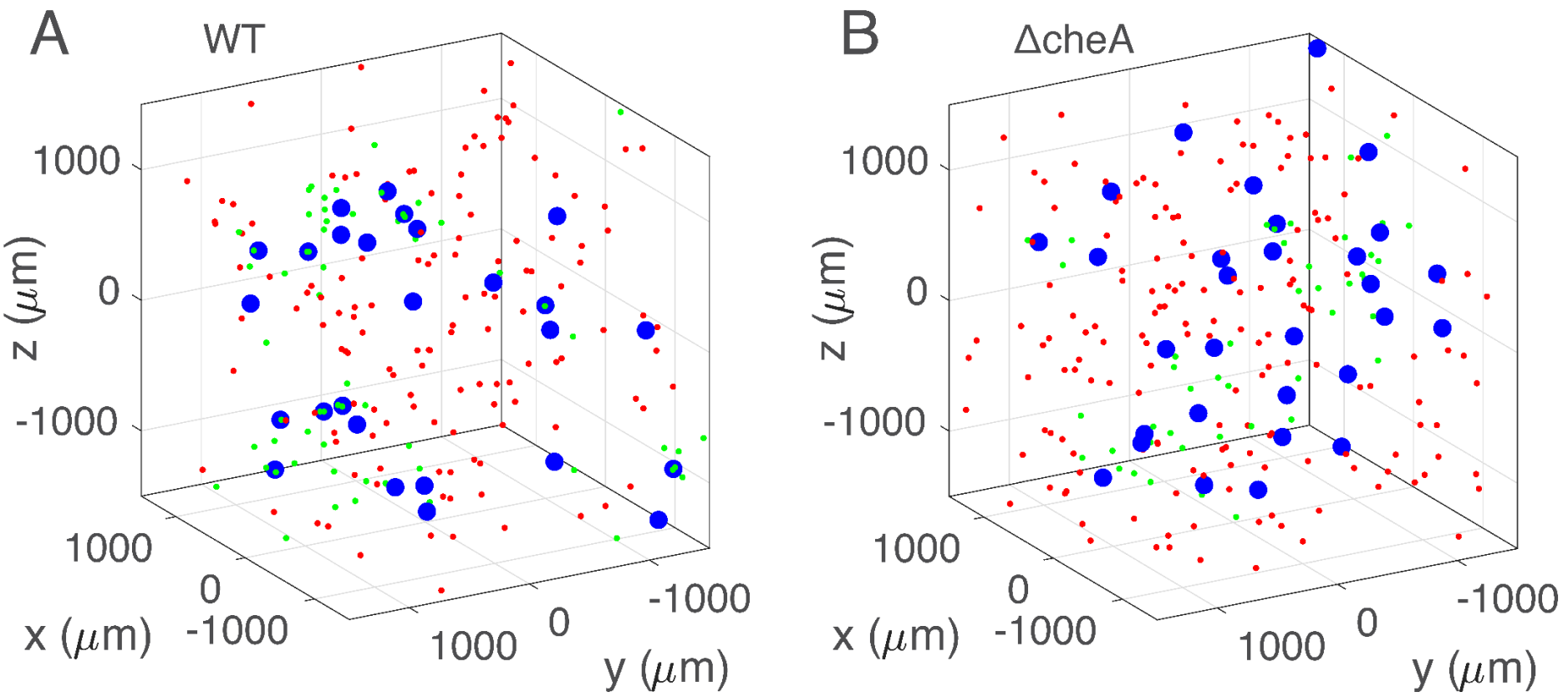

Figure 4.3 Spatial distribution of bacteria at the completion of the simulation (t = 3 hours). Results are shown for (**A**) wild type *Marinobacter adhaerens* as well as (**B**) non-chemotactic mutants (Δ*che*A). In each case, the *Synechococcus* cells are shown in blue, and bacteria are colour-coded based on whether their ambient nutrient concentration is higher (green) or lower (red) than 3 % of the nutrient concentration at the surface of a *Synechococcus* cell. For visual clarity, only small subset of the computation domain is shown. Results for non-motile cells (Δ*fli*C) are not presented, as they were equal to the non-chemotactic (Δ*che*A) mutants.

To quantify the differences in nutrient uptake between chemotactic and non-chemotactic cells, it is instructive to consider the average nutrient concentration experienced by each bacterial population as a function of time (Figure 4.4). For each value of ρ (*Synechococcus* density), both chemotactic and non-chemotactic populations began the simulation with the same mean nutrient exposure, because they were each seeded randomly in the domain. However, the nutrient exposure experienced by the chemotactic cells increased with time, reaching a higher equilibrium than the non-chemotactic cells (Figure. 4.4): the timescale necessary to reach the steady state decreased, with increasing ρ. At higher phytoplankton concentrations, it took less time for the chemotactic bacteria to reach their nearest phycosphere. However, the steady state value was attained early in the simulations in all *Synechococcus* concentration, indicating that three hours incubation is sufficient to capture the quantitative differences between the different bacterial phenotypes. In-line with the experimental observations, the relative increase in nutrient exposure due to chemotaxis is most pronounced at lower values of ρ, which is driven by the increase in background nutrient concentration for higher cell densities. At $\rho = 10^3$ cells ml^{-1}, the nutrient exposure of chemotactic cells was approximately twice that experienced by non-chemotactic cells. However, at $\rho = 10^5$ cells ml^{-1}, that relative advantage is reduced to ~20 %.

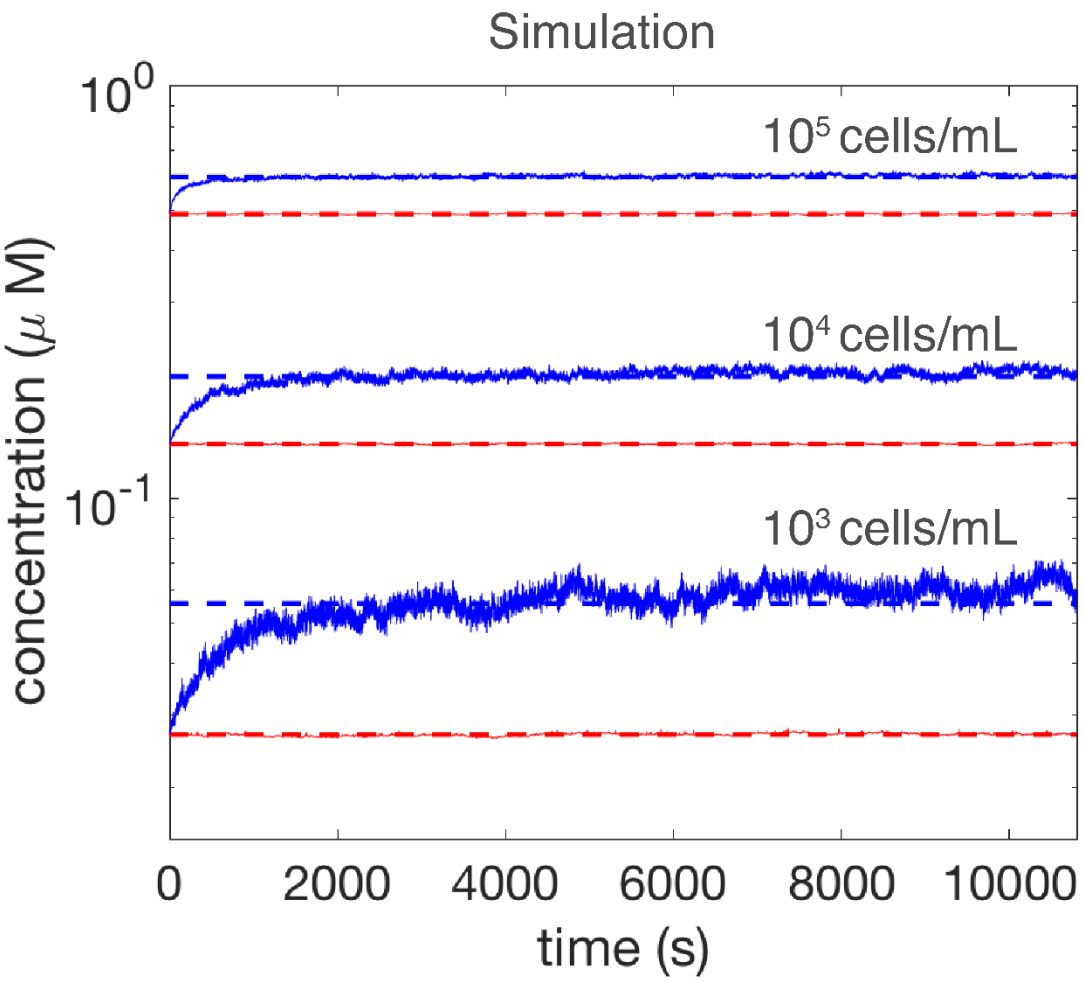

Figure 4.4 Potential uptake for wild type *Marinobacter adhaerens* (blue) and non-chemotactic mutants (red) as functions of time for three different phytoplankton concentrations, 10^3, 10^4 and 10^5 cells ml^{-1}. The potential uptake (vertical axis) was represented on a logarithmic scale. The mean value of each curve is represented by a dotted line. Results for non-motile cells (Δ*fli*C) are not presented, as they were equal to the non-chemotactic (Δ*che*A) mutants.

Although the relative advantage of chemotaxis is clear in these simulations, it is noteworthy that the overall nutrient uptake by the heterotrophic bacteria is strongly affected by changes in the value of ρ. Similarly to the experimental observations, increasing the phytoplankton concentration by a factor of 10 has a greater effect on the bacterial uptake than the inclusion of chemotaxis (Figure. 4.5).

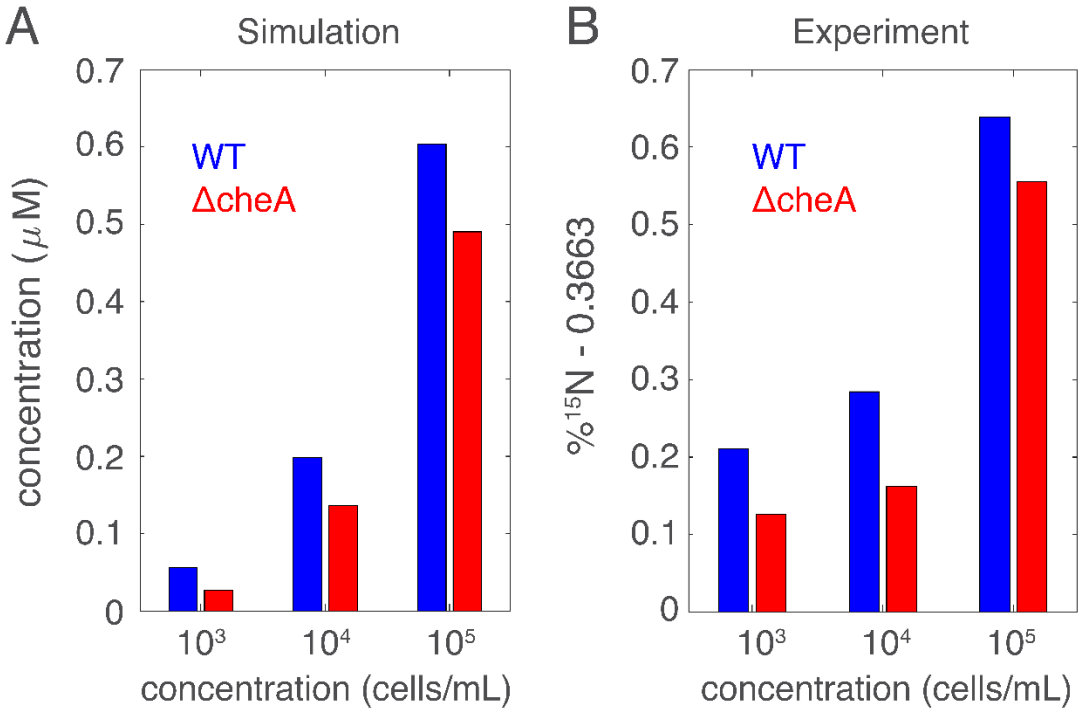

Figure 4.5 Population-averaged nutrient concentration for *Marinobacter adhaerens* WT (blue) and Δ*che*A (red) cells, for three different *Synechococcus* concentrations. Results are shown for (**A**) numerical simulations as well as (**B**) NanoSIMS experiments. The results highlight the advantage conferred by chemotaxis across several orders of magnitude in ρ. Results for non-motile cells (Δ*fli*C) are not presented, as they were equal to the non-chemotactic (Δ*che*A) mutants.

Here we demonstrate the importance of bacterial behaviour in the consumption of chemicals released by small phytoplankton. While the potential importance of bacterial chemotaxis in the pelagic ocean has been mostly derived from laboratory observations of bacterial chemotaxis (Stocker *et al.*, 2008; Smriga *et al.*, 2016) and theoretical approaches (Fenchel 2001; Kiørboe & Jackson 2001; Stocker & Seymour 2012; Seymour et al. 2017), our application of NanoSIMS to directly quantify and compare nutrient uptake provides the first direct quantitative evidence for the beneficial role of bacterial chemotaxis within patchy pelagic seascapes. Significantly, we show that chemotaxis imparts a significant advantage to heterotrophic bacterial cells responding to the phycosphere associated with small picocyanobacteria, which had once been thought too small to generate a phycosphere that could be detected by swimming bacteria (Jackson, 1987; Seymour *et al.*, 2017). This provides a new mechanism by which pelagic autotrophs and heterotrophs may interact, within both ecological and metabolic contexts, across the vast regions of the oligotrophic ocean where phototrophic biomass is dominated by small picocyanobacteria. As a consequence, chemotaxis may play an even greater role in ocean microbial ecology and biogeochemistry than previously been thought.

5 Chapter 5 - General Discussion

This thesis has delivered important new insights into our understanding of the intimate interactions between one of the smallest and numerically dominant photosynthetic organisms in the ocean, the picocyanobacteria *Synechococcus* and heterotrophic bacteria. This was achieved by applying cutting-edge single cell analytical approaches, including Secondary Ion Mass Spectrometry (SIMS), to identify microscale metabolic interactions that would have otherwise remained unobserved using traditional bulk-scale analysis techniques. These single cell approaches enabled me to demonstrate the occurrence of reciprocal chemical exchanges between *Synechococcus* and heterotrophic bacteria, along with the potentially important, but until now over-looked, role of bacterial behaviour in these interactions. These observations provide transformative insights into the complex metabolic exchanges taking place between abundant phototrophic microbes and heterotrophic bacteria in the ocean and have implications for our understanding of microbial ecology and biogeochemistry of large parts of the ocean where picocyanobacteria dominate the phototrophic biomass.

5.1 From the bulk-scale to the micro-scale

Bulk-scale approaches, such as Elemental Analyser-Isotope Ratio Mass Spectrometry, in combination with stable isotope tracers, have often been used in microbial ecology for measuring the transfer and assimilation of chemicals across different compartments of the microbial food-web (Montoya *et al.*, 1996; Boschker *et al.*, 1998; Hinrichs *et al.*, 1999). For example, in microbial oceanography, metabolic activity is often measured through the incorporation if isotopes (e.g. ^{13}C, ^{15}N) by the total biomass collected from large volumes (1-10 L) of seawater. Whilst bulk-scale approaches remain fundamental for quantifying microbial-mediated processes, they are disconnected from the metabolic dynamics that take place at the microbial scale (Stocker, 2015). The results presented in **Chapter 2** contrast the advantages and disadvantages of measurements of ^{15}N uptake by *Synechococcus* using three mass spectrometers, each with different resolution: EA-IRMS (bulk-scale), Time of Flight-Secondary Ion Mass Spectrometry (1-5 µm) and nano-scale secondary ion mass spectrometry (sub-50 nm). EA-IRMS was suitable for bulk measurements because of its high accuracy, low cost and the simplicity of sample preparation, making it ideal for analysing large numbers of samples (e.g. those collected during lengthy oceanographic voyages) when quantification of the background average

suffices. However, the results obtained using this method preclude insights into the metabolic dynamics occurring at the single-cell level. In contrast, ToF-SIMS allows for molecular characterisation at the micrometre-scale. Yet the small size of *Synechococcus* cells fell below the limits of instrument resolution, meaning it was not possible to distinguish between either single cells or aggregates of cells and in addition, the detection of specific organic compounds was vastly restricted. Nevertheless, this technique did allow for the measurement of an increase in the incorporation of ^{15}N into C_3N^- and CNO^-, both of which are signatures for peptides. Finally, the sub-micron resolution of NanoSIMS allowed for very high spatial -resolution measurements, revealing high levels of variability in ^{15}N enrichment between *Synechococcus* cells, indicating metabolic heterogeneity between individual cells or unequal distribution of nitrogen isotopes during cell division. The findings of **Chapter 2**, therefore, revealed the relative strengths and limitations of the three techniques, and critically, highlighted the importance of examining microbial-mediated processes at the single cell level. Based on these results, I chose to apply NanoSIMS in both **Chapters 3** and **4**, in order to address some fundamental ecological questions related to the metabolic interactions of *Synechococcus* with heterotrophic bacteria at the microscale.

5.2 Metabolic interaction between *Synechococcus* and heterotrophic bacteria

Due to their abundance, the interactions between *Synechococcus* and heterotrophic bacteria likely play a crucial role in marine biogeochemical cycles (Partensky, Blanchot, et al. 1999; Whitman et al. 1998). However, despite evidence of physical (Malfatti and Azam, 2009) and metabolic interactions (Christie-Oleza *et al.*, 2017) between these two partners, the dynamics of nutrient exchange at the single cell-level have been largely overlooked. The results presented in **Chapter 3** demonstrate the occurrence of reciprocal nitrogen and carbon exchange between ^{15}N-labelled *Synechococcus* and two bacterial strains isolated from cultures of this *Cyanobacterium* (*Erythrobacter* MG_01 and *Shimia* MG_02 – both pre-enriched with ^{13}C), highlighting the distinctive metabolic dynamics of these associations. The significant increase in ^{15}N enrichment of free-living *Erythrobacter* MG_01 and *Shimia* MG_02 indicated that they increasingly consumed *Synechococcus*-derived organic nitrogen exuded into the surrounding medium over time. *Erythrobacter* MG_01 assimilated 3-times more ^{15}N than *Shimia* MG_02, highlighting different metabolic features of these two bacteria at the single-cell level. Perhaps surprisingly, given the small size of *Synechococcus*, both heterotrophic bacteria were also

found physically attached to individual *Synechococcus* cells. Quantification of ^{15}N enrichment in these cells revealed that attachment led to an order of magnitude higher levels of enrichment than by non-attached cells. These attached cells maintained a high level of enrichment over time, suggesting that attached bacteria not only experience constant high levels of nutrients, but also exploit them more quickly than non-attached cells, thus consequently cycling nutrients at a higher rate, highlighting the ecological advantage of maintaining close spatial proximity.

Studies of interactions between eukaryotic phytoplankton and heterotrophic bacteria have demonstrated complex interdependencies with the bacterial partners benefiting from exuded organic compounds, while reciprocally supplying growth promoters (e.g. IAA) (Amin *et al.*, 2015) and vitamins (e.g. vitamin B12) to the phytoplankton (Croft *et al.*, 2005). In the association between *Synechococcus* and heterotrophic bacteria, it has been demonstrated that the latter provide regenerated nitrogen in the form of ammonia to the picocyanobacteria, in exchange for nitrogen-based organic compounds (Christie-Oleza *et al.*, 2017). Our results confirm the transfer of nitrogenous compounds from the *Synechococcus* to heterotrophic bacteria, and also provides further complexity to our current understanding of the interactions between these groups of bacteria. NanoSIMS analysis revealed a transfer of ^{13}C-labelled molecules from both *Erythrobacter* MG_01 and *Shimia* MG_02 to *Synechococcus*. Interestingly, *Shimia* MG_02, which took up less ^{15}N from *Synechococcus*, transferred 6-times more ^{13}C than *Erythrobacter* MG_01. While the potentially photoheterotrophic metabolism of *Synechococcus* has been widely reported (Cottrell and Kirchman, 2009), these results are striking because they indicate that associated heterotrophic bacteria may contribute to the organic carbon requirements of *Synechococcus* cells. Therefore, future studies should aim to identify heterotrophic partners that promote nutrient cycling in association with *Synechococcus*, *in situ*, and to characterise the specific metabolites exchanged within this microbial consortium in order to disentangle the complex chemical network connecting these two associates. Such research focus would greatly enhance existing knowledge on the role of heterotrophic bacteria in sustaining the productivity of one of key photosynthetic organisms in the oceans.

The capacity of bacteria to exploit *Synechococcus*-derived organic matter, as demonstrated in **Chapter 3**, raised questions about the implications of bacterial behaviour

in the establishment of *Synechococcus*-heterotrophic bacteria interactions. This led me to investigate the role of bacterial chemotaxis and motility in the exploitation of organic matter exuded by *Synechococcus* at the single-cell level in **Chapter 4**.

5.3 The role of bacterial behaviour in the exploitation of *Synechococcus* phycosphere

Chemotaxis – the ability of motile bacteria to modulate their movement in response to chemical gradients – can increase the encounter rate of marine heterotrophic bacteria with phytoplankton cells (Stocker & Seymour 2012). This is important because in the open oceans, the distance between a heterotrophic bacterium and the nearest photosynthetic organism can be hundreds to thousands of body lengths and efficient chemical exchanges will often require intimate spatial associations (Seymour et al. 2017). There is growing evidence that chemotactic behaviour by marine bacteria might promote interactions between phytoplankton and heterotrophic bacteria, increasing bacterial consumption of organic matter within the phycosphere, and even affect biogeochemical cycling processes and marine productivity (Stocker *et al.*, 2008; Smriga *et al.*, 2016). However, results presented in **Chapter 4** provide the first direct quantification of the role of chemotaxis in exploiting the *Synechococcus* phycosphere at the micro-scale, showing that bacterial chemotaxis enhances uptake of *Synechococcus* derived organic material. I coupled NanoSIMS measurements and a mathematical model to unravel the spatiotemporal dynamics of *Synechococcus*-derived nitrogen uptake by a chemotactic bacterium and two different impaired mutants, for three densities of *Synechococcus* mimicking real environmental scenarios. At low *Synechococcus* densities, chemotaxis enhanced the bacterial uptake of ^{15}N-labeled photosynthates by up to 2.4-folds relative to non-motile mutants. Conversely, at high *Synechococcus* densities, although ^{15}N uptake increased there were no statistically-distinguishable difference between the three different bacteria phenotypes, likely as a result of the higher volume of nutrients released into the bulk media. The mathematical model not only strengthened these findings by predicting similar responses based on the same conditions and cell densities that were used experimentally, but also allowed further exploration of the dynamics of nutrient exploitation for the three bacterial phenotypes. The model predicted that, at low *Synechococcus* density, chemotactic bacteria experience higher concentrations of nutrients in a shorter timeframe than non-chemotactic bacteria. Furthermore, it showed that the size of the *Synechococcus* phycosphere was large enough to be detected and

exploited by chemotactic cells, but was still too small to retain most bacteria. By the end of the experiment, 33 % of the chemotactic population were located within the *Synechococcus* phycosphere compared to only 14 % of the non-chemotactic cells. These findings provide clear quantitative evidence that chemotaxis increases consumption of nutrients, and overturns the paradigm that the *Synechococcus* phycosphere is too small to be detectable chemotactically. Despite previous studies that have shown that chemotactic bacteria are attracted towards *Synechococcus* exudates (Seymour *et al.*, 2010), the identity of specific chemical cues is still unknown. However, mass spectrometry-based studies are deciphering the composition of *Synechococcus* exudates, revealing that they are mainly constituted of low molecular weight compounds (Fiore *et al.*, 2015; Ma, Coleman and Waldbauer, 2018). Therefore, future studies should aim to test the chemotactic response of *Synechococcus*-associated bacteria towards specific exuded chemicals to address which are the molecular triggers of this interaction. In addition, within the spirit of the work by Smriga et al. (2016), direct microscopic observation of chemotactic responses towards the small phycosphere of single *Synechococcus* cells might verify the weak trapping effect predicted by the mathematical model.

5.4 An intricate network at the single-cell level

The results presented in this thesis fill several gaps in the existing knowledge surrounding the interactions occurring between one of the most abundant photosynthetic organism on Earth – the cyanobacterium *Synechococcus* – and heterotrophic bacteria. The application of high-resolution imaging techniques coupled with stable isotopes labelling and combined with traditional microbiology allowed to zoom in on these complex and dynamic interactions - which I have synthesized in Figure 5.1. Together, these results provide the first comprehensive study at the single-cell level of a partnership that has been previously overlooked but that shapes the ocean biogeochemistry. Additionally, the datasets generated in this thesis should be integrated into modelling frameworks in order to quantify and predict more accurately the impact of these single-cell interactions onto global biogeochemical cycles.

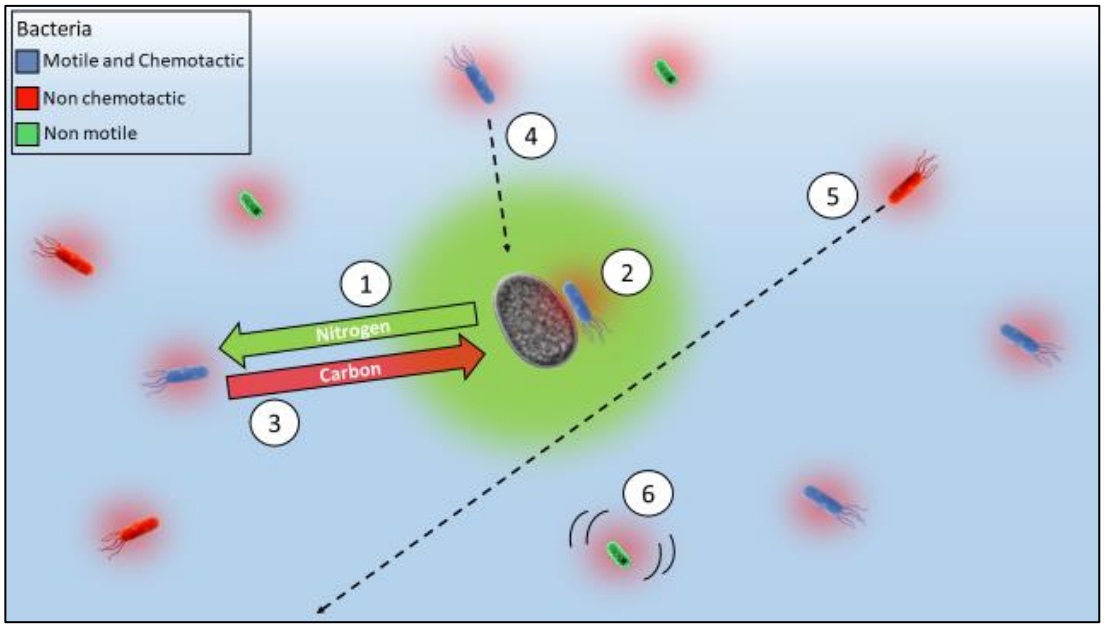

Figure 5.1 Schematic representation of the single-cell interactions between *Synechococcus* (grey in the centre) and heterotrophic bacteria (Blue, Red and Green) summarising main findings of this thesis: (1) *Synechococcus* cell exudes organic Nitrogen (green halo) which is consumed by heterotrophic bacteria. (2) Bacteria that can attach to *Synechococcus* have access to higher concentrations of Nitrogen than those not attached. (3) In return, heterotrophic bacteria release organic Carbon (red halo) that is consumed by *Synechococcus*. Bacterial behaviour plays an important role on the transfer of nutrients. In fact, (4) bacteria that are both motile and chemotactic consume more *Synechococcus*-derived Nitrogen as they have higher chances of encountering cells than (5) non chemotactic and (6) non motile cells.

5.5 Conclusion remarks

My PhD thesis has expanded knowledge on the micro-scale metabolic interactions between two ubiquitous, ecologically important and numerically abundant groups of marine microbes - *Synechococcus* and heterotrophic bacteria. This research ultimately permitted a focussed understanding of the biochemical dynamics of these interactions that will likely define the chemistry of large parts of the ocean. My thesis has shown that (i) *Synechococcus* and heterotrophic bacterial cells participate in reciprocal exchanges of nutrients that are facilitated by microscale proximity of cells; (ii) heterotrophic bacteria rapidly assimilate nitrogenous compounds exuded by *Synechococcus*; (iii) *Synechococcus* assimilates organic carbon supplied by heterotrophic bacteria and (iv) chemotaxis by heterotrophic bacteria substantially enhances uptake of *Synechococcus*-derived substrates, indicating that marine bacteria have a greater capacity to exploit the phycosphere associated with picoplankton than previously thought. These results highlight the potentially profound significance of microscale ecological interactions among pelagic microorganisms, even within the oligotrophic ocean, where picocyanobacteria dominate phototrophic biomass.

6 References

Achlatis, M. *et al.* (2018) 'Single-cell measurement of ammonium and bicarbonate uptake within a photosymbiotic bioeroding sponge', *ISME Journal*. Springer US, pp. 1–11. doi: 10.1038/s41396-017-0044-2.

Ackermann, M. (2015) 'A functional perspective on phenotypic heterogeneity in microorganisms', *Nature Reviews Microbiology*. Nature Publishing Group, 13(8), pp. 497–508. doi: 10.1038/nrmicro3491.

Adams, D. G. (2000) 'Heterocyst formation in cyanobacteria', *Current Opinion in Microbiology*, 3(6), pp. 618–624. doi: 10.1016/S1369-5274(00)00150-8.

Aharonovich, D. and Sher, D. (2016) 'Transcriptional response of Prochlorococcus to co-culture with a marine Alteromonas: Differences between strains and the involvement of putative infochemicals', *ISME Journal*. Nature Publishing Group, 10(12), pp. 2892–2906. doi: 10.1038/ismej.2016.70.

Alonso, C. *et al.* (2012) 'HISH-SIMS analysis of bacterial uptake of algal-derived carbon in the Rio de la Plata estuary', *Systematic and Applied Microbiology*. Elsevier GmbH., 35(8), pp. 541–548. doi: 10.1016/j.syapm.2012.08.004.

Amaro, A. M. *et al.* (2005) 'Identification and characterization of potentially algal-lytic marine bacteria strongly associated with the toxic dinoflagellate Alexandrium catenella', *Journal of Eukaryotic Microbiology*, 52(3), pp. 191–200. doi: 10.1111/j.1550-7408.2005.00031.x.

Amin, S. *et al.* (2015) 'Interaction and signalling between a cosmopolitan phytoplankton and associated bacteria', *Nature*. doi: 10.1038/nature14488.

Amin, S. A. *et al.* (2009) 'Photolysis of iron-siderophore chelates promotes bacterial-algal mutualism.', *Proceedings of the National Academy of Sciences of the United States of America*. National Academy of Sciences, 106(40), pp. 17071–6. doi: 10.1073/pnas.0905512106.

Amin, S., Parker, M. S. and Armbrust, E. V. (2012) 'Interactions between Diatoms and Bacteria', *Microbiology and Molecular Biology Reviews*, 76(3), pp. 667–684. doi: 10.1128/MMBR.00007-12.

Aota, Y. and Nakajima, H. (2001) 'Mutualistic relationships between phytoplankton and bacteria caused by carbon excretion from phytoplankton', *Ecological Research*, 16(2), pp. 289–299. doi: 10.1046/j.1440-1703.2001.00396.x.

Arandia-Gorostidi, N. *et al.* (2017) 'Elevated temperature increases carbon and nitrogen fluxes between phytoplankton and heterotrophic bacteria through physical attachment', *ISME Journal*, 11(3), pp. 641–650. doi: 10.1038/ismej.2016.156.

Azam, F. (1998) 'Microbial control of oceanic carbon flux: the plot thickens'.

Azam, F., Fenchel, T. and Field, J. (1983) 'The ecological role of water-column microbes in the sea.', *Marine ecology ...*, 10, pp. 257–263. Available at: http://www.soest.hawaii.edu/oceanography/courses/OCN621/Spring2011/Azam et al_loop.pdf (Accessed: 31 August 2014).

Azam, F. and Long, R. A. (2001) 'Sea snow microcosms', *Nature*, 414(June), pp. 495–498.

Azam, F. and Malfatti, F. (2007) 'Microbial structuring of marine ecosystems.', *Nature reviews. Microbiology*, 5(10), pp. 782–91. doi: 10.1038/nrmicro1747.

Beamson, G. and Briggs, D. (1992) 'High resolution monochromated X-ray photoelectron spectroscopy of organic polymers : A comparison between solid state data for organic polymers and gas phase data for small molecules', *Molecular Physics*, 76(4), pp. 919–936. doi: 10.1080/00268979200101761.

Behringer, G. *et al.* (2018) 'Bacterial communities of diatoms display strong conservation across strains and time', *Frontiers in Microbiology*, 9(APR), pp. 1–15. doi: 10.3389/fmicb.2018.00659.

Beliaev, A. S. *et al.* (2014) 'Inference of interactions in cyanobacterial-heterotrophic co-cultures via transcriptome sequencing', *ISME Journal*. Nature Publishing Group, 8(11), pp. 2243–2255. doi: 10.1038/ismej.2014.69.

Bell, W. H. and Mitchell, R. (1972) 'Chemotactic and Growth Responses Of Marine Bacteria to Algal Extracellular Products', *The Biological Bullettin*, 143(2), pp. 265–277. doi: 10.2307/2383716.

Berges, a. J. *et al.* (2001) 'Evolution of an Artificial Seawater Medium:Improvements in Enriched Seawater,Artificial Water Over the Last Two Decades', *J.Phycol*, 37, pp. 1138–1145. doi: 10.1046/j.1529-8817.2001.01052.x.

Biddanda, B. and Benner, R. (1997) 'Carbon, nitrogen, and carbohydrate fluxes during the production of particulate and dissolved organic matter by marine phytoplankton', *Limnology and Oceanography*, 42(3), pp. 506–518. doi: 10.4319/lo.1997.42.3.0506.

Biller, S. J., Coe, A. and Chisholm, S. W. (2016) 'Torn apart and reunited: Impact of a heterotroph on the transcriptome of Prochlorococcus', *ISME Journal*. Nature Publishing Group, 10(12), pp. 2831–2843. doi: 10.1038/ismej.2016.82.

Bjørnsen, P. K. (1988) 'Phytoplankton exudation of organic matter: Why do healthy cells do it?', *Limnology and Oceanography*, 33(1), pp. 151–154. doi: 10.4319/lo.1988.33.1.0151.

Blackburn, N., Fenchel, T. and Mitchell, J. (1998) 'Microscale Nutrient Habitats Patches Shown by in PLanktonic Chemotactic', *Science*, 282(5397), pp. 2254–2256. doi: 10.1126/science.282.5397.2254.

Bonnet, S. *et al.* (2016) 'Diazotroph derived nitrogen supports diatom growth in the South West Pacific: A quantitative study using nanoSIMS', *Limnology and Oceanography*, 61(5), pp. 1549–1562. doi: 10.1002/lno.10300.

Boschker, H. T. S. *et al.* (1998) 'Direct linking of microbial populations to specific biogeochemical processes by 13C-labelling of biomarkers', *Nature*, 392(6678), pp. 801–804. doi: 10.1038/33900.

Boschker, H. T. S. and Middelburg, J. J. (2002) 'Stable isotopes and biomarker in microbial ecology', *FEMS Microbiology Ecology*, 40(January), pp. 85–95.

Bowen, J. D. *et al.* (1993) 'Simulating bacterial clustering around phytoplankton cells in a turbulent ocean', *Limnology and Oceanography*, 38(1), pp. 36–51.

Bratbak, G. and Thingstad, T. (1985) 'Phytoplankton-bacteria interactions: an apparant paradox? Analysis of a model system with both competition and commensalism ', *Marine Ecology Progress Series*, 25, pp. 23–30. doi: 10.3354/meps025023.

Bronk, D. a (1999) 'Rates of NH4+ uptake, intracellular transformation and dissolved organic nitrogen release in two clones of marine Synechococcus spp.', *Journal of Plankton Research*, 21(7), pp. 1337–1353. doi: 10.1093/plankt/21.7.1337.

Buchan, A. *et al.* (2014) 'Master recyclers: features and functions of bacteria associated with phytoplankton blooms.', *Nat Rev Microbiol*. Nature Publishing Group, 12(August), pp. 686–698. doi: 10.1038/nrmicro3326.

Buchan, A. and Moran, M. A. (2005) 'MINIREVIEW Overview of the Marine Roseobacter Lineage †', 71(10), pp. 5665–5677. doi: 10.1128/AEM.71.10.5665.

Carpenter, K. J. *et al.* (2018) 'Single-Cell View of Carbon and Nitrogen Acquisition in the Mixotrophic Alga Prymnesium parvum (Haptophyta) Inferred From Stable Isotope Tracers and NanoSIMS', *Fronitiers in Marine Science*, 5(May), pp. 1–11. doi: 10.3389/fmars.2018.00157.

Chen, L. J. *et al.* (2011) 'Characterization and quantification of nanoparticle-antibody conjugates on cells using C60 ToF SIMS in the event-by-event bombardment/detection mode', *International Journal of Mass Spectrometry*. Elsevier B.V., 303(2–3), pp. 97–102. doi: 10.1016/j.ijms.2011.01.001.

Chen, M.-H. *et al.* (2011) 'Shimia isoporae sp. nov., isolated from the reef- building coral Isopora palifera', *International journal of systematic and evolutionary microbiology*, 61(2011), pp. 823–827. doi: 10.1099/ijs.0.022848-0.

Choi, D. H. and Cho, B. C. (2006) 'Shimia marina gen. nov., sp. nov., a novel bacterium of the Roseobacter clade isolated from biofilm in a coastal fish farm', *International Journal of Systematic and Evolutionary Microbiology*, 56(8), pp. 1869–1873. doi: 10.1099/ijs.0.64235-0.

Christie-Oleza, J. a. *et al.* (2017) 'Nutrient recycling facilitates long-term stability of marine microbial phototroph-heterotroph interactions', *Nature Microbiology*. Nature Publishing Group, 2(June). doi: 10.1038/nmicrobiol.2017.100.

Christie-Oleza, J. A. *et al.* (2015) 'Functional distinctness in the exoproteomes of marine Synechococcus', *Environmental microbiology*, 17(10), pp. 3781–3794. doi: 10.1111/1462-2920.12822.

Christie-Oleza, J. A., Scanlan, D. J. and Armengaud, J. (2015) '"You produce while I clean up", a strategy revealed by exoproteomics during Synechococcus-Roseobacter interactions', *Proteomics*, 15(20), pp. 3454–3462. doi: 10.1002/pmic.201400562.

Cole, J. J. (1982) 'Interactions Between Bacteria and Algae in Aquatic Ecosystems', *Annual Review of Ecology and Systematics*, 13(1), pp. 291–314. doi: 10.1146/annurev.es.13.110182.001451.

Cottrell, M. T. and Kirchman, D. L. (2009) 'Photoheterotrophic microbes in the Arctic Ocean in summer and winter.', *Applied and environmental microbiology*. American Society for Microbiology, 75(15), pp. 4958–66. doi: 10.1128/AEM.00117-09.

Crespi, B. J. (2001) 'The evolution of social behavior in microorganisms', *Trends in Ecology & Evolution*, 16(4), pp. 178–183. doi: 10.1016/S0169-5347(01)02115-2.

Croft, M. T. *et al.* (2005) 'Algae acquire vitamin B12 through a symbiotic relationship with bacteria.', *Nature*, 438(7064), pp. 90–93. doi: 10.1038/nature04056.

Denner, E. B. M. *et al.* (2002) 'Erythrobacter citreus sp. nov., a yellow-pigmented bacterium that lacks bacteriochlorophyll a, isolated from the western Mediterranean Sea', *International Journal of Systematic and Evolutionary Microbiology*, (2002), pp. 1655–1661. doi: 10.1099/ijs.0.01885-0.Abbreviations.

Dumont, M. G. and Murrell, J. C. (2005) 'Stable isotope probing - linking microbial identity to function', 3(June), pp. 499–504.

Durham, B. P. *et al.* (2014) 'Cryptic carbon and sulfur cycling between surface ocean plankton', *Proc Natl Acad Sci U S A*, in review(2), pp. 453–457. doi: 10.1073/pnas.1413137112.

Eakins, B. and Sharman, G. (2010) *Volumes of the World's Oceans from ETOPO1*. NOAA National Geophysical Data Center, Boulder, CO). Available at: https://www.ngdc.noaa.gov/mgg/global/etopo1_ocean_volumes.html (Accessed: 17 August 2018).

Evrard, V. *et al.* (2010) 'Carbon and nitrogen flows through the benthic food web of a photic subtidal sandy sediment', *Marine Ecology Progress Series*, 416, pp. 1–16. doi: 10.3354/meps08770.

Falkowski, P. G. (1994) 'The role of phytoplankton photosynthesis in global biogeochemical cycles', *Photosynthesis Research*, 39(3), pp. 235–258. doi: 10.1007/BF00014586.

Falkowski, P. G., Fenchel, T. and Delong, E. F. (2008) 'The microbial engines that drive earth's biogeochemical cycles', *Science*, 320(5879), pp. 1034–1039. doi: 10.1126/science.1153213.

Fearn, S. (2015) *An introduction to time-of-flight secondary ion mass spectrometry (ToF-SIMS) and its application to materials science*. IOP Publishing, Bristol, UK. doi: 10.1088/978-1-6817-4088-1ch5.

Fenchel, T. (2001) 'Eppur si muove: Many water column bacteria are motile', *Aquatic Microbial Ecology*, 24(2), pp. 197–201. doi: 10.3354/ame024197.

Field, C. B. *et al.* (1998) 'Primary production of the biosphere: integrating terrestrial and oceanic components', *Science (New York, N.Y.)*. American Association for the Advancement of Science, 281(5374), pp. 237–40. doi: 10.1126/SCIENCE.281.5374.237.

Finzi-Hart, J. a *et al.* (2009) 'Fixation and fate of C and N in the cyanobacterium Trichodesmium using nanometer-scale secondary ion mass spectrometry.', *Proceedings of the National Academy of Sciences of the United States of America*, 106(15), pp. 6345–6350. doi: 10.1073/pnas.0810547106.

Fiore, C. L. *et al.* (2015) 'Release of ecologically relevant metabolites by the cyanobacterium Synechococcus elongates CCMP 1631', *Environmental microbiology*, 17(10), pp. 3949–3963. doi: 10.1111/1462-2920.12899.

Fitzsimons, I. C. W., Harte, B. and Clark, R. M. (2000) 'SIMS stable isotope measurement: counting statistics and analytical precision', *Mineralogical Magazine*. De Gruyter, 64(01), pp. 59–83. doi: 10.1180/002646100549139.

Flombaum, P. *et al.* (2013) 'Present and future global distributions of the marine Cyanobacteria Prochlrococcus and Synechococcus', *Pnas*, 110(24), pp. 9824–9829. doi: 10.1073/pnas.1307701110/-/DCSupplemental.www.pnas.org/cgi/doi/10.1073/pnas.1307701110.

Fogg, G. E. (1983) 'The Ecological Significance of Extracellular Products of Phytoplankton Photosynthesis', *Botanica Marina*, 26(1), pp. 3–14. doi: 10.1515/botm.1983.26.1.3.

Foster, R. A., Sztejrenszus, S. and Kuypers, M. M. M. (2013) 'Measuring carbon and N2 fixation in field populations of colonial and free-living unicellular cyanobacteria using nanometer-scale secondary ion mass spectrometry1', *Journal of Phycology*, 49(3),

pp. 502–516. doi: 10.1111/jpy.12057.

Foster, R. a *et al.* (2011) 'Nitrogen fixation and transfer in open ocean diatom-cyanobacterial symbioses.', *The ISME journal*. Nature Publishing Group, 5(9), pp. 1484–1493. doi: 10.1038/ismej.2011.26.

Fukao, T., Kimoto, K. and Kotani, Y. (2010) 'Production of transparent exopolymer particles by four diatom species', *Fisheries Science*. Springer Japan, 76(5), pp. 755–760. doi: 10.1007/s12562-010-0265-z.

Gao, D., Huang, X. and Tao, Y. (2015) 'A critical review of NanoSIMS in analysis of microbial metabolic activities at single-cell level', *Critical Reviews in Biotechnology*, (July), pp. 1–7. doi: 10.3109/07388551.2015.1057550.

Garside, C. (1981) 'Nitrate and ammonium uptake in the apex of the New York Bight', 26(4), pp. 731–739.

Gaworzewska, E. T. and Carlile, M. J. (1982) 'Positive Chemotaxis of Rhizobium leguminosarum and other Bacteria towards Root Exudates from Legumes and other Plants', *Microbiology*, 128(6), pp. 1179–1188. doi: 10.1099/00221287-128-6-1179.

del Giorgio, P. a and Duarte, C. M. (2002) 'Respiration in the open ocean', *Nature*, 420(6914), pp. 379–384. doi: 10.1038/nature01165.

Glibert, P. M. and Ray, R. T. (1990) 'Different patterns of growth and nitrogen uptake in two clones of marineSynechococcus spp.', *Marine Biology*, 107(2), pp. 273–280. doi: 10.1007/BF01319826.

Goecke, F. *et al.* (2013) 'Algae as an important environment for bacteria - phylogenetic relationships among new bacterial species isolated from algae', *Phycologia*, 52(1), pp. 14–24. doi: 10.2216/12-24.1.

Grant, M. A. *et al.* (2014) 'Direct exchange of vitamin B12 is demonstrated by modelling the growth dynamics of algal–bacterial cocultures', *The ISME Journal*. Nature Publishing Group, 8(7), pp. 1418–1427. doi: 10.1038/ismej.2014.9.

Grossart, H. P. *et al.* (2004) 'Antagonistic activity of bacteria isolated from organic aggregates of the German Wadden Sea', *FEMS Microbiology Ecology*, 47(3), pp. 387–396. doi: 10.1016/S0168-6496(03)00305-2.

Grossart, H. P. *et al.* (2007) 'Comparison of cell-specific activity between free-living and attached bacteria using isolates and natural assemblages', *FEMS Microbiology Letters*, 266(2), pp. 194–200. doi: 10.1111/j.1574-6968.2006.00520.x.

Guillard, R. R. L. (1975) 'Culture of phytoplankton for feeding marine invertebrates', in Smith, W. L., and Chanley, M. H. (ed.) *Culture of Marine Invertebrate Animals*. New York: Plenum Press, pp. 29–60.

Hall, T. (1999) 'BioEdit: a user-friendly biological sequence alignment editor and analysis program for Windows 95/98/NT', *Nucleic Acids Symposium Series*, pp. 95–98. doi: citeulike-article-id:691774.

Hellebust, J. (1965) 'Excretion of some organic compounds by marine phytoplankton', *Limnology and Oceanography*, 10(2), pp. 192–206.

Hillion, F. *et al.* (2008) 'The effect of QSA on S, C, O and Si isotopic ratio measurements', *Geochimica et Cosmochimica Acta Supplement*, 72, p. A377.

Hinrichs, K.-U. *et al.* (1999) 'Methane - consuming archaebacteria in marine sediments', *Nature(Letters to nature)*, 398(April), p. 802805.

Hoefler, B. C. and Straight, P. D. (2014) 'Imaging Mass Spectrometry, Metabolism, and New Views of the Microbial World', *Natural Products Analysis*, pp. 349–396. doi: 10.1002/9781118876015.ch10.

Huh, D. and Paulsson, J. (2011) 'Non-genetic heterogeneity from stochastic partitioning at cell division', *Nature Genetics*, 43(2), pp. 95–100. doi: 10.1038/ng.729.

Iuculano, F. *et al.* (2017) 'Prochlorococcus as a possible source for transparent exopolymer particles (TEP)', *Frontiers in Microbiology*, 8(APR), pp. 1–11. doi: 10.3389/fmicb.2017.00709.

Jackson, G. a (1987) 'Stimulating chemosensory responses of marine microorganisms', *Limnological Oceanography*, 32(6), pp. 1–14. Available at: https://stellar.mit.edu/S/course/1/fa14/1.88/courseMaterial/topics/topic12/studyMaterial/JacksonLOM(1987)32_1253-1266/JacksonLOM(1987)32_1253-1266.pdf%5Cnfile:///Users/seb/Dropbox/Library.papers3/Articles/1987/Jackson/Limnological Oceanography 1987 Jackson.

Jasti, S. *et al.* (2005) 'Phylogenetic diversity and specificity of bacteria closely associated with Alexandrium spp. and other phytoplankton', *Applied and Environmental Microbiology*, 71(7), pp. 3483–3494. doi: 10.1128/AEM.71.7.3483-3494.2005.

Johnson, D. R. *et al.* (2012) 'Metabolic specialization and the assembly of microbial communities', *ISME Journal*. Nature Publishing Group, 6(11), pp. 1985–1991. doi: 10.1038/ismej.2012.46.

Kaur, A. *et al.* (2018) '100 Days of marine Synechococcus–Ruegeria pomeroyi interaction: A detailed analysis of the exoproteome', *Environmental Microbiology*, 20(2), pp. 785–799. doi: 10.1111/1462-2920.14012.

Kazamia, E. *et al.* (2012) 'Mutualistic interactions between vitamin B12-dependent algae and heterotrophic bacteria exhibit regulation', *Environmental Microbiology*. Wiley/Blackwell (10.1111), 14(6), pp. 1466–1476. doi: 10.1111/j.1462-2920.2012.02733.x.

Kilburn, M. R. and Clode, P. L. (2014) 'Elemental and Isotopic Imaging of Biological Samples Using NanoSIMS', in *Electron Microscopy: Methods and Protocols*, pp. 733–755. doi: 10.1007/978-1-62703-776-1.

Kiørboe, T. and Jackson, G. A. (2001) 'Marine snow, organic solute plumes, and optimal chemosensory behavior of bacteria', *Limnology and Oceanography*. Wiley-Blackwell, 46(6), pp. 1309–1318. doi: 10.4319/lo.2001.46.6.1309.

Kirchman, D. L. (2002) 'The ecology of Cytophaga-Flavobacteria in aquatic environments', *FEMS Microbiology Ecology*. Oxford University Press, 39(2), pp. 91–100. doi: 10.1111/j.1574-6941.2002.tb00910.x.

Koch, A. L. (2001) 'Oligotrophs versus copiotrophs', *BioEssays*, 23(7), pp. 657–661. doi: 10.1002/bies.1091.

Kopf, S. H. *et al.* (2015) 'Heavy water and ^{15}N labelling with NanoSIMS analysis reveals growth rate-dependent metabolic heterogeneity in chemostats', *Environmental Microbiology*, 17(7), pp. 2542–2556. doi: 10.1111/1462-2920.12752.

Krupke, A. *et al.* (2013) 'In situ identification and N2 and C fixation rates of uncultivated cyanobacteria populations', *Systematic and Applied Microbiology*. Elsevier GmbH., 36(4), pp. 259–271. doi: 10.1016/j.syapm.2013.02.002.

Lauro, F. M. *et al.* (2009) 'The genomic basis of trophic strategy in marine bacteria', *Proceedings of the National Academy of Sciences*, 106(37), pp. 15527–15533. doi: 10.1073/pnas.0903507106.

Lechene, C. *et al.* (2006) 'High-resolution quantitative imaging of mammalian and bacterial cells using stable isotope mass spectrometry', *J Biol*, pp. 1–30. Available at: http://scholar.google.com/scholar?hl=en&btnG=Search&q=intitle:High-resolution+quantitative+imaging+of+mammalian+and+bacterial+cells+using+stable+isotope+mass+spectrometry#6 (Accessed: 16 September 2014).

Lechene, C. P. *et al.* (2007) 'Quantitative imaging of nitrogen fixation by individual bacteria within animal cells.', *Science (New York, N.Y.)*, 317(5844), pp. 1563–6. doi: 10.1126/science.1145557.

Legendre, L. and Rassoulzadegan, F. (1995) 'Plankton and nutrient dynamics in marine waters', *Ophelia*. Taylor & Francis Group , 41(1), pp. 153–172. doi: 10.1080/00785236.1995.10422042.

Lidstrom, M. E. and Konopka, M. C. (2010) 'The role of physiological heterogeneity in microbial population behavior', *Nature Chemical Biology*, 6(10), pp. 705–712. doi: 10.1038/nchembio.436.

Ma, X., Coleman, M. L. and Waldbauer, J. R. (2018) 'Distinct molecular signatures in dissolved organic matter produced by viral lysis of marine cyanobacteria', *Environmental Microbiology*. Wiley/Blackwell (10.1111). doi: 10.1111/1462-2920.14338.

Malfatti, F. and Azam, F. (2009) 'Atomic force microscopy reveals microscale networks and possible symbioses among pelagic Marine Bacteria', *Aquatic Microbial Ecology*, 58(1), pp. 1–14. doi: 10.3354/ame01355.

Malmcrona-Friberg, K., Goodman, A. and Kjelleberg, S. (1990) 'Chemotactic Responses of Marine Vibrio sp. Strain S14 (CCUG 15956) to Low-Molecular-Weight Substances under Starvation and Recovery Conditions.', *Applied and environmental microbiology*. American Society for Microbiology, 56(12), pp. 3699–704. Available at: http://www.ncbi.nlm.nih.gov/pubmed/16348373 (Accessed: 3 August 2018).

Marañón, E. *et al.* (2004) 'Significance and mechanisms of photosynthetic production of dissolved organic carbon in a coastal eutrophic ecosystem', *Limnology and Oceanography*, 49(5), pp. 1652–1666. doi: 10.4319/lo.2004.49.5.1652.

Marie, D. *et al.* (1997) 'Enumeration and Cell Cycle Analysis of Natural Populations of Marine Picoplankton by Flow Cytrometry Using the Nucleic Acid Stain SYBR Green I', *Applied and Enviornmental Microbiology*, 63(1), pp. 186–193. doi: 10.1111/j.1365-294X.2009.04480.x.

Matwiyoff, N. A. and Ott, D. G. (1973) 'Stable Isotope Tracers in the Life Sciences and Medicine', 181(4105), pp. 1125–1132.

Mayali, X. and Azam, F. (2004) 'Algicidal bacteria in the sea and their impact on algal blooms', *Journal of Eukaryotic Microbiology*, 51(2), pp. 139–144. doi: 10.1111/j.1550-7408.2004.tb00538.x.

Mayali, X., Franks, P. J. S. and Burton, R. S. (2011) 'Temporal attachment dynamics by distinct bacterial taxa during a dinoflagellate bloom', *Aquatic Microbial Ecology*, 63(2), pp. 111–122. doi: 10.3354/ame01483.

Mccarthy, J. J., Garside, C. and Nevins, J. L. (1992) 'Nitrate supply and phytoplankton

uptake kinetics in the euphotic layer of a Gulf Stream warm-core ring', *Deep Sea Research Part A, Oceanographic Research Papers*. Pergamon Press plc, 39, pp. S393–S403. doi: 10.1016/S0198-0149(11)80021-X.

Mcnichol, J. *et al.* (2018) 'Primary productivity below the seafloor at deep-sea hot springs', *Proceedings of the National Academy of Sciences of the United States of America*, pp. 1–6. doi: 10.1073/pnas.1804351115.

Van Den Meersche, K. *et al.* (2004) 'Carbon-nitrogen coupling and algal-bacterial interactions during an experimental bloom: Modeling a13C tracer experiment', *Limnology and Oceanography*, 49(3), pp. 862–878. doi: 10.4319/lo.2004.49.3.0862.

Van Den Meersche, K., Soetaert, K. and Middelburg, J. J. (2011) 'Plankton dynamics in an estuarine plume: A mesocosm 13C and 15N tracer study', *Marine Ecology Progress Series*, 429, pp. 29–43. doi: 10.3354/meps09097.

Mesibov, R. and Adler, J. (1972) 'Chemotaxis toward amino acids in Escherichia coli.', *Journal of bacteriology*. American Society for Microbiology, 112(1), pp. 315–26. Available at: http://www.ncbi.nlm.nih.gov/pubmed/4562400 (Accessed: 3 August 2018).

Mitchell, J. G., Okubo, A. and Fuhrman, J. A. (1985) 'Microzones surrounding phytoplankton form the basis for a stratified marine microbial ecosystem', *Nature*. Nature Publishing Group, 316(6023), pp. 58–59. doi: 10.1038/316058a0.

Montoya, J. P. *et al.* (1996) 'A Simple , High-Precision , High-Sensitivity Tracer Assay for N (inf2) Fixation . These include : A Simple , High-Precision , High-Sensitivity Tracer Assay for N 2 Fixation', *Applied and Environmental Microbiology*, 62(3), pp. 986–993.

Moore, L. R. *et al.* (2002) 'Utilization of different nitrogen sources by the marine cyanobacteria \textit{Prochlorococcus} and \textit{Synechococcus}', *Limnology and Oceanography*, 47(4), pp. 989–996. doi: 10.4319/lo.2002.47.4.0989.

Morana, C. *et al.* (2014) 'Production of dissolved organic matter by phytoplankton and its uptake by heterotrophic prokaryotes in large tropical lakes', *Limnology and Oceanography*, 59(4), pp. 1364–1375. doi: 10.4319/lo.2014.59.4.1364.

Morel, A. *et al.* (1993) 'Prochlorococcus and Synechococcus - a Comparative-Study of Their Optical-Properties in Relation To Their Size and Pigmentation', *Journal of Marine Research*, 51(3), pp. 617–649. doi: 10.1357/0022240933223963.

Morris, R. M. *et al.* (2002) 'SAR11 clade dominates ocean surface bacterioplankton communities', *Nature*, 420(6917), pp. 806–810. doi: 10.1038/nature01240.

Muccio, Z. and Jackson, G. P. (2009) 'Isotope ratio mass spectrometry', *The Analyst*, 134(2), pp. 213–222. doi: 10.1039/B808232D.

Musat, N. *et al.* (2008) 'A single-cell view on the ecophysiology of anaerobic phototrophic bacteria.', *Proceedings of the National Academy of Sciences of the United States of America*, 105(46), pp. 17861–17866. doi: 10.1073/pnas.0809329105.

Musat, N. *et al.* (2012) 'Detecting metabolic activities in single cells, with emphasis on nanoSIMS', *FEMS Microbiology Reviews*, 36(2), pp. 486–511. doi: 10.1111/j.1574-6976.2011.00303.x.

Musat, N. *et al.* (2014) 'The effect of FISH and CARD-FISH on the isotopic composition of 13C- and 15N-labeled Pseudomonas putida cells measured by nanoSIMS', *Systematic and Applied Microbiology*. Elsevier GmbH., 37(4), pp. 267–

276. doi: 10.1016/j.syapm.2014.02.002.

Musat, N. *et al.* (2016) 'Tracking microbial interactions with NanoSIMS', *Current Opinion in Biotechnology*. Elsevier Ltd, 41, pp. 114–121. doi: 10.1016/j.copbio.2016.06.007.

Obernosterer, I. and Herndl, G. J. (1995) 'Phytoplankton extracellular release and bacterial growth: Dependence on the inorganic N:P ratio', *Marine Ecology Progress Series*, 116(1–3), pp. 247–258. doi: 10.3354/meps116247.

Paerl, H. W. (1977) 'Role of heterotrophic bacteria in promoting N2 fixation by Anabaena in aquatic habitats', *Microbial Ecology*, 4(3), pp. 215–231. doi: 10.1007/BF02015078.

Partensky, F., Blanchot, J. and Vaulot, D. (1999) 'Differential distribution and ecology of Prochlorococcus and Synechococcus in oceanic waters : a review', *Bulletin de l'Institut océanographique*, 19(19), pp. 457–475. Available at: http://cat.inist.fr/?aModele=afficheN&cpsidt=1218663.

Partensky, F., Hess, W. R. and Vaulot, D. (1999) 'Prochlorococcus, a marine photosynthetic prokaryote of global significance', *Microbiol.Mol Biol.Rev.*, 63(1), pp. 106–127. doi: doi:1092-2172/99/$04.00.

Passarelli, M. K. *et al.* (2017) 'The 3D OrbiSIMS - Label-free metabolic imaging with subcellular lateral resolution and high mass-resolving power', *Nature Methods*, 14(12), pp. 1175–1183. doi: 10.1038/nmeth.4504.

Passarelli, M. K. and Winograd, N. (2011) 'Lipid imaging with time-of-flight secondary ion mass spectrometry (ToF-SIMS)', *Biochimica et Biophysica Acta - Molecular and Cell Biology of Lipids*. Elsevier B.V., 1811(11), pp. 976–990. doi: 10.1016/j.bbalip.2011.05.007.

Pel, R., Hoogveld, H. and Floris, V. (2003) 'Using the hidden isotopic heterogeneity in phyto- and zooplankton to unmask disparity in trophic carbon transfer', *Limnology and Oceanography*, 48(6), pp. 2200–2207. doi: 10.4319/lo.2003.48.6.2200.

Pelz, O. *et al.* (1998) 'Tracing the assimilation of organic compounds using δ13C analysis of unique amino acids in the bacterial peptidoglycan cell wall', *FEMS Microbiology Ecology*, 25(3), pp. 229–240. doi: 10.1016/S0168-6496(97)00097-4.

Pernice, M. *et al.* (2012) 'A single-cell view of ammonium assimilation in coral–dinoflagellate symbiosis', *The ISME Journal*. Nature Publishing Group, 6(7), pp. 1314–1324. doi: 10.1038/ismej.2011.196.

Pernice, M. *et al.* (2015) 'A nanoscale secondary ion mass spectrometry study of dinoflagellate functional diversity in reef-building corals', *Environmental microbiology*, 17(10), pp. 3570–3580. doi: 10.1111/1462-2920.12518.

Philippot, L. *et al.* (2013) 'Going back to the roots: the microbial ecology of the rhizosphere', *Nature Reviews Microbiology*. Nature Publishing Group, 11(11), pp. 789–799. doi: 10.1038/nrmicro3109.

Ploug, H. *et al.* (2010) 'Carbon and nitrogen fluxes associated with the cyanobacterium Aphanizomenon sp. in the Baltic Sea', *ISME Journal*. Nature Publishing Group, 4(9), pp. 1215–1223. doi: 10.1038/ismej.2010.53.

Popa, R. *et al.* (2007) 'Carbon and nitrogen fixation and metabolite exchange in and between individual cells of Anabaena oscillarioides', *ISME Journal*, 1(4), pp. 354–360. doi: 10.1038/ismej.2007.44.

Post, D. M. (2002) ‘Using stable isotopes to estimate trophic position: models, methos, and assumptions. ’, *Ecology*, 83(3), pp. 703–718. doi: Doi 10.2307/3071875.

Rädecker, N. *et al.* (2018) ‘Using Aiptasia as a model to study metabolic interactions in Cnidarian-Symbiodinium symbioses’, *Frontiers in Physiology*, 9(MAR). doi: 10.3389/fphys.2018.00214.

Raina, J. B. *et al.* (2017) ‘Subcellular tracking reveals the location of dimethylsulfoniopropionate in microalgae and visualises its uptake by marine bacteria’, *eLife*, 6, pp. 1–17. doi: 10.7554/eLife.23008.

Samo, T. J. *et al.* (2018) ‘Attachment between heterotrophic bacteria and microalgae influences symbiotic microscale interactions’, *Environmental Microbiology*. Wiley/Blackwell (10.1111). doi: 10.1111/1462-2920.14357.

Sanni, O. D. *et al.* (2002) ‘Classification of adsorbed protein static ToF-SIMS spectra by principal component analysis and neural networks’, *Surface and Interface Analysis*. Wiley-Blackwell, 33(9), pp. 715–728. doi: 10.1002/sia.1438.

Sarmento, H. and Gasol, J. M. (2012) ‘Use of phytoplankton-derived dissolved organic carbon by different types of bacterioplankton’, *Environmental Microbiology*, 14(9), pp. 2348–2360. doi: 10.1111/j.1462-2920.2012.02787.x.

Schäfer, H. and Abbas, B. (2002) ‘Genetic diversity of ’satellite’bacteria present in cultures of marine diatoms’, *FEMS Microbiology …*, 42(1), pp. 25–35. doi: 10.1111/j.1574-6941.2002.tb00992.x.

Schindelin, J. *et al.* (2012) ‘Fiji: An open-source platform for biological-image analysis’, *Nature Methods*, 9(7), pp. 676–682. doi: 10.1038/nmeth.2019.

Schreiber, F. *et al.* (2016) ‘Phenotypic heterogeneity driven by nutrient limitation promotes growth in fluctuating environments’, *Nature Microbiology*. Nature Publishing Group, 1(6), pp. 1–7. doi: 10.1038/nmicrobiol.2016.55.

Seyedsayamdost, M. R. *et al.* (2011) ‘The Jekyll-and-Hyde chemistry of Phaeobacter gallaeciensis.’, *Nature chemistry*, 3(4), pp. 331–335. doi: 10.1038/nchem.1002.

Seymour, J. R. *et al.* (2008) ‘A microfluidic chemotaxis assay to study microbial behavior in diffusing nutrient patches’, *Limnology and Oceanography: Methods*. Wiley-Blackwell, 6(9), pp. 477–488. doi: 10.4319/lom.2008.6.477.

Seymour, J. R. *et al.* (2010) ‘Chemotactic response of marine bacteria to the extracellular products of Synechococcus and Prochlorococcus’, *Aquatic Microbial Ecology*, 59(2), pp. 161–168. doi: 10.3354/ame01400.

Seymour, J. R. *et al.* (2017) ‘Zooming in on the phycosphere: The ecological interface for phytoplankton-bacteria relationships’, *Nature Microbiology*, 2(May). doi: 10.1038/nmicrobiol.2017.65.

Seymour, J. R., Marcos, and Stocker, R. (2009) ‘Resource Patch Formation and Exploitation throughout the Marine Microbial Food Web’, *The American Naturalist*, 173(1), pp. E15–E29. doi: 10.1086/593004.

Seymour, J. R., Seuront, L. and Mitchell, J. G. (2007) ‘Microscale gradients of planktonic microbial communities above the sediment surface in a mangrove estuary’, *Estuarine, Coastal and Shelf Science*, 73(3–4), pp. 651–666. doi: 10.1016/j.ecss.2007.03.004.

Sher, D. *et al.* (2011) ‘Response of Prochlorococcus ecotypes to co-culture with diverse

marine bacteria', *ISME Journal*. Nature Publishing Group, 5(7), pp. 1125–1132. doi: 10.1038/ismej.2011.1.

Sjövall, P., Johansson, B. and Lausmaa, J. (2006) 'Localization of lipids in freeze-dried mouse brain sections by imaging TOF-SIMS', *Applied Surface Science*, 252(19), pp. 6966–6974. doi: 10.1016/j.apsusc.2006.02.126.

Smith, D. F. and Wiebe, W. J. (1976) 'Constant release of photosynthate from marine phytoplankton.', *Applied and environmental microbiology*. American Society for Microbiology, 32(1), pp. 75–9. Available at: http://www.ncbi.nlm.nih.gov/pubmed/987750 (Accessed: 20 August 2018).

Smriga, S. *et al.* (2016) 'Chemotaxis toward phytoplankton drives organic matter partitioning among marine bacteria', *Proceedings of the National Academy of Sciences*, 113(6), pp. 1576–1581. doi: 10.1073/pnas.1512307113.

Son, K., Guasto, J. S. and Stocker, R. (2013) 'Bacteria can exploit a flagellar buckling instability to change direction', *Nature Physics*. Nature Publishing Group, 9(8), pp. 494–498. doi: 10.1038/nphys2676.

Son, K., Menolascina, F. and Stocker, R. (2016) 'Speed-dependent chemotactic precision in marine bacteria', *Proceedings of the National Academy of Sciences*, 113(31), pp. 8624–8629. doi: 10.1073/pnas.1602307113.

Sonnenschein, E. C. *et al.* (2011) 'Development of a genetic system for Marinobacter adhaerens HP15 involved in marine aggregate formation by interacting with diatom cells', *Journal of Microbiological Methods*. Elsevier B.V., 87(2), pp. 176–183. doi: 10.1016/j.mimet.2011.08.008.

Sonnenschein, E. C. *et al.* (2012) 'Chemotaxis of Marinobacter adhaerens and its impact on attachment to the diatom Thalassiosira weissflogii', *Applied and Environmental Microbiology*, 78(19), pp. 6900–6907. doi: 10.1128/AEM.01790-12.

Stocker, R. *et al.* (2008) 'Rapid chemotactic response enables marine bacteria to exploit ephemeral microscale nutrient patches', *Proceedings of the National Academy of Sciences*, 105(11), pp. 4209–4214. doi: 10.1073/pnas.0709765105.

Stocker, R. (2012) 'Marine Microbes See a Sea of Gradients', *Science*, 338(6107), pp. 628–633. doi: 10.1126/science.1208929.

Stocker, R. (2015) 'The 100 μm length scale in the microbial ocean', *Aquatic Microbial Ecology*, 76(3), pp. 189–194. doi: 10.3354/ame01777.

Stocker, R. and Seymour, J. R. (2012) 'Ecology and Physics of Bacterial Chemotaxis in the Ocean', *Microbiology and Molecular Biology Reviews*, 76(4), pp. 792–812. doi: 10.1128/MMBR.00029-12.

Stocker, R. and Seymour, J. R. (2012) 'Ecology and Physics of Bacterial Chemotaxis in the Ocean Ecology and Physics of Bacterial Chemotaxis in the Ocean', 76(4). doi: 10.1128/MMBR.00029-12.

Strom, S. L. (2008) 'Microbial ecology of ocean biogeochemisrty: a community perspective', 320, pp. 1043–1045.

Su, J. Q. *et al.* (2007) 'Isolation and characterization of a marine algicidal bacterium against the toxic dinoflagellate Alexandrium tamarense', *Harmful Algae*, 6(6), pp. 799–810. doi: 10.1016/j.hal.2007.04.004.

Suttle, C. A. (2005) 'Viruses in the sea', *Nature*, 437(7057), pp. 356–361. doi:

10.1038/nature04160.

Tai, V. *et al.* (2009) 'Whole-genome microarray analyses of Synechococcus-Vibrio interactions', *Environmental Microbiology*, 11(10), pp. 2698–2709. doi: 10.1111/j.1462-2920.2009.01997.x.

Tang, Y. Z., Koch, F. and Gobler, C. J. (2010) 'Most harmful algal bloom species are vitamin B1 and B12 auxotrophs.', *Proceedings of the National Academy of Sciences of the United States of America*. National Academy of Sciences, 107(48), pp. 20756–61. doi: 10.1073/pnas.1009566107.

Tarquinio, F. *et al.* (2018) 'Microorganisms facilitate uptake of dissolved organic nitrogen by seagrass leaves', *ISME Journal*. Springer US, pp. 1–5. doi: 10.1038/s41396-018-0218-6.

Teeling, H. *et al.* (2012) 'Substrate-controlled succession of marine bacterioplankton populations induced by a phytoplankton bloom.', *Science (New York, N.Y.)*. American Association for the Advancement of Science, 336(6081), pp. 608–11. doi: 10.1126/science.1218344.

Terrado, R. *et al.* (2017) 'Autotrophic and heterotrophic acquisition of carbon and nitrogen by a mixotrophic chrysophyte established through stable isotope analysis', *ISME Journal*. Nature Publishing Group, 11(9), pp. 2022–2034. doi: 10.1038/ismej.2017.68.

Thiel, V. *et al.* (2007) 'Analysis of archaeal core ether lipids using Time of Flight-Secondary Ion Mass Spectrometry (ToF-SIMS): Exploring a new prospect for the study of biomarkers in geobiology', *Geobiology*, 5(1), pp. 75–83. doi: 10.1111/j.1472-4669.2006.00093.x.

Thompson, A. W. *et al.* (2012) 'Unicellular cyanobacterium symbiotic with a single-celled eukaryotic alga.', *Science (New York, N.Y.)*, 337(6101), pp. 1546–50. doi: 10.1126/science.1222700.

Thornton, D. C. O. (2014) 'Dissolved organic matter (DOM) release by phytoplankton in the contemporary and future ocean', *European Journal of Phycology*, 49(1), pp. 20–46. doi: 10.1080/09670262.2013.875596.

van Tol, H. M., Amin, S. a and Armbrust, E. V. (2017) 'Ubiquitous marine bacterium inhibits diatom cell division', *ISME Journal*. Nature Publishing Group, 11(1), pp. 31–42. doi: 10.1038/ismej.2016.112.

Turner, J. T. (2002) 'Zooplankton fecal pellets, mrine snow and sinking phytoplankton blooms.', *Aquatic Microbial Ecology*, 27, pp. 57–102. doi: Doi 10.3354/Ame027057.

Vaidyanathan, S. *et al.* (2008) 'Subsurface biomolecular imaging of Streptomyces coelicolor using secondary ion mass spectrometry', *Analytical Chemistry*, 80(6), pp. 1942–1951. doi: 10.1021/ac701921e.

Wagner, M. (2009) 'Single-cell ecophysiology of microbes as revealed by Raman microspectroscopy or secondary ion mass spectrometry imaging.', *Annual review of microbiology*, 63, pp. 411–29. doi: 10.1146/annurev.micro.091208.073233.

Wagner, M. S. *et al.* (2002) 'Limits of detection for time of flight secondary ion mass spectrometry (ToF-SIMS) and X-ray photoelectron spectroscopy (XPS): detection of low amounts of adsorbed protein', *Journal of Biomaterials Science, Polymer Edition*. Taylor & Francis Group , 13(4), pp. 407–428. doi: 10.1163/156856202320253938.

Wang, B. X. *et al.* (2010) 'A novel marine bacterium algicidal to the toxic dinoflagellate

Alexandrium tamarense', *Letters in Applied Microbiology*, 51(5), pp. 552–557. doi: 10.1111/j.1472-765X.2010.02936.x.

Wang, H. *et al.* (2015) 'Identification of Genetic Modules Mediating the Jekyll and Hyde Interaction of Dinoroseobacter shibae with the Dinoflagellate Prorocentrum minimum', *Frontiers in Microbiology*. Frontiers, 6, p. 1262. doi: 10.3389/fmicb.2015.01262.

Waterbury, J. B. *et al.* (1979) 'Widespread occurance of a unicellular, marine, planktonic, cyanobacterium', *Nature*, pp. 293–294.

Watrous, J. D. and Dorrestein, P. C. (2011) 'Imaging mass spectrometry in microbiology.', *Nature reviews. Microbiology*. Nature Publishing Group, 9(9), pp. 683–694. doi: 10.1038/nrmicro2634.

Weisburg, W. G. *et al.* (1991) '16S ribosomal DNA amplification for phylogenetic study', *Journal of Bacteriology*, 173(2), pp. 697–703. doi: n.a.

Whitman, W. B., Coleman, D. C. and Wiebe, W. J. (1998) 'Prokaryotes: the unseen majority', *Proc Natl Acad Sci U S A*, 95(12), pp. 6578–6583. doi: 10.1073/pnas.95.12.6578.

Woebken, D. *et al.* (2012) 'Identification of a novel cyanobacterial group as active diazotrophs in a coastal microbial mat using NanoSIMS analysis.', *The ISME journal*. Nature Publishing Group, 6(7), pp. 1427–39. doi: 10.1038/ismej.2011.200.

Worrich, A. *et al.* (2017) 'Mycelium-mediated transfer of water and nutrients stimulates bacterial activity in dry and oligotrophic environments', *Nature Communications*, 8(iDiv). doi: 10.1038/ncomms15472.

Wu, H. X. *et al.* (2012) 'Erythrobacter pelagi sp. nov., a member of the family Erythrobacteraceae isolated from the Red Sea', *International Journal of Systematic and Evolutionary Microbiology*, 62(6), pp. 1348–1353. doi: 10.1099/ijs.0.029561-0.

Xie, B. *et al.* (2013) 'Chlamydomonas reinhardtii thermal tolerance enhancement mediated by a mutualistic interaction with vitamin B12-producing bacteria', *The ISME Journal*. Nature Publishing Group, 7(8), pp. 1544–1555. doi: 10.1038/ismej.2013.43.

Zheng, Q. *et al.* (2018) 'Dynamics of Heterotrophic Bacterial Assemblages within Synechococcus Cultures.', *Applied and environmental microbiology*. American Society for Microbiology, 84(3), p. AEM.01517-17. doi: 10.1128/AEM.01517-17.

Zimmermann, M. *et al.* (2015) 'Phenotypic heterogeneity in metabolic traits among single cells of a rare bacterial species in its natural environment quantified with a combination of flow cell sorting and NanoSIMS', *Frontiers in Microbiology*, 6(MAR), pp. 1–11. doi: 10.3389/fmicb.2015.00243.

Appendix A

Supplementary Information for Chapter 2

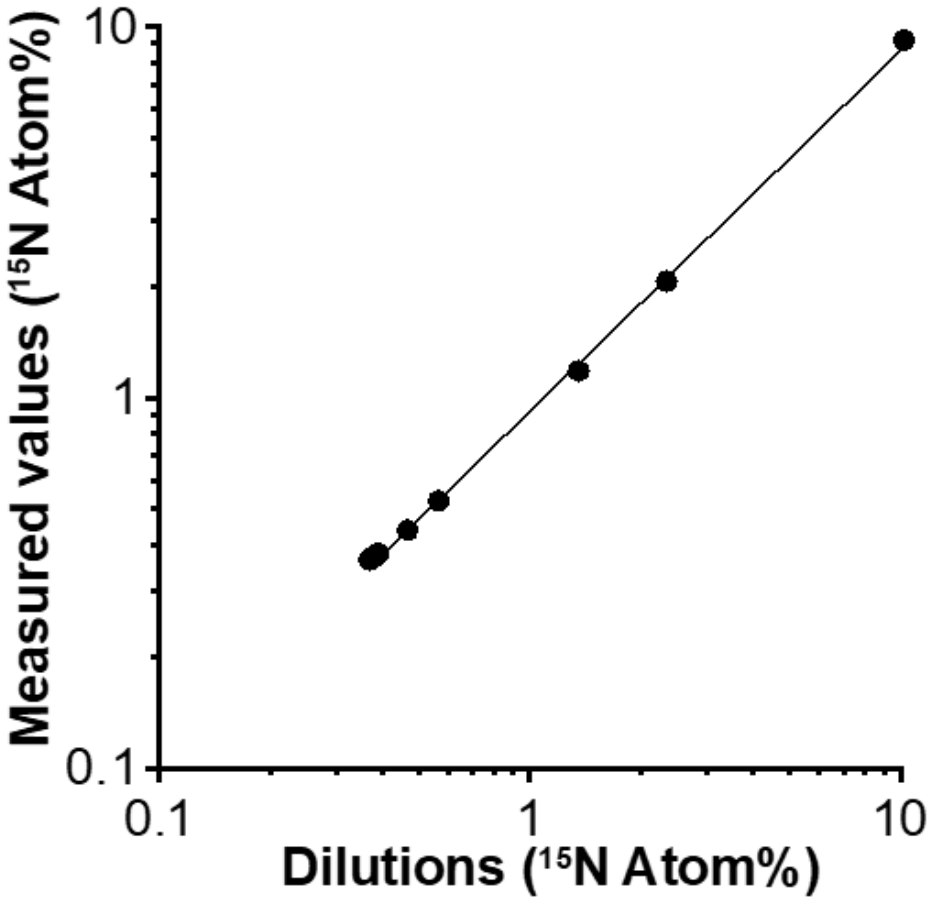

Supplementary Figure 2.1 Dilution series of glutamic acid standards (with increasing proportion of ^{15}N) measured with EA-IRMS.

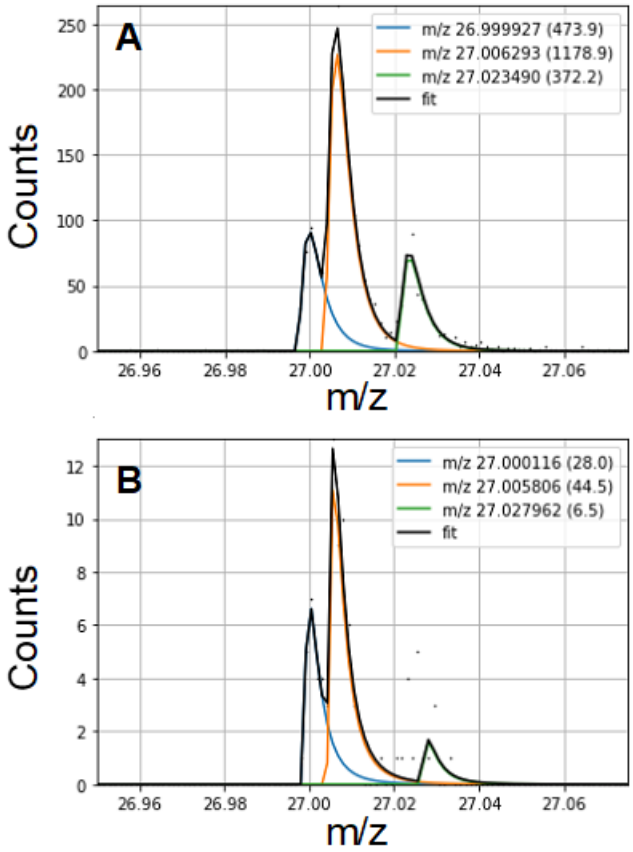

Supplementary Figure 2.2 Examples of ToF-SIMS spectra showing quality of asymmetric peak fitting for sample T1: (a) typical high-quality fit (standard error 0.993) observed when peak heights have sufficient counts (>20) and, (b) poor quality fit (standard error 0.884) where peak height <20 counts and approaching detection limit of the instrument. Peak masses are shown, along with the accumulated counts beneath each peak. Note $^{11}B^{16}O^-$ at m/z 27.00422 cannot be resolved.

Supplementary Table 2.1 Pairwise comparison of negative control (T_0) against 15 minutes (T_1) of each respective instrument with T-Test (EA-IRMS) and Mann-Whitney U-test (NanoSIMS and ToF-SIMS).

Method	Pairwise comparison	Test	U-value	*t*	*p*-value
EA-IRMS	T0/15 min	t-test	-	-51.42	0.000
ToF-SIMS	T0/15 min	Mann-Whitney	133	-	0.002
NanoSIMS	T0/15 min	Mann-Whitney	44	-	0.000

Supplementary Table 2.2 Summary of Kruskal-Wallis test and Dunn's post hoc test with Bonferroni adjustment. The column 'data-points' reports the number of replicate per each method; the replicate for ToF-SIMS and NanoSIMS correspond to single cells. *Only two replicates for time-point 5 were analyzed with EA-IRMS as one replicate was lost.

Sample	Data-points	Mean (At%)	SE	Kruskal-Wallis test *p*-value	Post hoc pairwise comparisons	Test Statistic	Std. Error	Std. Test Statistic	Bonferroni Adjusted *p*-value
T0	EA-IRMS = 3	0.371	0.001	0.000	EA-IRMS/ToF-SIMS	28.198	13.556	-2.666	0.023
	ToF-SIMS = 23	0.460	0.016		ToF-SIMS/NanoSIMS	-36.145	5.564	5.068	0.000
	NanoSIMS = 50	0.374	0.001		EA-IRMS/NanoSIMS	-7.947	13.127	-0.605	1
15 min	EA-IRMS = 3	0.516	0.002	0.006	EA-IRMS/ToF-SIMS	-3.833	14.761	-0.260	1
	ToF-SIMS = 25	0.543	0.017		ToF-SIMS/NanoSIMS	18.321	5.881	3.115	0.006
	NanoSIMS = 56	0.481	0.012		EA-IRMS/NanoSIMS	14.488	14.284	1.014	0.931
30 min	EA-IRMS = 3	0.700	0.005	0.010	EA-IRMS/ToF-SIMS	-7.310	15.844	-0.461	1
	ToF-SIMS = 29	0.751	0.024		ToF-SIMS/NanoSIMS	17.948	5.942	3.021	0.008
	NanoSIMS = 58	0.642	0.024		EA-IRMS/NanoSIMS	10.638	15.468	0.688	1
60 minutes	EA-IRMS = 3	1.273	0.006	0.000	EA-IRMS/ToF-SIMS	2.278	14.491	0.157	1
	ToF-SIMS = 18	1.242	0.043		ToF-SIMS/NanoSIMS	24.824	6.257	3.967	0.000
	NanoSIMS = 59	0.920	0.050		EA-IRMS/NanoSIMS	27.102	13.753	1.971	0.146
120 minutes	EA-IRMS = 3	2.995	0.009	0.000	EA-IRMS/ToF-SIMS	7.368	14.616	0.504	1
	ToF-SIMS = 19	2.869	0.176		ToF-SIMS/NanoSIMS	23.208	6.206	3.740	0.001
	NanoSIMS = 59	1.965	0.099		EA-IRMS/NanoSIMS	30.576	13.924	2.196	0.084
240 minutes	EA-IRMS = 2*	7.460	0.006	0.051	EA-IRMS/ToF-SIMS	NA	NA	NA	NA
	ToF-SIMS = 20	5.898	0.383		ToF-SIMS/NanoSIMS	NA	NA	NA	NA
	NanoSIMS = 53	5.225	0.266		EA-IRMS/NanoSIMS	NA	NA	NA	NA
360 minutes	EA-IRMS = 3	12.887	0.057	0.000	EA-IRMS/ToF-SIMS	26.513	21.683	1.223	0.664
	ToF-SIMS = 52	11.608	0.587		ToF-SIMS/NanoSIMS	23.576	6.665	3.537	0.001
	NanoSIMS = 71	9.219	0.375		EA-IRMS/NanoSIMS	50.089	21.524	2.327	0.060

Appendix B

Supplementary Information for Chapter 3

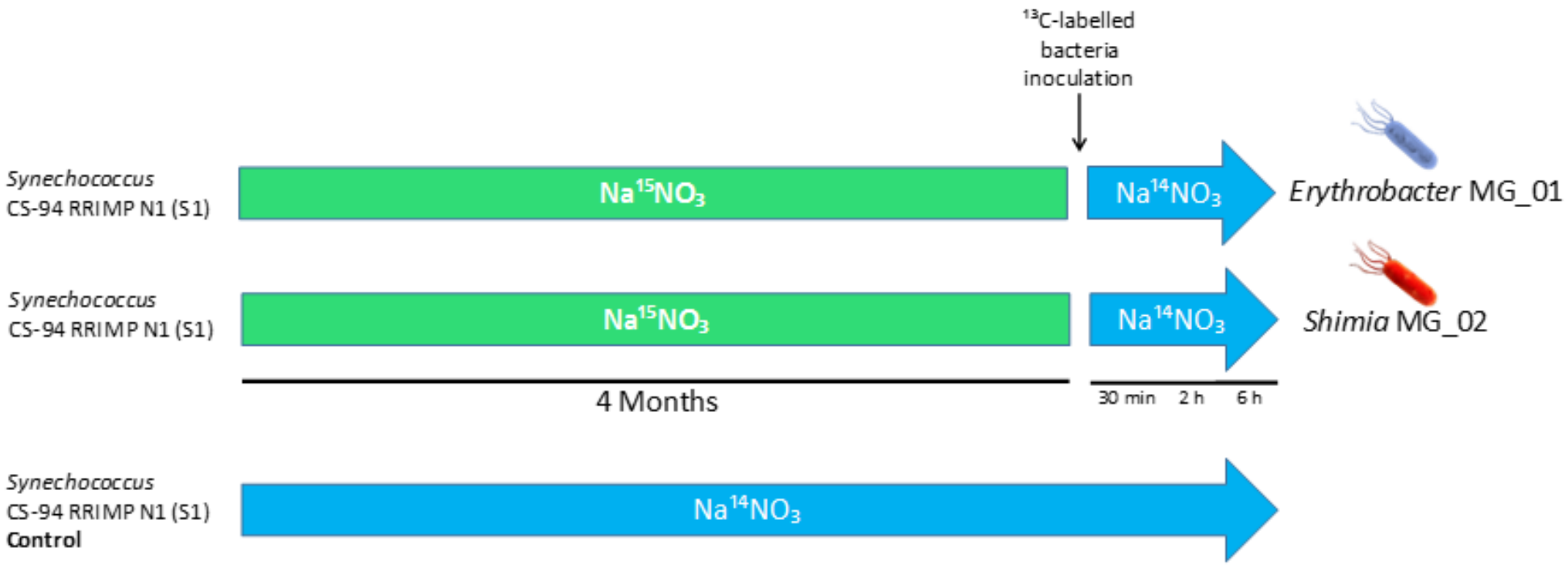

Supplementary Figure 3.1 Experimental design showing isotopic labelling of *Synechococcus* CS-94 RRIMP N1 (S1) culture, inoculation of ^{13}C-labelled bacteria previously isolated from the culture and the time of incubation used for the experiment.

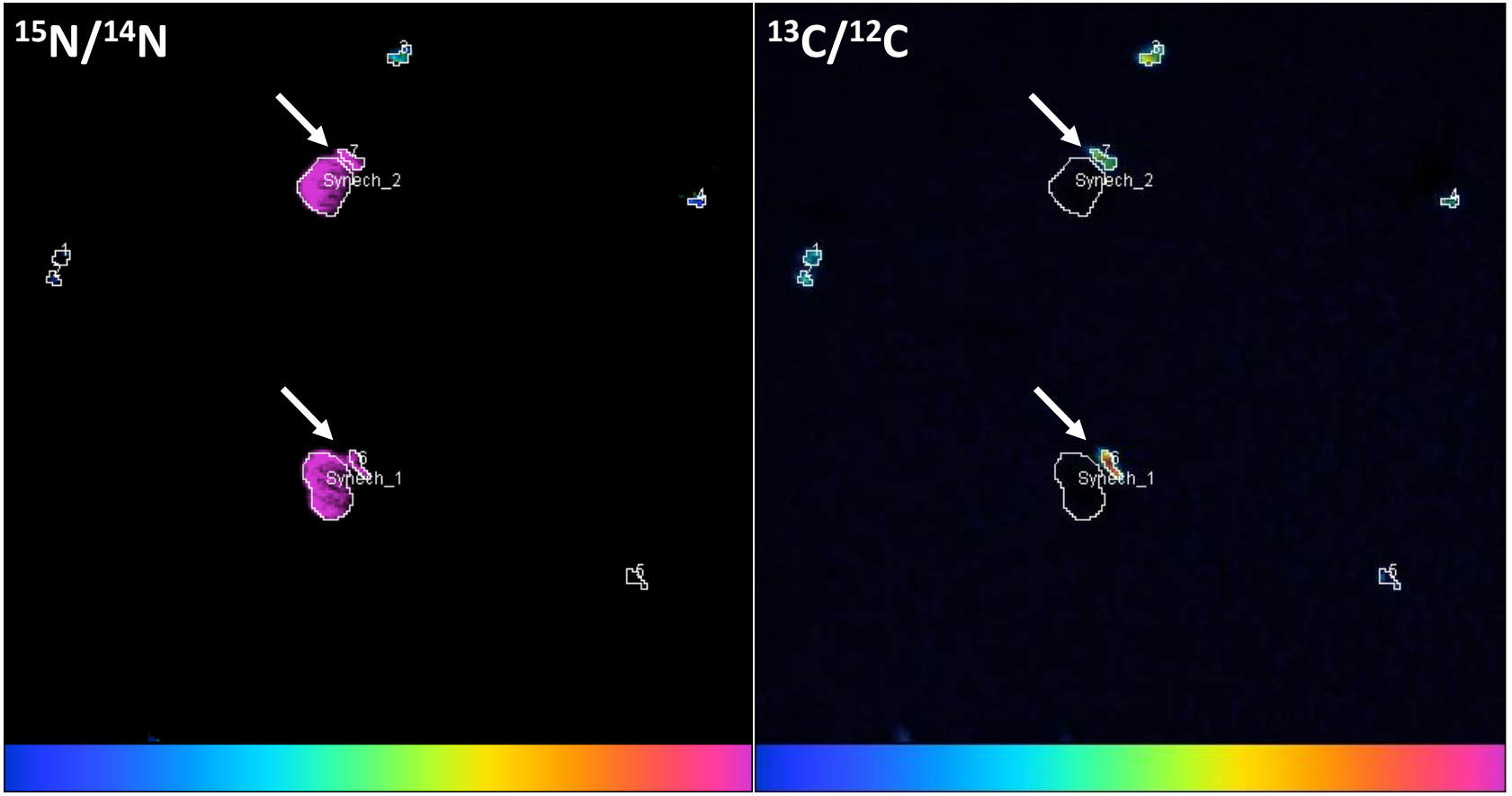

Supplementary Figure 3.2 Hue Saturation Images (HSI) showing the Regions of Interest (ROI) drawn to obtain isotopic quantification of each single cell. The arrows show attachments between single *Synechococcus* cells (Synech_1 and Synech_2) and heterotrophic bacteria (numbers). To avoid overlaps of the respective ROIs of the two cell types, $^{13}C/^{12}C$ HSI images (right panel), which show the unique ^{13}C signature of bacteria, were used as a mask for drawing ROIs around single heterotrophic bacteria cells. The same ROIs appear also in the $^{15}N/^{14}N$ HSI image (left panel). When cells were attached, the ROIs of each cell type were well separated.

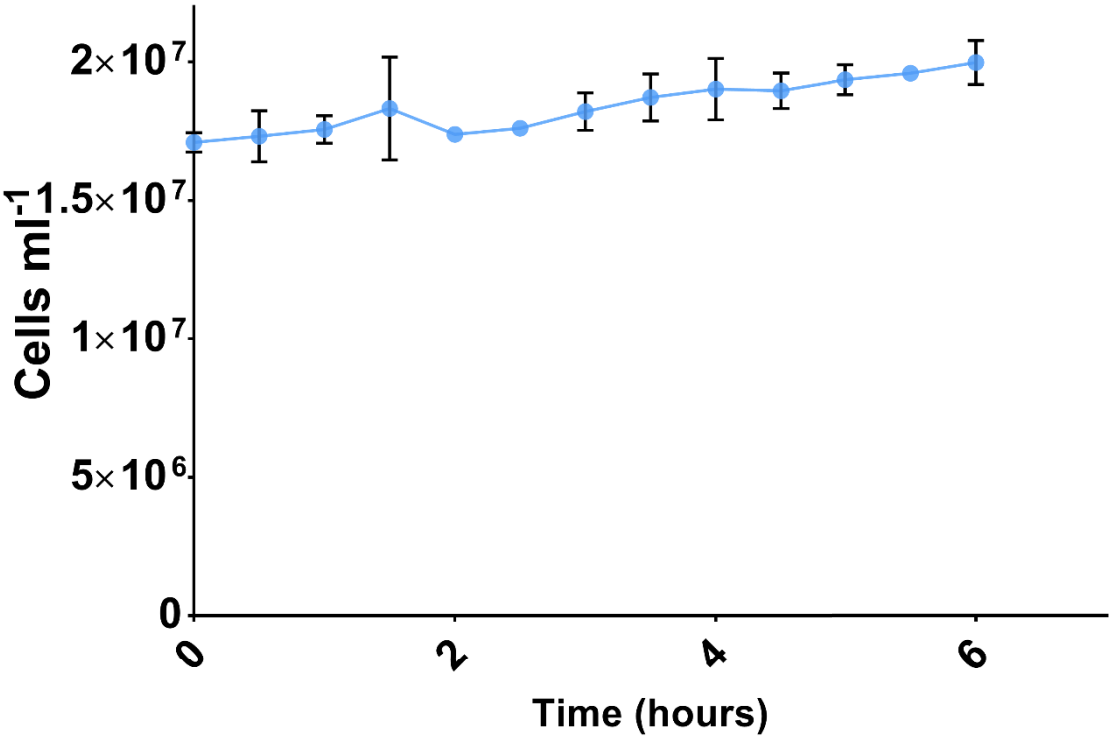

Supplementary Figure 3.3 Growth of *Synechococcus* sp. over six-hours at same light and temperature conditions used during the experiment. Samples were collected every 30 minutes (n = 5). Error bars = standard deviation.

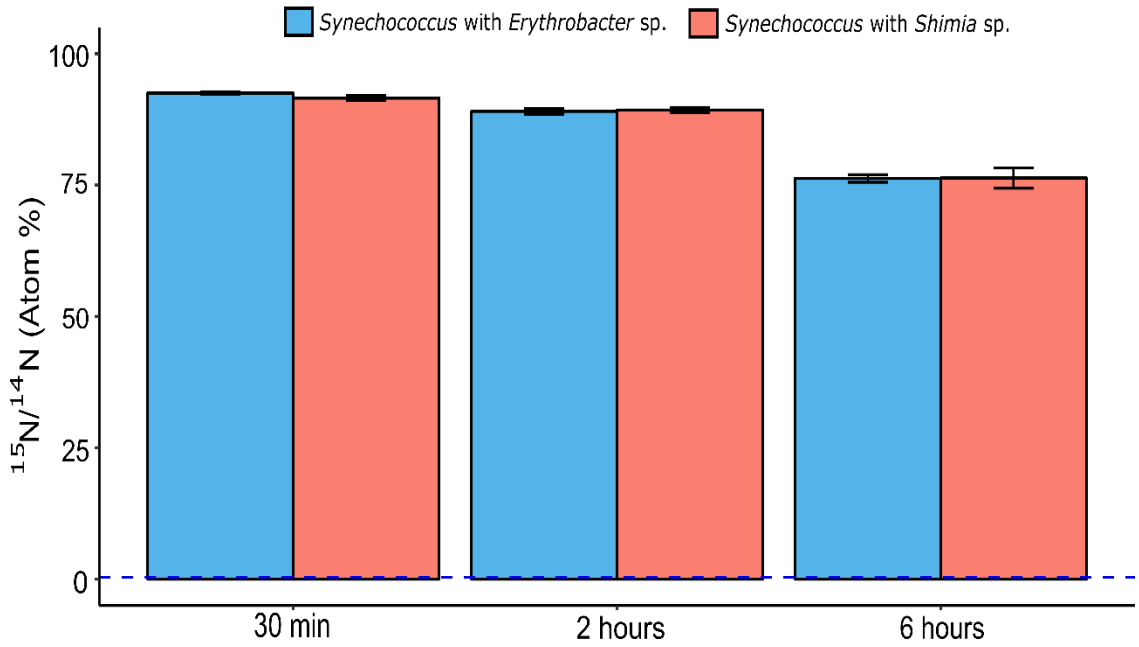

Supplementary Figure 3.4 Decreasing ^{15}N enrichment of *Synechococcus* cells in co-incubation with *Erythrobacter* sp. MG_01 (blue) and *Shimia* sp. MG_02 (pink) (**A**); Error bars: standard errors; dashed line: $^{15}N/^{14}N$ ratio in natural abundance calculated from the control (0.367 % ± 0.002 mean ± SEM, n = 154); *Synechococcus* with *Erythrobacter* sp. MG_01: 30 minutes (92.519 % ± 0.247 mean ± SEM, n = 48), 2 hours (89.070 % ± 0.0.525 mean ± SEM, n = 54), 6 hours (76.279 % ± 0.695. mean ± SEM, n = 147); Shimia MG_02: 30 minutes (91.582 % ± 0.433 mean ± SEM, n = 26), 2 hours (89.283 % ± 0.493 mean ± SEM, n = 49), 6 hours (75.964 % ± 1.963 mean ± SEM, n = 24).

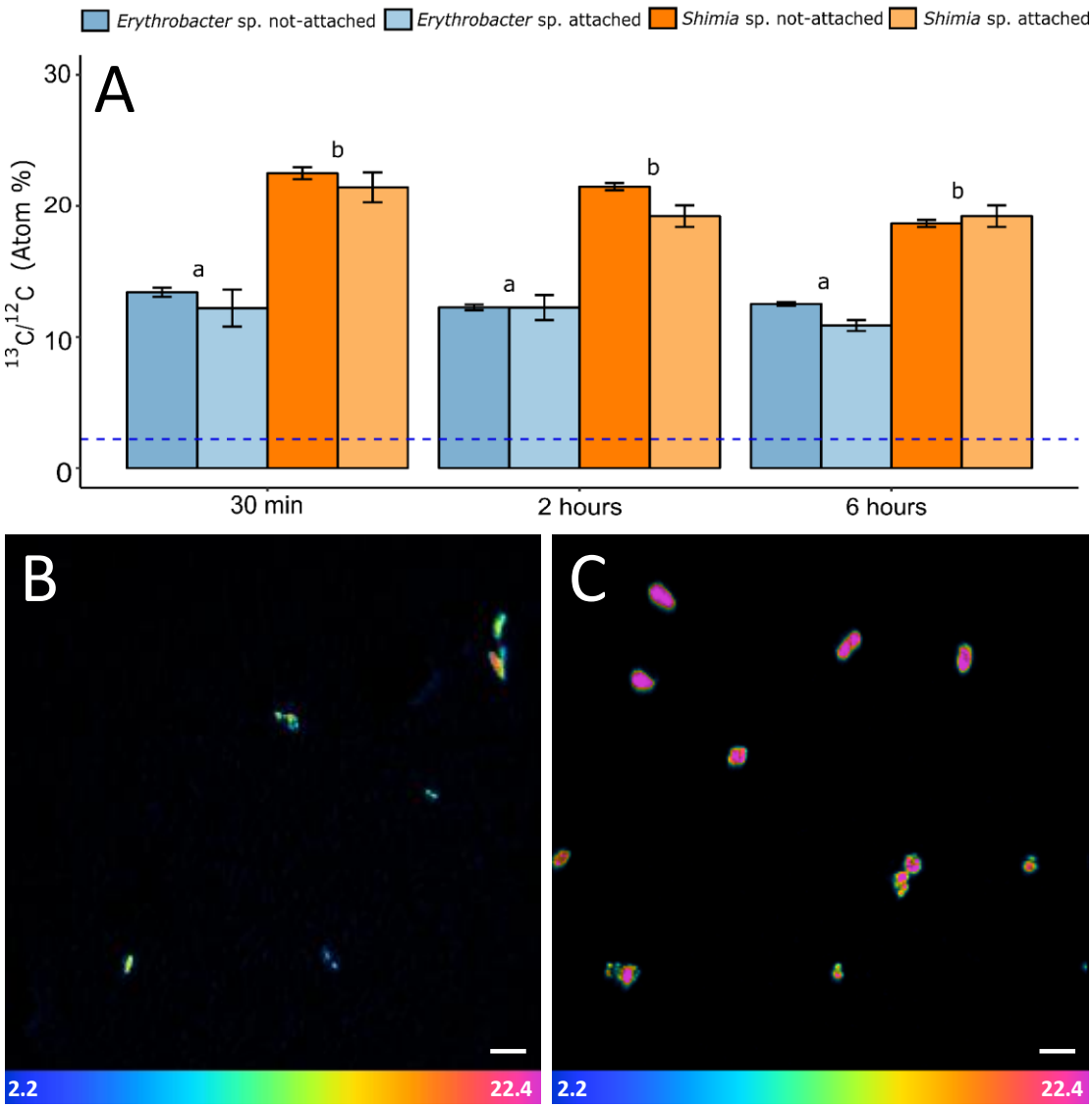

Supplementary Figure 3.5 ^{13}Carbon signature of *Erythrobacter* sp. MG_01 (blue) and *Shimia* sp. MG_02 (orange) (**A**); Error bars: standard errors; dashed line: $^{13}C/^{12}C$ ratio in natural abundance calculated from the control (2.176 % ± 0.006 mean ± SEM, n = 154); *Erythrobacter* sp. MG_01 not-attached: 30 minutes (13.416 % ± 0.349 mean ± SEM, n = 71), 2 hours (12.261 % ± 0.215 mean ± SEM, n = 132), 6 hours (12.517 % ± 0.149 mean ± SEM, n = 283); *Shimia* MG_02 not-attached: 30 minutes (22.486 % ± 0.456 mean ± SEM, n = 150), 2 hours (21.463 % ± 0.273 mean ± SEM, n = 270), 6 hours (18.663 % ± 0.268 mean ± SEM, n = 237); *Erythrobacter* MG_01 attached: 30 minutes (12.207 % ± 1.411 mean ± SEM, n = 8), 2 hours (12.254 % ± 0.955 mean ± SEM, n = 13), 6 hours (10.874 % ± 0.416 mean ± SEM, n = 20); *Shimia* MG_02 attached: 30 minutes (21.414 % ± 1.144 mean ± SEM, n = 19), 2 hours (20.594 % ± 0.507 mean ± SEM, n = 38), 6 hours (19.217 % ± 0.819 mean ± SEM, n = 21). Representative NanoSIMS images showing $^{13}C/^{12}C$ ratio distribution in the samples: *Erythrobacter* sp. MG_01 (**B**) and *Shimia* sp. MG_02 (**C**) at 30 minutes; Blue = $^{13}C/^{12}C$ ratio in natural abundance, calculated from the control; Magenta = mean of *Shimia* sp. MG_02 at 30 minutes. Scale bars: 2 µm.

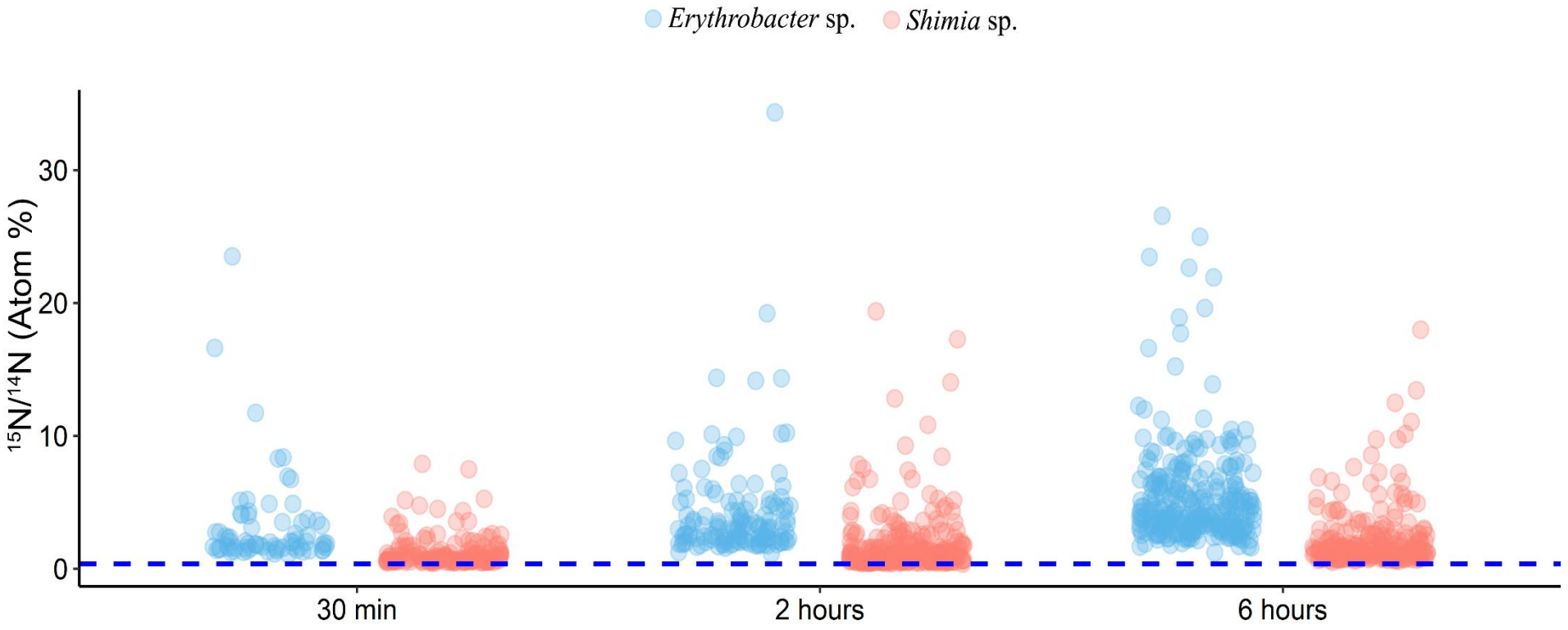

Supplementary Figure 3.6 Scatterplots showing the distribution of ^{15}N enrichment of single bacterial cells measured over six hours. Dashed line: $^{15}N/^{14}N$ ratio in natural abundance calculated from the control (0.367 % ± 0.002 mean ± SEM, n = 154).

Supplementary Table 3.1 Pairwise comparison with Mann-Whitney U-test to compare ^{15}N enrichment across bacterial groups

Bacteria	Timepoint	Not-attached – *Erythrobacter* MG_01						Not-attached - *Shimia* MG_02					
		30 minutes		2 hours		6 hours		30 minutes		2 hours		6 hours	
		U-value	*p*-value	U-value	*p*-value	U-value	*p*-value	U-value	*p*-value	U-value	*p*-value	U-value	*p*-value
Attached *Erythrobacter* MG_01	30 minutes	5	0.000	-	-	-	-	-	-	-	-	-	-
	2 hours	-	-	16	0.000	-	-	-	-	-	-	-	-
	6 hours	-	-	-	-	38	0.000	-	-	-	-	-	-
Attached *Shimia* MG_02	30 minutes	-	-	-	-	-	-	0.000	0.000	-		-	-
	2 hours	-	-	-	-	-	-	-	-	21	0.000	-	-
	6 hours	-	-	-	-	-	-	-	-	-	-	19	0.000
Not-attached *Shimia* MG_02	30 minutes	1646	0.000	-	-	-	-	-	-	-	-	-	-
	2 hours	-	-	5012	0.000	-	-	-	-	-	-	-	-
	6 hours	-	-	-	-	8412	0.000	-	-	-	-	-	-

Supplementary Table 3.2 Summary of Kruskal-Wallis test and Dunn's post hoc test with Bonferroni adjustment to compare ^{15}N enrichment within bacterial groups

Group tested	Single cells analyzed	Mean (At%)	SE	Kruskal-Wallis test *p*-value	Post hoc pairwise comparisons	Test Statistic	Std. Error	Std. Test Statistic	Bonferroni Adjusted *p*-value
***Erythrobacter* MG_01 Not-attached**	control = 154 30 minutes = 71 2 hours = 132 6 hours = 283	0.367 3.194 4.243 5.422	0.002 0.419 0.343 0.224	0.000	control / 30 minutes control / 2 hours control /6 hours 30 minutes/2 hours 30 minutes/6 hours 2 hours/6 hours	-206.092 -284.848 -364.973 -78.757 -158.882 -80.125	26.523 21.931 18.515 27.212 24.542 19.488	-7.770 -12.988 -19.713 -2.894 -6.474 -4.111	0.000 0.000 0.000 0.023 0.000 0.000
***Erythrobacter* MG_01 Attached**	control = 154 30 minutes = 8 2 hours = 13 6 hours = 20	0.367 28.401 27.625 28.887	0.002 4.094 2.278 1.744	0.000	control / 30 minutes control / 2 hours control / 6 hours 30 minutes/2 hours 30 minutes/6 hours 2 hours/6 hours	-99.625 -96.346 -97.400 3.279 2.225 -1.054	20.465 16.300 13.414 25.360 23.609 20.106	-4.868 -5.911 -7261 0.129 0.094 -0.052	0.000 0.000 0.000 1 1 1
***Shimia* MG_02 Not-attached**	control = 154 30 minutes = 150 2 hours = 270 6 hours =237	0.367 1.294 1.786 2.225	0.002 0.101 0.145 0.151	0.000	control / 30 minutes control / 2 hours control / 6 hours 30 minutes/2 hours 30 minutes/6 hours 2 hours/6 hours	-337.683 -377.399 -480.014 -39.716 -142.330 -102.615	26.874 23.656 24.247 23.856 24.442 20.852	-12.566 -15.954 -19.797 -1.665 -5.823 -4.921	0.000 0.000 0.000 0.576 0.000 0.000
***Shimia* MG_02 Attached**	control = 154 30 minutes = 19 2 hours = 38 6 hours = 21	0.367 21.048 24.907 21.717	0.002 2.602 1.375 1.729	0.000	control / 30 minutes control / 2 hours control / 6 hours 30 minutes/2 hours 30 minutes/6 hours 2 hours/6 hours	-64.211 -79.289 -69.727 -15.079 -5.517 9.562	10.992 8.588 10.392 11.883 13.245 11.330	-5.842 -9.232 -6.710 -1.269 -0.417 0.844	0.000 0.000 0.000 1 1 1

Supplementary Table 3.3 Pairwise comparison with Mann-Whitney U-test to compare ^{13}C enrichment across bacterial groups

Bacteria	Timepoint	control		Not-attached – *Shimia* MG_02						Attached - *Shimia* MG_02					
				30 minutes		2 hours		6 hours		30 minutes		2 hours		6 hours	
		U-value	*p*-value	U-value	*p*-value	U-value	*p*-value	U-value	*p*-value	U-value	*p*-value	U-value	*p*-value	U-value	*p*-value
control		-	-	0.000	0.000	0.000	0.000	0.000	0.000	0.000	0.000	0.000	0.000	0.000	0.000
Not-attached *Erythrobacter* MG_01	30 minutes	0.000	0.000	694	0.000	-	-	-	-	-	-	-	-	-	-
	2 hours	0.000	0.000	-	-	1727	0.000	-	-	-	-	-	-	-	-
	6 hours	0.000	0.000	-	-	-	-	6745	0.000	-	-	-	-	-	-
Attached *Erythrobacter* MG_01	30 minutes	0.000	0.000	-	-	-	-	-	-	12	0.000	-		-	-
	2 hours	0.000	0.000	-	-	-	-	-	-	-	-	26	0.000	-	-
	6 hours	0.000	0.000	-	-	-	-	-	-	-	-	-	-	9	0.000

Appendix C

Supplementary Information for Chapter 4

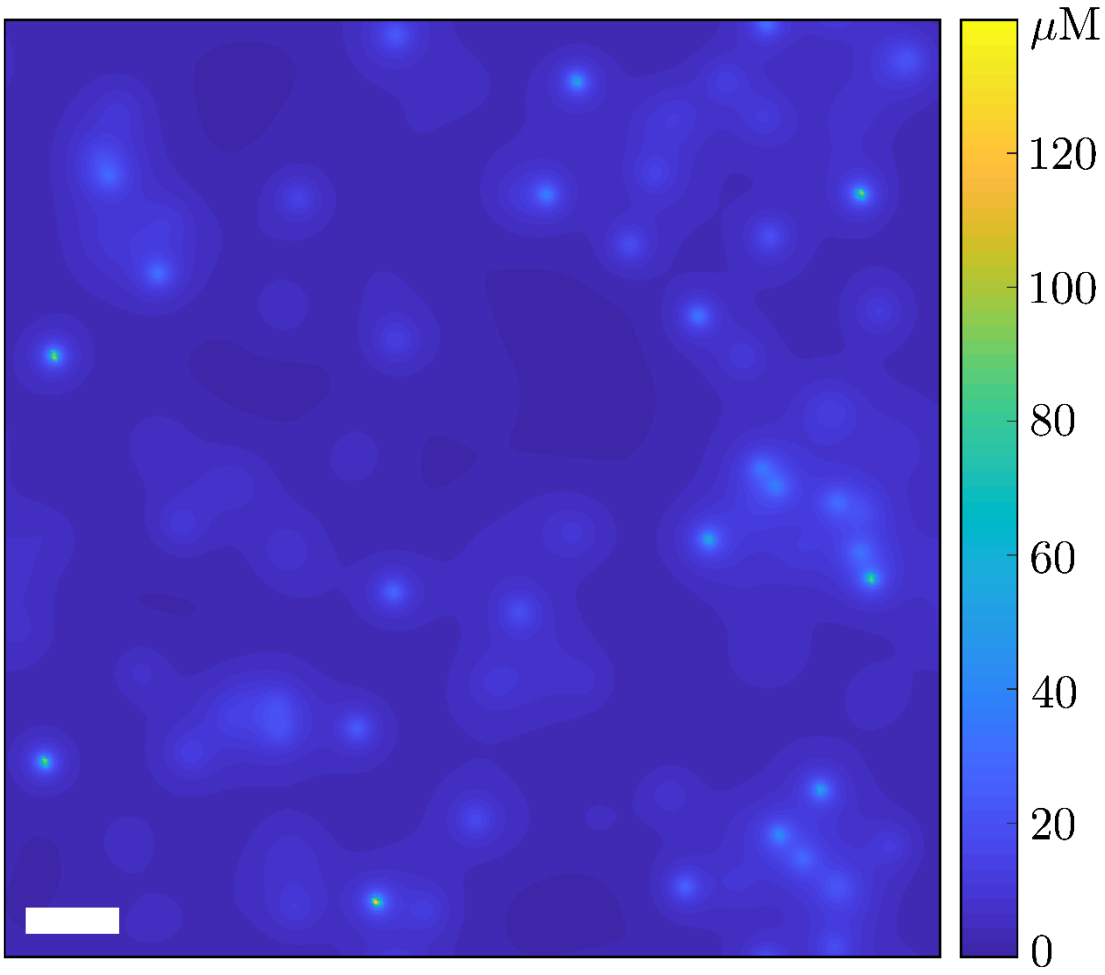

Supplementary Figure 4.1 DOM concentration within a 2D cross-section of the full 3D pro file. Results correspond to a *Synechococcus* density of $\rho = 10^3$ cells/mL. The white scale bar represents 1 mm.

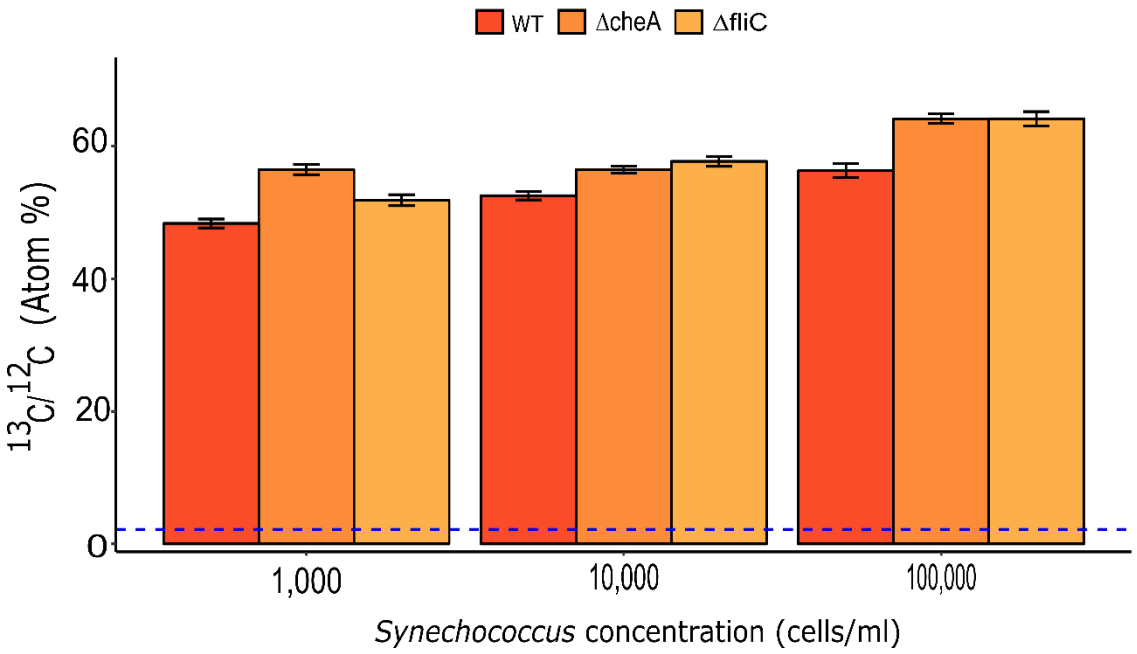

Supplementary Figure 4.2 ^{13}Carbon signature of *Marinobacter adhaerens* HP15 wild type (WT), motile and non-chemotactic (Δ*che*A), and non-motile (Δ*fli*C) at different Synechococcus concentrations: concentration 1,000 cells ml^{-1} (WT: 48.337 % ± 0.666, n = 376; Δ*che*A: 56.466 % ± 0.761, n = 262; Δ*fli*C: 51.836 % ± 0.839, n = 166; mean ± SEM); concentration 10,000 cells ml^{-1} (WT: 52.533 % ± 0.647, n = 470; Δ*che*A: 56.443 % ± 0.548, n = 419; Δ*fli*C: 57.694 % ± 0.772, n = 286; mean ± SEM); concentration 100,000 cells ml^{-1} (WT: 56.299 % ± 1.079, n = 181; Δ*che*A: 64.119 % ± 0.725, n = 172; Δ*fli*C: 64.126 % ± 1.076, n = 195; mean ± SEM); Error bars: standard errors; dashed line: $^{13}C/^{12}C$ ratio in natural abundance calculated from the control (2.185 % ± 0.005 mean ± SEM, n = 102).

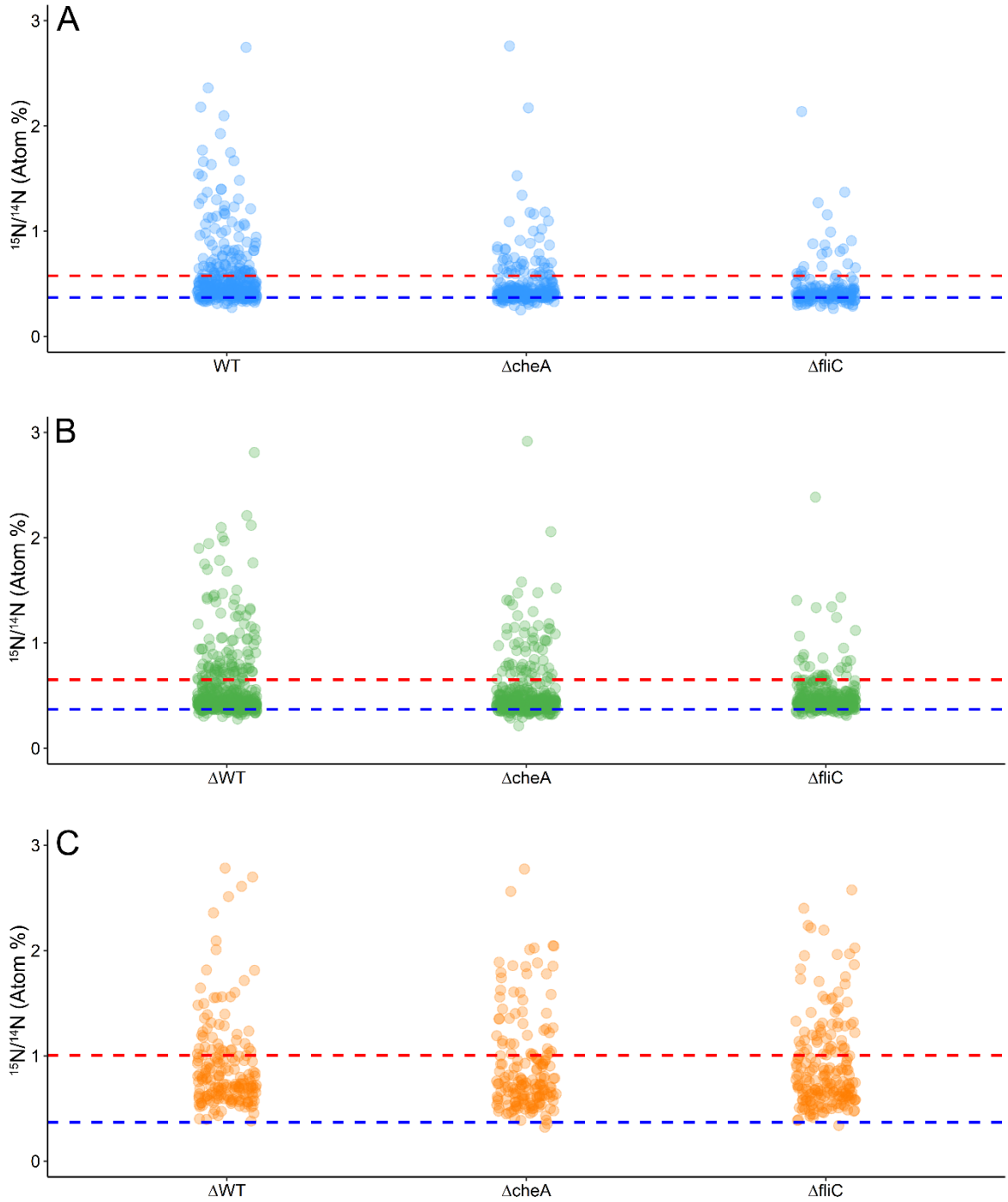

Supplementary Figure 4.3 Scatterplots showing the distribution of ^{15}N enrichment of single bacterial cells measured at different *Synechococcus* concentrations: 1,000 cells ml^{-1} (**A**), 10,000 cells ml^{-1} (**B**) and 100,000 cells ml^{-1} (**C**). Dashed blue line: $^{15}N/^{14}N$ ratio in natural abundance calculated from the control (0.374 % ± 0.001 mean ± SEM, n = 120). Dashed red line: mean values calculated from the WT bacteria (**A:** 0.577 %, n = 376; **B:** 0.651 %, n = 470; **C:** 1.005 %, n = 181).

Supplementary Table 4.1 Summary of Kruskal-Wallis test and Dunn's post hoc test with Bonferroni adjustment to compare ^{15}N enrichment of *M. adhaerens* strains within same *Synechococcus* concentration

Group tested	Single cells of *M. adhaerens* analyzed	Mean (At%)	SE	Kruskal-Wallis test *p*-value	Post hoc pairwise comparisons	Test Statistic	Std. Error	Std. Test Statistic	Bonferroni Adjusted *p*-value
***Synechococcus* 1,000 cells/ml**	control = 102	0.367	0.002	0.000	control / WT	-353.458	29.214	-12.099	0.000
	WT = 376	0.577	0.017		control / Δ*che*A	-258.790	30.541	-8.474	0.000
	Δ*che*A = 262	0.492	0.016		control / Δ*fli*C	-196.149	32.922	-5.958	0.000
	Δ*fli*C = 166	0.458	0.016		WT / Δ*che*A	94.688	21.059	4.495	0.000
					WT / Δ*fli*C	157.308	24.385	6.451	0.000
					Δ*che*A / Δ*fli*C	62.641	25.959	2.413	0.095
***Synechococcus* 10,000 cells/ml**	control = 102	0.367	0.002	0.000	control / WT	-507.936	40.283	-12.609	0.000
	WT = 470	0.651	0.049		control / Δ*che*A	-428.018	40.718	-10.512	0.000
	Δ*che*A = 419	0.528	0.016		control / Δ*fli*C	-486.024	42.531	-11.428	0.000
	Δ*fli*C = 286	0.502	0.012		WT / Δ*che*A	79.918	24.778	3.225	0.008
					WT / Δ*fli*C	21.913	27.657	0.428	1
					Δ*che*A / Δ*fli*C	-58.006	28.286	-2.051	0.242
***Synechococcus* 100,000 cells/ml**	control = 102	0.367	0.002	0.000	control / WT	-329.268	23.249	-14.162	0.000
	WT = 71	1.005	0.072		control / Δ*che*A	-310.860	23.468	-13.246	0.000
	Δ*che*A = 132	0.921	0.043		control / Δ*fli*C	-320.177	22.947	-13.953	0.000
	Δ*fli*C = 283	0.907	0.031		WT / Δ*che*A	-18.407	19.996	0.921	1
					WT / Δ*fli*C	-9.091	19.382	0.469	1
					Δ*che*A / Δ*fli*C	--9.316	19.643	-0.474	1